Mon. Not. R. Astron. Soc. **367,** 1329–1366 (2006) doi:10.1111/j.1365-2966.2006.10148.x

Elemental abundance survey of the Galactic thick disc

Bacham E. Reddy,[1⋆] David L. Lambert[2] and Carlos Allende Prieto[2]

[1]*Indian Institute of Astrophysics, Bangalore 560034, India*
[2]*The W.J. McDonald Observatory, University of Texas, Austin, TX 78712, USA*

Accepted 2005 December 6. Received 2005 November 8

ABSTRACT

We have performed an abundance analysis for F- and G- dwarfs of the Galactic thick-disc component. A sample of 176 nearby ($d \leqslant 150$ pc) thick-disc candidate stars was chosen from the *Hipparcos* catalogue and subjected to a high-resolution spectroscopic analysis. Using accurate radial velocities combined with the *Hipparcos* astrometry, kinematics (U, V and W) and Galactic orbital parameters were computed. We estimate the probability for a star to belong to the thin disc, the thick disc or the halo. With a probability $P \geqslant 70$ per cent taken as certain membership, we assigned 95 stars to the thick disc, 13 to the thin disc, and 20 to the halo. The remaining 48 stars in the sample cannot be assigned with reasonable certainty to one of the three components.

Abundances of C, O, Na, Mg, Al, Si, Ca, Sc, Ti, V, Cr, Mn, Fe, Co, Ni, Cu, Zn, Y, Ba, Ce, Nd and Eu have been obtained. The abundances for the thick-disc stars are compared with those for the thin-disc members from Reddy et al. The ratios of α-elements (O, Mg, Si, Ca and Ti) to iron for thick-disc stars show a clear enhancement compared to thin-disc members in the range $-0.3 <$ [Fe/H] < -1.2. There are also other elements – Al, Sc, V, Co, and possibly Zn – which show enhanced ratios to iron in the thick disc relative to the thin disc. The abundances of Na, Cr, Mn, Ni and Cu (relative to Fe) are very similar for thin- and thick-disc stars. The dispersion in abundance ratios [X/Fe] at given [Fe/H] for thick-disc stars is consistent with the expected scatter due to measurement errors, suggesting a lack of 'cosmic' scatter.

A few stars classified as members of the thick disc by our kinematic criteria show thin-disc abundances. These stars, which appear older than most thin-disc stars, are also, on average, younger than the thick-disc population. They may have originated early in the thin-disc history, and been subsequently scattered to hotter orbits by collisions. The thick disc may not include stars with [Fe/H] > -0.3. The observed compositions of the thin and thick discs seem to be consistent with the models of galaxy formation by hierarchical clustering in a Lambda cold dark matter (ΛCDM) universe.

Key words: stars: abundances – stars: kinematics – Galaxy: abundances – Galaxy: evolution.

1 INTRODUCTION

Stars of the solar neighbourhood are overwhelmingly members of the Galactic disc, with a small admixture of halo stars. The assignment of a star to the disc or the halo is based on the differences in chemical composition and kinematics. The local disc population is subdivided into stars of the thin disc and others belonging to the thick disc, with the chemical composition and kinematics again playing a role in effecting this subdivision.

The modern division of the disc into the thin and thick disc was proposed by Gilmore & Reid (1983). Star counts led them to divide the disc population in the solar neighbourhood into a thin disc with a scaleheight of 300 pc, and a thick disc with the much greater scaleheight of 1450 pc. Thin-disc stars outnumber thick-disc stars by about 20 to one in the Galactic plane. Many other estimates of the scaleheights and relative densities of the thin- and thick-disc populations now exist (e.g. Buser, Rong & Karaali 1999; Ojha 2001; Cabrera-Lavers, Garzón & Hammersley 2005; Juric et al. 2005). The thick-disc stars are generally older than most thin-disc stars. The metallicity distribution of the thick-disc population is shifted to lower values relative to the distribution for the thin disc by about 0.5 dex. Although both distributions can be reasonably approximated by Gaussians with a full width at half-maximum of roughly 0.5 dex, the thick disc includes a tail at lower metallicities. In contrast to the thin-disc stars, which orbit the Galactic Centre on

⋆E-mail: ereddy@iiap.res.in

nearly circular orbits, the thick-disc stars are on moderately elliptical orbits that typically reach higher distances from the plane. Thick-disc stars revolve around the Galactic Centre slower than those in the thin disc.

The origin of the thick disc has occasioned much debate. Keys to the origin lie within the kinematics and composition of the thick-disc stars. A number of recent spectroscopic studies have set out to compare the chemical compositions of the thick- and thin-disc stars. This avenue was explored by Gratton et al. (1996) and Fuhrmann (1998). Gratton et al. showed that O/Fe ratios for thick-disc stars are distinctly different from thin-disc stars, but similar to halo stars. Fuhrmann confirmed this based on the Mg abundances and showed a clear-cut difference in the Mg/Fe ratio for thick and thin F-G dwarf stars of the same [Fe/H].[1] These studies stimulated several investigations of elemental abundances in samples of thick- and thin-disc stars – see, for example, Prochaska et al. (2000), Feltzing, Bensby & Lundström (2003), Reddy et al. (2003, hereafter Paper I), Bensby, Feltzing & Lundström (2003, 2004), Bensby et al. (2005), and Mishenina et al. (2004). Although the pattern of abundance differences between thick and thin disc is emerging, many details remain obscure, largely, one suspects, because these investigations cover small numbers of thick-disc stars: Prochaska et al. considered 10, Bensby and colleagues analysed 36, and Mishenina et al. less than 30 stars. Considering that the thick disc may span a range of 1 dex in [Fe/H], these samples, even when combined, are probably too small to define in detail the differences between compositions of thick- and thin-disc stars over their full range in [Fe/H], even if the two disc components were themselves chemically homogeneous as a function of metallicity. Additionally, different definitions of what constitutes a thick-disc star have been adopted by different authors.

Tens of thousands of thick-disc stars at a few kpc from the plane have been spectroscopically observed as part of the Sloan Digital Sky Survey (SDSS) (York et al. 2000; Adelman-McCarthy et al. 2006). These spectra, however, have a much lower resolving power than the surveys mentioned above and, although, they may yield abundance ratios for a number of metals that produce strong spectral lines, they have, to this date, been used to derive iron abundances only (Allende Prieto et al. 2006).

Exploration of the chemical compositions of local thin-disc stars is now well advanced. In particular, several surveys have investigated many elements in F-G dwarfs whose spectra are amenable to quantitative analysis. Our recent study of 26 elements in 181 F-G dwarfs (Paper I) was the precursor for the work presented in this paper. The vast majority of the 181 stars belong to the thin disc, as judged (see below) by their kinematics. Our Paper I sample may be combined with other large samples to which thin-disc stars are the major contributor: for example, Edvardsson et al. (1993) for 189 stars, and Chen et al. (2000) for 90 stars. A key result of our 2003 survey was the finding that 'cosmic' scatter in an abundance ratio [X/Fe] at a given [Fe/H] for thin-disc stars was less than the small measurement errors. Here, we apply the same analytical techniques to a large sample of thick stars for which the cosmic scatter and, indeed, the form of the run of [X/Fe] with [Fe/H] was not known at the outset of this project. There were clear indications of the sign and magnitude of some abundance differences between thick and thin disc, as recognized by Fuhrmann (1998) and Prochaska et al. (2000), and further examined by Bensby and colleagues, and by Mishenina et al. (2004).

The present survey provides abundances for 23 elements from C to Eu for 176 stars in the solar neighbourhood, of which 95 are attributed to the thick disc. The full sample is introduced in the next section. The observations and abundance analysis are based closely on Paper I's approach described in Sections 3 and 4. Full results, and comparisons with other studies are given in Section 5. Chemical evolution of the thick disc and the evolution of the Galactic disc are discussed in Section 6. This section includes discussion on stars which have thick-disc kinematics and thin-disc abundances (TKTA), disc heating, and merger scenarios. Concluding remarks are given in Section 7.

2 THE THICK-DISC SAMPLE

2.1 Preliminary selection

Stars were first selected from the *Hipparcos* catalogue, according to the following criteria: a declination north of -30° so that they were observable from the W. J. McDonald Observatory; a $B-V$ colour corresponding to an effective temperature of 5000–6500 K which eliminates the cool dwarfs with rich line spectra and the hotter dwarfs where rapid rotation may broaden lines; and an absolute visual magnitude in the range $2.5 \leqslant M_V \leqslant 6.0$ indicating evolution off the zero-age main-sequence (ZAMS) so that an age determination is possible; a distance of less than 150 pc to avoid significant uncertainties in the observed trigonometric parallaxes, and the introduction of a reddening correction. Application of these criteria provided about 9300 stars from the catalogue's total of 118 218.

The *Hipparcos* catalogue was the sole source of parallaxes and proper motions. Our initial selection of thick-disc candidates was based on the space motions computed using radial velocities collected from several catalogues: the *Hipparcos* Input Catalogue, Carney et al. (1994), Barbier-Brossat & Figon (2000), and Malaroda, Levato & Galliani (2001). These sources provided radial velocity data for 1970 of the 9300 stars. The space velocities U, V and W were computed, where U is directed towards the Galactic Centre, V is directed in the sense of Galactic rotation (clockwise as seen from the North Galactic Pole), and W is directed towards the North Galactic Pole. Then, the velocities, $U_{\rm LSR}$, $V_{\rm LSR}$ and $W_{\rm LSR}$, relative to the local standard of rest (LSR) were calculated assuming the solar motion of $(U, V, W) = (10.0, 5.3, 7.2)\,{\rm km\,s^{-1}}$, as derived by Dehnen & Binney (1998) from the *Hipparcos* data. After calculation of their $U_{\rm LSR}$, $V_{\rm LSR}$ and $W_{\rm LSR}$, a selection by $V_{\rm LSR}$ and $W_{\rm LSR}$ was made to increase the yield of thick-disc (and halo) stars: $V_{\rm LSR} \leqslant -40\,{\rm km\,s^{-1}}$ and $|W_{\rm LSR}| \geqslant 30\,{\rm km\,s^{-1}}$. These criteria led to a sample of 213 stars which was reduced to 176 when inspection of spectra revealed stars with broad lines and the double-lined spectroscopic binaries.

In the final computation of the U, V and W for the 176 stars, we made extensive use of three new sources of radial velocities: Latham et al. (2002), Nidever et al. (2002) and Nordström et al. (2004). The agreement between these sources for stars in common corresponds to about $\sigma = 0.2\,{\rm km\,s^{-1}}$. For 146 of the 176 stars, the radial velocity is given in one or more of these sources. For the remaining 30 stars, we derived the radial velocity from our spectra with an accuracy of about $0.5\,{\rm km\,s^{-1}}$.

Space velocities were recomputed using the new radial velocities. We examined the effects of errors in the input parameters (parallax, proper motion, and radial velocity), assuming these errors are uncorrelated. The uncertainties in $U_{\rm LSR}$, $V_{\rm LSR}$ and $W_{\rm LSR}$ are

[1] Here and throughout this paper, we use the so-called *bracket* notation to indicate the chemical-abundance ratios of two elements X and Y: $[{\rm X/Y}] \equiv \log[N({\rm X})/N({\rm Y})] - \log[N({\rm X})/N({\rm Y})]_\odot$, where N indicates number density.

calculated as the quadratic sum of the individual uncertainties in the input parameters. In a typical case, the Galactic velocity components are accurate to about 5 km s^{-1}. An uncertain parallax (say, 30 per cent accuracy) can lead to a much larger uncertainty; there are 12 stars for which the uncertainty in one of the component velocities is as large as 30–50 km s^{-1}.

2.2 Membership probabilities

In developing an understanding of the differences between the thin and thick discs, an obvious prerequisite is a reliable method, even if statistical, of assigning a star to the thin or thick disc, and of recognizing stars for which an assignment cannot be made with fair certainty. Since our goal is to quantify the differences in the chemical composition between the thin and thick disc, composition cannot be a consideration in determining membership. Kinematic criteria are invoked for this purpose. We follow recent studies in developing and applying the criteria. The criteria are blunt instruments; the kinematics of, especially, thin-disc stars, but one suspects also of thick-disc stars, are complicated.

The thin disc, as represented by the F-G dwarfs in the solar vicinity, is neither a monolithic structure nor cleanly separated from the thick disc in the ($U_{\rm LSR}, V_{\rm LSR}, W_{\rm LSR}$) space. Structures include moving groups or stellar streams which are seen as regions of enhanced stellar density in phase space (see Nordström et al. 2004; Famaey et al. 2005). In addition, the mean location of stars and the dispersion about their mean velocity are dependent on the age of the stars.

Characteristics of thick-disc stars are the generally negative $V_{\rm LSR}$ and the larger $W_{\rm LSR}$ (relative to the thin disc). At present, thick-disc stars with accurate $U_{\rm LSR}$, $V_{\rm LSR}$ and $W_{\rm LSR}$ velocities are too few in number to identify moving groups, should they exist. It is commonly agreed that the dispersions in the $U_{\rm LSR}$, $V_{\rm LSR}$ and $W_{\rm LSR}$ velocities of the thick-disc stars exceed those of the thin-disc stars.

There are regions in the ($U_{\rm LSR}$, $V_{\rm LSR}$, $W_{\rm LSR}$) space where both thin- and thick-disc stars may occur. In such boundary layers shared by thin and thick stars, one must resort to a probability argument. Boundary layers also exist mixing thick disc with halo stars and again a probability argument must be used.

In this paper, the method of assigning the probability for each star to either the thin disc, the thick disc, or the halo is basically that adopted in the earlier studies by Bensby et al. (2003, 2004) and Mishenina et al. (2004). We assume the sample is a mixture of the three populations. These populations are each assumed to be represented by Gaussian distribution functions for the velocity components $U_{\rm LSR}$, $V_{\rm LSR}$ and $W_{\rm LSR}$, with given mean values and dispersions. (The well-known age dependence of the quantities for the thin disc is ignored.) The remaining required ingredients are the relative numbers of thin-disc, thick-disc, and halo stars.

Given these assumptions, the equations establishing the probability that a star belongs to the thin disc ($P_{\rm thin}$), the thick disc ($P_{\rm thick}$), or the halo ($P_{\rm halo}$) are

$$P_{\rm thin} = f_1 \frac{P_1}{P},\ P_{\rm thick} = f_2 \frac{P_2}{P},\ P_{\rm halo} = f_3 \frac{P_3}{P}, \quad (1)$$

where

$$P = \sum f_i P_i,$$

$$P_i = K_i \exp\left[-\frac{U_{\rm LSR}^2}{2\sigma_{U_i}^2} - \frac{(V_{\rm LSR} - V_{\rm ad})^2}{2\sigma_{V_i}^2} - \frac{W_{\rm LSR}^2}{2\sigma_{W_i}^2}\right]$$

and

$$K_i = \frac{1}{(2\pi)^{3/2}\sigma_{U_i}\sigma_{V_i}\sigma_{W_i}}\ (i = 1, 2, 3) \quad (2)$$

Table 1. Given are the velocity dispersions, the asymmetric drift velocities relative to LSR, ($V_{\rm ad}$), and the fractional population of three stellar components: thin, thick and the halo.

Component	σ_U	σ_V	σ_W	$V_{\rm ad}$	Fraction
Thin disc	43	28	17	−9	0.93
Thick disc	67	51	42	−48	0.07
Halo	131	106	85	−220	0.006

and $V_{\rm ad}$ is the asymmetric drift, the mean Galactic rotation velocity for each stellar population relative to the LSR.

The parameters (values of σ, and the mean velocities) defining the Gaussian distribution functions and the population fractions f_i, given in Table 1, are taken from Robin et al. (2003; but see, also Ojha et al. 1996, 1999; Soubiran, Bienaymé & Siebert 2003). The asymmetric drifts $V_{\rm ad}$ given by Robin et al. are referred to the Sun and, therefore, we have corrected them for the solar motion relative to the LSR $V_\odot = +5.3$ km s^{-1}. The mean values of $U_{\rm LSR}$ and $W_{\rm LSR}$ for any of the three populations are taken to be zero. For the thin disc, the estimates refer to stars of 5–7 Gyr in age, which is an average value for our sample (see Section 4.5), but this result is also in excellent agreement with the value inferred by Allende Prieto et al. (2004) from FGK stars in the solar neighbourhood.

The relative numbers of thin-disc, thick-disc, and halo stars in the solar vicinity are taken to be $f_1 = 0.93$, $f_2 = 0.07$, and $f_3 = 0.006$, respectively. As a check, we have used Nordström et al.'s (2004) survey of Galactic F-G dwarfs in the solar neighbourhood to estimate the fractions of the three components. If we assume that all the stars having $V_{\rm LSR}$ between −150 and −40 km s^{-1} belong to the thick-disc, stars with $V_{\rm LSR} > -40$ km s^{-1} are part of the thin-disc, and the rest are halo stars, we find fractions of 94, 5 and 1 per cent. The differences between Robin et al.'s (2003) and these fractions are small and have no impact on the resolution of the sample into three components based on probabilities.[2] Our adopted fractions also compare well with the ratios $\rho_{\rm thick}/\rho_{\rm thin}$ of 4 and 9 per cent derived at the solar radius from star counts by Juric et al. (2005) using the SDSS and by Cabrera-Lavers et al. (2005) based on the Two-Micron All-Sky Survey (2MASS), respectively.

The probabilities – $P_{\rm thin}$, $P_{\rm thick}$ and $P_{\rm halo}$ – and the associated errors due to errors in the velocities $U_{\rm LSR}$, $V_{\rm LSR}$ and $W_{\rm LSR}$ were computed. [Our program reproduces the probabilities given by Bensby et al. (2003, 2005) and Mishenina et al. (2004), when their input data are adopted.] We consider that a probability ($P_{\rm thick}$ – error) in excess of 70 per cent suffices to assign a star to either the thin disc, thick disc, or halo. Table 2 lists 95 thick stars with $P_{\rm thick}$ given in column 12, 13 thin-disc stars with $P_{\rm thin}$ in column 12, and 20 halo stars with $P_{\rm halo}$ in column 12. Of the sample of 176 stars, there remain 48 stars with 34 belonging to either the thick or the thin disc, with about equal probability, and 14 belong to the thick disc or the halo, with approximately equal probability. In Table 2, $P_{\rm thick}$ is given for these 48 stars. (The same procedure applied to the 181 'thin' disc stars of Paper I yielded 175 thin disc, just two thick stars with the other four assignable with roughly equal probability to either the thin or the thick disc.)

The present sample and that from Paper I are shown in Fig. 1 with the velocities, $U_{\rm LSR}$, $V_{\rm LSR}$ and $W_{\rm LSR}$, plotted against

[2] Venn et al. (2004) seemed to have computed membership probabilities on the assumption that the fractional populations are the same for the three components. This assumption can give very different and misleading results.

Table 2. Atmospheric parameters and kinematic data for the program stars. The columns 1–11 are self explanatory. The value in column 5 is the heliocentric radial velocity(R_V). Errors for the values in columns 5–8 are discussed in the text. See text for explanatory note about the probability (per cent P) in column 12.

Star HIP	[Fe/H]	$T_{\rm eff}$ (K)	log g (cm s^{-2})	R_V	$U_{\rm LSR}$ (km s^{-1})	$V_{\rm LSR}$	$W_{\rm LSR}$	$R_{\rm m}$ (kpc)	e	$Z_{\rm max}$ (kpc)	τ_9 (Gyr)	per cent P
					Thick disc							
3086	−0.23	5697	4.14	−29.2	−159	−50	56	8.55	0.51	0.70	$7.9^{+2.4}_{-1.8}$	95 ± 1
3185	−0.65	5344	3.81	−45.3	−37	−84	45	6.20	0.40	0.43	$11.3^{+2.7}_{-2.2}$	87 ± 0
3441	−0.50	5723	4.50	−108.3	89	−66	86	7.08	0.39	1.13	...	96.±0
4039	−1.24	5803	3.92	−5.3	−116	−92	46	6.75	0.52	0.47	$13.0^{+2.6}_{-2.1}$	95 ± 1
4544	−0.87	5832	4.51	−112.2	−33	−133	−74	5.35	0.61	0.81	...	90 ± 6
5122	−0.62	5204	3.80	8.9	−93	−73	48	6.93	0.42	0.50	$12.6^{+3.0}_{-2.4}$	91 ± 2
5315	−0.47	5014	3.45	−94.0	59	−117	44	5.68	0.56	0.41	$8.8^{+6.7}_{-3.8}$	96 ± 1
5336	−0.86	5300	4.67	−99.6	−31	−154	−27	4.99	0.72	0.22	...	91 ± 1
5775	−0.59	5547	4.62	81.8	−59	−97	−74	6.10	0.47	0.90	...	96 ± 1
6159	−0.67	5653	4.56	−6.7	148	−68	−40	7.78	0.52	0.43	...	93 ± 9
6607	−0.41	5454	4.59	84.7	−15	−80	−68	6.26	0.36	0.71	...	97 ± 0
7961	−0.64	5565	3.96	−8.6	−86	−71	40	6.83	0.41	0.37	$10.7^{+2.9}_{-2.3}$	78 ± 1
8674	−0.60	5455	4.62	41.8	28	−88	−43	6.10	0.41	0.37	...	86 ± 11
9080	−0.37	5162	4.65	−14.2	−83	−85	52	6.53	0.45	0.48	...	96 ± 1
10652	−0.67	5499	4.58	−20.5	−90	−86	90	6.61	0.46	1.21	...	93 ± 2
12579	−0.80	5770	4.60	−12.5	−2	−54	−67	6.84	0.24	0.70	...	94 ± 13
13366	−0.70	5669	4.19	7.0	45	−99	−74	5.97	0.47	0.83	$11.8^{+4.3}_{-3.2}$	96 ± 1
15405	−0.73	5107	3.56	17.8	−137	−95	−40	6.91	0.57	0.39	$10.2^{+8.3}_{-4.6}$	94 ± 1
17147	−0.87	5722	4.50	121.0	−100	−80	−38	6.74	0.46	0.35	...	88 ± 2
17666	−1.03	5000	4.50	76.0	−108	−99	−73	6.04	0.55	0.78	...	93 ± 3
22020	−0.35	5604	4.27	28.1	−71	−85	−53	6.43	0.43	0.52	...	95 ± 14
22060	−0.63	5610	4.61	172.1	−184	−66	52	8.75	0.59	0.65	...	89 ± 7
23080	−0.32	5334	4.60	38.5	−46	−67	55	6.65	0.33	0.54	...	88 ± 1
24030	−1.00	5738	4.64	−15.7	20	−88	97	6.18	0.39	1.22	...	95 ± 1
25860	−0.35	5543	4.56	48.1	−14	−74	−59	6.38	0.34	0.59	...	94 ± 8
26452	−0.89	5749	4.64	−37.7	3	−96	47	5.93	0.43	0.44	...	94 ± 1
26828	−0.34	6180	4.12	77.7	−63	−81	40	6.42	0.42	0.35	$3.20^{+3.6}_{-1.7}$	80 ± 1
27128	−0.81	5802	4.16	180.7	−162	−68	−66	8.11	0.56	0.91	$12.3^{+2.8}_{-2.3}$	91 ± 0
29269	−0.68	5484	3.95	−32.0	−95	−85	−74	6.64	0.47	0.89	$12.2^{+3.7}_{-2.8}$	95 ± 1
31188	−0.59	5789	4.54	3.3	19	−26	71	7.68	0.12	0.77	...	92 ± 3
34642	−0.44	5747	4.14	−29.5	−13	−87	−55	6.09	0.40	0.53	$8.97^{+3.2}_{-2.4}$	95 ± 12
35989	−0.19	5185	4.60	6.3	−37	−41	−65	7.27	0.21	0.68	...	92 ± 13.
36849	−0.77	5843	4.40	−36.8	70	−84	−46	6.35	0.43	0.42	...	92 ± 17.
37233	−0.51	5627	4.01	52.8	13	−67	50	6.55	0.30	0.47	$9.3^{+2.6}_{-2.1}$	75 ± 2
38769	−0.79	5726	4.15	5.6	25	−65	69	6.63	0.30	0.74	$12.7^{+3.5}_{-2.8}$	97 ± 1
39893	−0.84	5249	4.69	−40.6	66	−127	−55	5.59	0.61	0.56	...	93 ± 3
40613	−0.62	5670	4.16	111.3	−27	−138	−36	5.18	0.65	0.30	$12.4^{+2.8}_{-2.3}$	94 ± 1
43393	−0.59	5256	4.65	33.4	32	−104	−79	5.88	0.47	0.93	...	95 ± 2
44075	−0.86	5783	4.09	149.6	−51	−111	86	6.25	0.39	0.87	$12.8^{+2.6}_{-2.2}$	92 ± 0
44347	−0.85	5798	4.62	−57.4	117	−64	31	7.34	0.45	0.29	...	70 ± 0
44860	−0.51	5654	4.27	65.5	−58	−67	−57	6.69	0.35	0.57	$12.6^{+3.8}_{-2.9}$	92 ± 5
45947	−0.46	4911	3.29	26.6	−16	−105	−60	5.77	0.48	0.60	$9.51^{+8.2}_{-4.4}$	97 ± 7
50005	−0.53	5394	4.64	60.1	101	−99	41	6.31	0.53	0.42	...	95 ± 4
50671	−0.48	5878	4.45	82.0	−60	−41	63	7.39	0.26	0.69	...	90 ± 1
50965	−0.57	5715	4.56	19.8	−51	−88	−84	6.26	0.42	1.02	...	96 ± 1
52673	−0.66	5541	4.62	74.7	52	−99	−39	5.97	0.47	0.35	...	92 ± 14
58843	−0.79	5663	4.63	6.8	109	−122	−52	6.01	0.63	0.53	...	91 ± 6
59233	−0.83	5333	3.71	−12.2	−181	−72	−37	8.38	0.60	0.38	...	91 ± 18
59750	−0.74	6069	4.44	−3.7	61	−61	−60	6.77	0.35	0.54	...	93 ± 2
60268	−0.72	5532	4.62	−81.8	6.7	−98	−37	5.86	0.45	0.32	...	88 ± 5
60956	−0.58	5362	4.63	6.1	7.3	−139	−64	5.21	0.63	0.73	...	91 ± 7
62240	−0.83	5663	4.46	−36.4	61	−68	−69	6.73	0.35	0.75	...	97 ± 4
64426	−0.71	5754	4.16	49.4	−72	−64	64	6.91	0.36	0.70	$11.3^{+3.4}_{-2.6}$	96 ±0

Table 2 – *continued*

Star HIP	[Fe/H]	$T_{\rm eff}$ (K)	log g (cm s^{-2})	R_V	$U_{\rm LSR}$ (km s^{-1})	$V_{\rm LSR}$	$W_{\rm LSR}$	$R_{\rm m}$ (kpc)	e	$Z_{\rm max}$ (kpc)	log τ_9 (Gyr)	per cent P
65449	−0.44	5383	3.84	−21.6	−141	−55	−37	7.97	0.48	0.38	$9.7^{+4.5}_{-3.1}$	85 ±2
70520	−0.62	5708	4.01	−48.2	96	−78	−65	6.79	0.45	0.75	$9.9^{+2.9}_{-2.2}$	97 ±0
70681	−1.10	5396	4.70	−46.7	−12	−41	−69	7.21	0.18	0.71	...	94 ± 7
71819	−0.14	5825	4.35	−18.1	−65	−101	38	6.01	0.50	0.33	...	94 ± 0
72407	−0.54	5567	4.56	1.5	−88	−60	48	7.10	0.38	0.47	...	81 ± 6
72803	−0.73	5159	3.57	−98.9	−98	−85	−45	6.65	0.47	0.40	$9.6^{+5.0}_{-3.3}$	94 ±1
74033	−0.85	5574	3.95	−59.9	−104	−120	33	5.99	0.62	0.28	$13.8^{+2.2}_{-1.9}$	94 ±2
74067	−0.75	5572	4.63	−61.1	−20	−60	−61	6.72	0.27	0.62	...	91 ± 3
81748	−0.01	5559	4.29	−76.0	−4	−65	−56	6.56	0.29	0.55	...	86 ± 4
84781	−0.29	5259	3.86	−93.9	−91	−60	49	7.17	0.35	0.54	$12.1^{+2.8}_{-2.3}$	85 ± 7
84803	−0.52	5524	3.87	−90.5	−47	−79	−51	6.36	0.39	0.49	$8.4^{+3.9}_{-2.6}$	91 ± 13
84862	−0.41	5605	4.49	−79.3	35	−76	−57	6.40	0.35	0.55	...	93 ± 1
85373	−0.82	5351	4.66	−74.1	−57	−103	75	5.99	0.49	0.87	...	95 ± 2
85378	−0.51	5709	4.22	−72.7	−55	−100	73	6.00	0.48	0.82	...	96 ± 0
85757	−0.70	5414	3.81	3.5	24	−75	71	6.40	0.34	0.78	$9.9^{+4.2}_{-2.9}$	98 ± 0
86013	−0.70	5630	4.58	−138.0	−156	−57	87	8.36	0.51	1.35	...	88 ± 6
86830	−0.59	5305	3.74	−82.6	165	−100	52	7.33	0.63	0.60	$11.5^{+3.8}_{-2.9}$	88 ± 5
87089	−0.30	5142	4.63	−96.3	−47	−120	47	5.58	0.56	0.44	...	96 ± 1
87533	−0.21	5727	3.97	−115.9	−68	−106	−33	5.93	0.52	0.28	$5.8^{+2.0}_{-1.5}$	93 ± 8
88039	−0.81	5680	4.01	−18.5	4	−108	83	5.73	0.49	0.99	$12.2^{+3.1}_{-2.5}$	94 ± 1
88166	−0.76	5305	4.67	−12.7	51	−97	75	6.06	0.46	0.85	...	96 ± 0
90393	−0.72	5541	3.97	−85.0	−56	−110	91	5.86	0.52	1.18	$13.5^{+2.3}_{-1.9}$	90 ± 3
94129	−0.27	5630	4.35	−45.3	5	−122	41	5.43	0.56	0.36	...	96 ± 0
96902	−0.29	5697	4.05	−104.7	−3	−109	−54	5.67	0.50	0.52	$6.9^{+2.4}_{-1.8}$	96 ± 2
97846	−0.18	5259	3.81	−73.1	−82	−49	55	7.33	0.33	0.58	$11.3^{+3.2}_{-2.5}$	85 ± 4
98020	−1.61	5170	4.73	−192.2	−142	−108	69	6.77	0.62	0.87	...	84 ± 0
98532	−1.13	5518	3.71	−14.0	84	−123	50	5.78	0.61	0.49	$11.1^{+4.2}_{-3.1}$	94 ± 3
99224	−0.12	5580	4.20	0.4	19	−87	−68	6.11	0.40	0.72	$9.9^{+3.0}_{-2.3}$	97 ± 1
104659	−1.07	5730	4.34	−45.3	102	−111	−51	6.16	0.57	0.51	$13.2^{+4.0}_{-3.1}$	94 ± 1
106947	−0.35	5305	4.63	−107.0	−55	−68	76	6.71	0.34	0.89	...	98 ± 0
107294	−1.14	5929	4.63	−95.0	139	−101	62	6.85	0.59	0.72	...	90 ± 6
108056	0.14	5928	4.39	−98.3	5	−67	118	6.72	0.28	1.73	...	92 ± 6
109384	−0.38	5126	4.64	−64.8	−5	−55	−59	6.84	0.24	0.59	...	85 ± 7
110291	−0.93	5729	4.55	−104.4	75	−87	37	6.31	0.46	0.33	...	84 ± 1
111517	−0.45	5471	3.88	−11.6	−88	−95	−107	6.45	0.49	1.59	$9.0^{+3.7}_{-2.6}$	84 ± 11
112666	−0.42	5208	4.62	−97.4	−31	−103	−70	5.80	0.48	0.77	...	96 ± 1
112811	−0.70	5347	4.64	−4.0	38	−84	−55	6.21	0.40	0.53	...	95 ± 11
113514	−0.63	5720	4.57	−119.8	−46	−128	33	5.51	0.58	0.24	...	95 ± 0
116421	−0.51	5617	4.15	−112.0	−55	−108	69	5.85	0.51	0.76	$11.7^{+2.6}_{-2.1}$	95 ± 0
117029	−0.77	5436	3.86	−71.7	−61	−99	89	6.12	0.47	1.15	$12.4^{+2.2}_{-1.9}$	93 ± 0
						Thin disc						
2909	−0.28	5634	4.15	24.9	38	−60	−21	6.75	0.29	0.18	$8.9^{+2.7}_{-2.1}$	88± 3
14086	−0.65	5075	3.72	42.6	18	−78	−13	6.27	0.36	0.10	$8.3^{+4.3}_{-2.8}$	78± 2
14241	−0.49	5457	4.61	−19.7	14	−63	33	6.60	0.29	0.28	...	75 ± 2
19696	−0.24	5554	4.45	−5.5	−2	−49	40	6.95	0.22	0.34	...	77 ± 3
26437	0.10	5911	4.40	−63.8	23	−55	−38	6.83	0.26	0.32	...	74 ± 3
39616	−0.41	5936	4.43	3.7	−53	−36	−35	7.48	0.23	0.30	...	87 ± 2
40118	−0.47	5484	4.58	28.4	−36	−55	−32	6.86	0.27	0.27	...	81 ± 2
64924	−0.03	5515	4.53	−8.4	−13	−41	−24	7.13	0.19	0.19	...	95 ± 0
73078	−0.11	5189	3.76	10.6	−26	11	21	8.87	0.09	0.18	$11.7^{+3.4}_{-2.6}$	98 ± 0
74933	−0.39	5712	4.24	9.3	9	−44	39	7.06	0.20	0.33	...	82 ± 0
81681	−0.38	5565	4.52	−41.0	1	−53	−38	6.85	0.24	0.32	...	77 ± 3
84506	0.09	5610	4.05	−62.6	−10	−45	−38	7.04	0.21	0.33	$5.70^{+2.0}_{-1.5}$	82 ± 5
86568	−0.40	5214	4.64	−51.3	−5	−71	28	6.40	0.32	0.23	...	74 ± 2

Table 2 – *continued*

Star HIP	[Fe/H]	$T_{\rm eff}$ (K)	log g (cm s^{-2})	R_V	$U_{\rm LSR}$ (km s^{-1})	$V_{\rm LSR}$	$W_{\rm LSR}$	$R_{\rm m}$ (kpc)	e	$Z_{\rm max}$ (kpc)	log τ_9 (yr)	per cent P
					Halo							
3026	−1.04	6060	4.47	−50.2	146	−231	−33	166.	0.99	57.2	...	97 ± 2
10449	−0.87	5566	4.64	27.9	−196	−196	65	6.46	0.94	0.77	...	75 ± 0
12294	−0.95	6069	4.58	54.6	−188	−149	69	6.97	0.80	0.81	...	99 ± 3
16072	−1.39	5608	4.72	−13.3	−31	−279	−49	4.88	0.76	0.46	...	99 ± 13
28671	−1.01	5357	4.69	−190.7	245	−234	99	361.	0.99	9.07	...	99 ± 0
52771	−1.98	5354	4.77	81.5	163	−339	102	7.44	0.63	1.74	...	99 ± 0
55592	−0.94	5886	4.60	97.2	−95	−239	13	24.9	0.99	5.54	...	96 ± 2
57450	−1.50	5315	4.74	64.0	−221	−270	60	7.48	0.89	0.77	...	99 ± 0
58229	−0.83	5740	4.61	167.9	−66	−201	57	27.5	0.99	3.01	...	73 ± 3
62882	−0.98	5619	3.83	152.6	280	−201	−103	61.9	0.99	2.28	$12.2^{+3.6}_{-2.8}$	99 ± 0
73385	−1.46	5435	3.86	175.6	51	−361	61	6.41	0.38	0.64	...	99 ± 0
78640	−1.34	5665	3.92	−152.3	119	−261	−16	5.25	0.86	0.12	$14.9^{+1.7}_{-1.6}$	99 ± 0
80837	−0.80	5724	4.10	−47.3	96	−258	−70	4.88	0.86	0.64	$13.3^{+2.4}_{-2.0}$	99 ± 0
86321	−0.87	5760	4.59	−241.8	−75	−260	−45	4.84	0.86	0.41	...	99 ± 0
86431	−0.54	5648	4.48	33.9	215	−112	91	8.55	0.74	1.63	...	78 ± 5
94449	−1.12	5545	3.68	−65.4	156	−310	60	6.61	0.73	0.69	$10.1^{+5.3}_{-3.5}$	99 ± 0
100568	−0.99	5566	4.67	−170.7	−145	−240	−65	8.76	0.96	1.48	...	99 ± 0
109067	−0.79	5362	4.69	−198.4	−24	−213	36	182.	0.99	9.61	...	73 ± 1
111549	−0.95	5704	4.13	−296.0	190	−261	41	6.39	0.90	0.33	$14.2^{+2.5}_{-2.1}$	99 ± 0
115704	−1.78	5691	4.65	−110.3	−167	−189	−49	5.96	0.90	0.53	...	88 ± 0
					Thin/thick disc							
5163	−0.74	5547	4.63	26.1	−21	−59	−38	6.74	0.27	0.35	...	31 ± 12
8720	−0.74	5079	4.70	−3.7	90	−59	−42	7.14	0.38	0.40	...	69 ± 44
10711	−0.69	5585	4.57	49.6	−82	−56	−43	7.19	0.35	0.42	...	64 ± 20
12381	−0.16	6151	4.24	45.9	26	−62	−46	6.65	0.29	0.45	...	58 ± 14
15126	−0.82	5305	4.68	88.1	145	−52	35	8.15	0.48	0.36	...	80± 12
15394	−0.27	5211	3.73	4.9	29	−52	−46	6.92	0.25	0.43	$10.6^{+4.2}_{-3.1}$	58 ± 15
16738	0.37	6000	3.99	60.0	−91	−62	37	7.07	0.39	0.34	...	62 ± 20
21227	−0.45	5701	4.48	65.7	−93	−71	17	6.90	0.42	0.14	...	41 ± 14
21306	−0.65	5532	4.63	−83.0	−120	−92	−23	6.72	0.53	0.21	...	86 ± 30
21703	0.15	5386	4.53	−19.7	23	−62	40	6.66	0.29	0.35	...	39 ± 1
21921	−0.41	5285	4.61	−33.0	30	−43	55	6.86	0.30	0.46	...	68 ± 6
24037	−0.49	5473	4.60	64.4	−9	−51	−52	6.92	0.23	0.48	...	58 ± 8
30990	−0.87	5655	3.99	61.3	−77	−58	45	7.06	0.35	0.43	$13.2^{+2.6}_{-2.2}$	58 ± 3
33382	−0.05	5513	4.49	−10.1	59	−55	−34	6.94	0.31	0.29	...	72 ± 4
34511	−0.15	5710	4.51	42.6	−24	−50	−39	6.94	0.24	0.34	...	76 ± 6
35148	−0.30	5710	4.16	41.5	22	−56	49	6.80	0.26	0.45	$9.0^{+2.5}_{-1.9}$	57 ± 6
40023	−0.12	5250	3.45	−45.0	49	−46	−45	7.16	0.25	0.41	$4.6^{+2.5}_{-1.6}$	39 ± 5
42734	−0.70	5635	4.03	57.9	−28	−65	38	6.59	0.30	0.30	$11.6^{+3.0}_{-2.4}$	40 ± 2
47588	−0.47	5610	4.06	41.1	14	−76	−48	6.72	0.26	0.59	$10.7^{+2.9}_{-2.3}$	77 ± 21
52015	−0.02	5641	4.03	42.8	24	−57	38	6.77	0.27	0.33	$6.32^{+2.1}_{-1.6}$	71 ± 3
53535	0.11	5575	4.03	−85.5	56	−68	−33	6.61	0.36	0.32	$5.9^{+1.9}_{-1.4}$	39 ± 8
54196	−0.39	5800	4.04	−0.9	−81	−46	−40	7.38	0.32	0.36	$6.9^{+2.2}_{-1.7}$	42 ± 7
64103	−0.21	5482	4.59	−57.2	−71	−43	−46	7.40	0.29	0.43	...	48 ± 6
74442	−0.23	5649	4.22	−60.4	20	−41	−48	7.17	0.20	0.45	...	38 ± 5
74443	−0.59	5116	4.68	−60.5	−29	−64	−40	6.62	0.30	0.36	...	43 ± 8
80162	−0.66	5058	4.67	−9.0	8	−83	37	6.16	0.38	0.32	...	61 ± 3
82265	0.09	5446	4.52	−75.3	−54	−58	−37	6.89	0.31	0.32	...	34 ± 5
85653	−0.43	5300	4.61	−83.8	−16	−50	−53	6.94	0.23	0.50	...	61 ± 3
89583	−0.20	5492	4.55	−57.1	−29	−51	−40	6.95	0.25	0.35	...	74 ± 7
90745	−0.50	5663	4.10	−77.3	−59	−62	39	6.83	0.33	0.35	$10.5^{+2.8}_{-2.2}$	47 ± 9
94615	0.20	5634	4.48	−81.4	−49	−54	38	6.93	0.29	0.32	...	30 ± 13
99938	−0.54	5732	4.48	−111.2	−105	−70	−36	7.04	0.44	0.33	...	74 ± 11
102081	0.09	5664	4.34	−57.7	−39	−46	−43	7.10	0.24	0.39	...	32 ± 7
115721	−0.46	5563	4.08	−55.2	4	−63	−55	6.63	0.28	0.53	$11.8^{+3.0}_{-2.4}$	81 ± 19

Table 2 – *continued*

Star HIP	[Fe/H]	$T_{\rm eff}$ (K)	log g (cm s^{-2})	R_V	$U_{\rm LSR}$ (km s^{-1})	$V_{\rm LSR}$	$W_{\rm LSR}$	$R_{\rm m}$ (kpc)	e	$Z_{\rm max}$ (kpc)	log τ_9 (yr)	per cent P
					Thick disc/halo							
7452	−1.53	5735	4.59	−151.2	34	−193	−46	4.45	0.90	0.38	...	97 ± 36
14594	−1.88	5522	4.55	−140.8	167	−118	−59	7.00	0.69	0.72	...	73 ± 9
20298	−0.84	5547	4.65	36.6	−94	−133	81	5.64	0.66	1.02	...	79 ± 13
23922	−0.66	5663	4.58	−107.8	42	−132	−116	5.46	0.62	1.74	...	38 ± 37
26617	−0.75	5429	4.67	127.2	−50	−224	33	93.8	0.99	140.	...	99 ± 34
42864	−1.47	5356	4.76	−13.7	16	−212	−39	583.	1.00	756.	...	98 ± 64
43595	−0.84	5506	4.67	49.9	−71	−148	−94	5.30	0.71	1.23	...	63 ± 62
48209	−0.65	5415	4.64	−35.2	−121	−125	−86	6.20	0.65	1.15	...	73 ± 21
51477	−1.25	5326	4.07	102.9	75	−173	−78	4.92	0.82	0.81	...	87 ± 24
60331	−0.64	5346	4.50	−152.0	−16	−105	−135	6.57	0.34	1.31	...	64 ± 3
62507	−0.24	5730	4.09	−42.0	−71	−79	−36	6.51	0.41	0.33	$6.8^{+2.3}_{-1.7}$	73 ± 11
71019	−0.39	5204	3.85	70.4	125	−109	−117	6.68	0.59	1.99	$13.0^{+2.8}_{-2.3}$	64 ± 39
85650	−0.39	5521	4.17	−31.8	147	−133	76	6.42	0.71	1.00	...	62 ± 20
107236	−0.5	5300	4.61	−41.2	−71	−80	34	6.48	0.42	0.30	...	72 ± 5

[Fe/H] – [Fe/H] for the present sample is given below. Also, shown is the Toomre diagram with $(U^2_{\rm LSR} + W^2_{\rm LSR})^{1/2}$ plotted against $V_{\rm LSR}$. The biases from the selection criteria for the present sample – $V_{\rm LSR} \leqslant -40\,{\rm km\,s^{-1}}$ and $|W_{\rm LSR}| \geqslant 30\,{\rm km\,s^{-1}}$ – are quite evident in the three panels involving [Fe/H]. In addition, the sample from Paper I was biased towards less than solar metallicities and, therefore, the thin disc is underrepresented at [Fe/H] ~ 0. The stars with approximately equal probability of membership of the thin or thick discs fall, as expected, at the thin–thick disc boundaries in the four panels.

Classification by probability with the parameters in Table 2 applied to our sample selected by our $V_{\rm LSR}$ and $W_{\rm LSR}$ criteria results in a collection of thin-disc stars that may be deemed unusual by purists. The computed orbits of the thin-disc stars are quite eccentric; compare the thin-disc entries in Table 2 with those in table 1 from Paper I – also see Fig. 1 or the different locations of these thin-disc stars and those from Paper I. The probability $P_{\rm thin} > 70$ per cent is largely set by the low $|W_{\rm LSR}|$ which in turn implies the star remains close to the Galactic plane. In several of the panels of Figs 1 and 3, these thin-disc stars fall at a boundary between the thin-disc stars of Paper I and the present thick-disc stars. Thus, one might regard them on kinematic grounds as either extreme representatives of the thin disc or the thick disc. Their compositions may resolve this ambiguity (see below).

An informative illustration of the dependence of $P_{\rm thick}$ on the velocity components $U_{\rm LSR}$, $V_{\rm LSR}$ and $W_{\rm LSR}$ is provided in Fig. 2. This gives equal probability contours for $P_{\rm thick}$ equal to 50, 70, 80 and $\geqslant$90 per cent for the range of $|U_{\rm LSR}| = 0$ to 200 km s^{-1}, $V_{\rm LSR} = +100$ to $-200\,{\rm km\,s^{-1}}$, and $|W_{\rm LSR}| = 0$ to $150\,{\rm km\,s^{-1}}$. In the figure, probabilities increase from outside ($P_{\rm thick} = 0.50$) to inside [$P_{\rm thick} = 0.97$ for panels (a)–(c) and to $P_{\rm thick} = 0.90$ for the panel (d)]. In these panels, if a star's $V_{\rm LSR}$ and $W_{\rm LSR}$ are such that these fall outside of the thick-disc $P_{\rm thick} = 0.50$ contour, the star most likely belongs to the halo and it is most likely a thin-disc star if it falls in the empty bottom right-hand corners of the plots.

2.3 Orbital parameters

Orbital parameters such as the eccentricity, maximum distance above the Galactic plane, the apogalactic and the perigalactic distance for the sample were computed using the same Galactic potential model adopted for Paper I. The distance of 8.5 kpc for the Sun from the Galactic Centre is adopted. The mean Galactocentric distance ($R_{\rm m}$) for each star is taken as the mean of the apogalactic and perigalactic distances. Key Galactic orbital parameters for the thick-disc sample are shown in Fig. 3 against [Fe/H] for both the current sample and that from Paper I. Again, it must be recognized that our selection criteria affect the distribution of points in the panels of Fig. 3.

3 OBSERVATIONS

High-resolution spectra of the program stars were obtained during the period 2002 December–2004 June at the Harlan J. Smith 2.7-m telescope of the W. J. McDonald Observatory, using the 2dcoudé echelle spectrometer (Tull et al. 1995) with a 2048 × 2048 Tektronix CCD as detector.

Spectral coverage at a resolving power of about 60 000 was complete from 3500 to 5600 Å and substantial but incomplete from 5600 to about 9000 Å. The Echelle spectroscopic data were reduced to one-dimensional spectra with y-axis as normalized flux and x-axis as wavelength, using spectral reduction program IRAF[3] as outlined in Paper I. The final reduced spectra have signal-to-noise ratio (S/N) $\approx$ 100–200. Selection and measurement of suitable absorption lines followed the procedures described in Paper I.

4 ANALYSIS

The local thermodynamic equilibrium (LTE) abundance analysis was modelled as closely as possible on that described in Paper I. The model atmosphere grid and the methods of determining the fundamental atmospheric parameters were retained. A minor alteration in the determination of the effective temperature for about 40 stars is noted below. The line list and basic atomic data were taken over from Paper I. The abundance analysis was again performed with the 2002 version of the code MOOG (Sneden 1973). The reader interested in the details is referred to Paper I.

[3] IRAF is distributed by the National Optical Astronomical Observatories, which are operated by the Association of Universities for Research in Astronomy, Inc., under contract to the National Science Foundation.

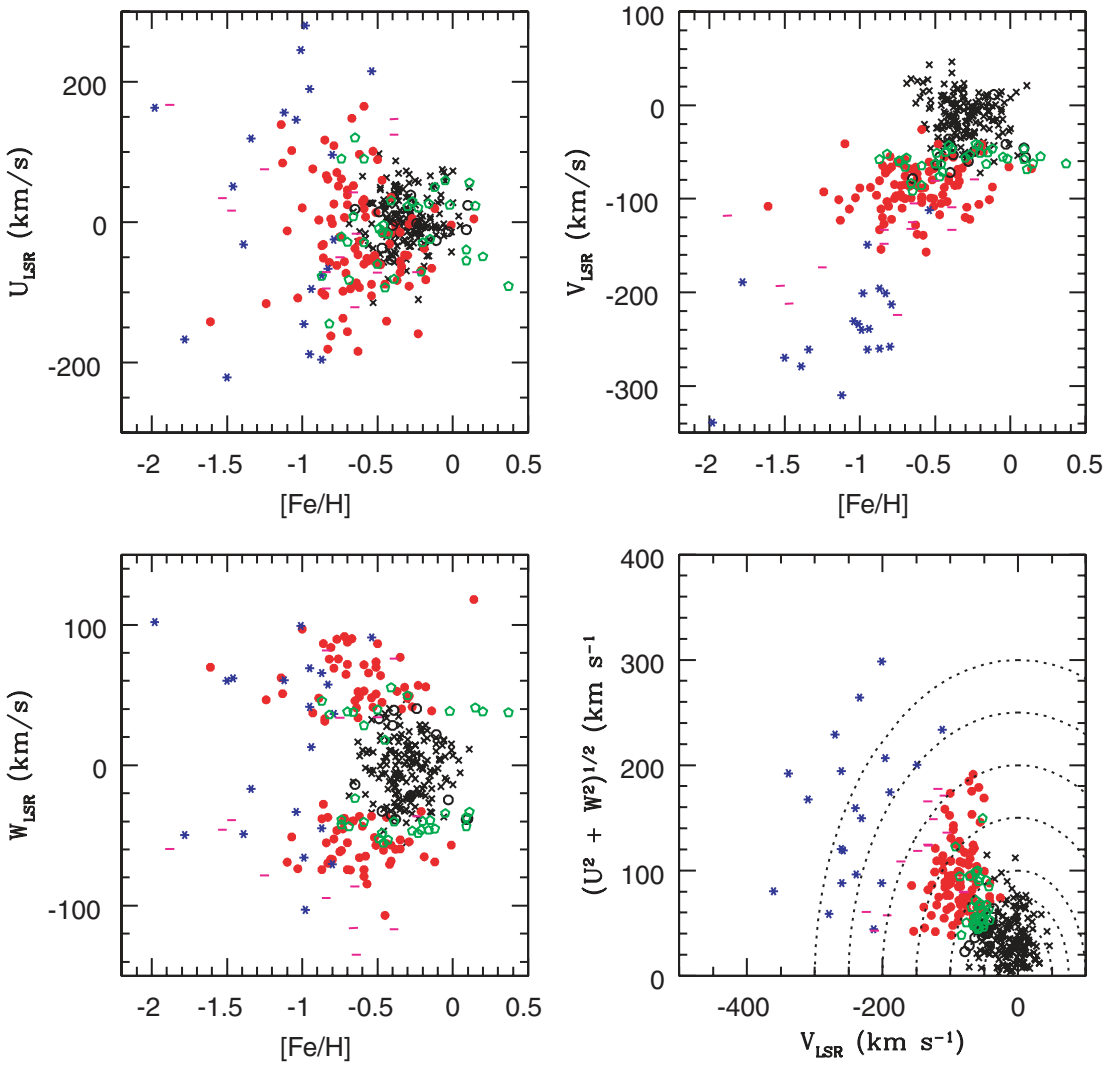

Figure 1. Plots of $U_{\rm LSR}$, $V_{\rm LSR}$ and $W_{\rm LSR}$ against [Fe/H] for our present sample of stars and that from Paper I. Also plotted is the Toomre diagram: $(U^2_{\rm LSR} + W^2_{\rm LSR})^{1/2}$ against $V_{\rm LSR}$. The current sample is separated into five different groups based on the probability P: thick-disc (red filled circles), thin-disc (black open circles), halo (blue star symbols), stars with equal probabilities between thin and thick (green pentagons) and between thick and halo (magenta bars), and the 173 thin-disc stars from Paper I (black crosses).

The distribution of stars in our sample with $T_{\rm eff}$, log g, and [Fe/H] is shown in Fig. 4 where is also given the distribution of log g with [Fe/H]. This figure may be compared with its counterpart in Paper I. The comparison shows the anticipated difference in the [Fe/H] range of the two samples. A point of note is that the samples differ in the spans of $T_{\rm eff}$; the thin-disc stars are in the mean systematically warmer than the present sample with the peak in the thick-disc distribution being about 300 K cooler than that in Paper I.

4.1 The effective temperature

In Paper I, effective temperatures ($T_{\rm eff}$) were estimated from a star's Strömgren $(b-y)$ colour using the calibration provided by Alonso, Arribas & Martinez-Roger (1996) who obtained $T_{\rm eff}$ from the infrared flux method (IRFM). The *uvbyβ* data were adopted from the Hauck & Mermilliod's (1997) catalogue. This approach was used for the 135 of the 176 stars in the present sample for which the Strömgren photometry has been reported.

An alternative approach was developed for the other 41 stars. We chose to use the $(V-K)$ colour and the corresponding calibration, again from Alonso et al. The V magnitude was taken from the *Hipparcos* catalogue. The K magnitude is not available for all of these stars, but the 2MASS catalogue[4] (Cutri et al. 2003) provides the magnitudes $K_{\rm s}$ for all 41 stars. To estimate a possible systematic offset between the ($K_{\rm s}$) magnitudes of the 2MASS and the Alonso et al. scale (K), we took a sample of 100 stars from the 2MASS catalogue with observations from Alonso et al. (1996). The mean difference is very small: $(K_{\rm s} - K) = -0.004$ with a σ of 0.09 and no trend (Fig. 5). Therefore, we adopted the 2MASS $K_{\rm s}$ and equated it with K.

The $(b-y)$ and $(V-K) \equiv (V-K_{\rm s})$ colours give very similar $T_{\rm eff}$ values – see Fig. 6. The mean difference $T_{\rm eff}(b-y) - T_{\rm eff}(V-K) = -15$ K with a $\sigma = 69$ K with a few outliers. For the

[4] This publication makes use of data products from the 2MASS, which is a joint project of the University of Massachusetts and the Infrared Processing and Analysis Centre/California Institute of Technology, funded by the National Aeronautics and Space Administration (NASA) and the National Science Foundation

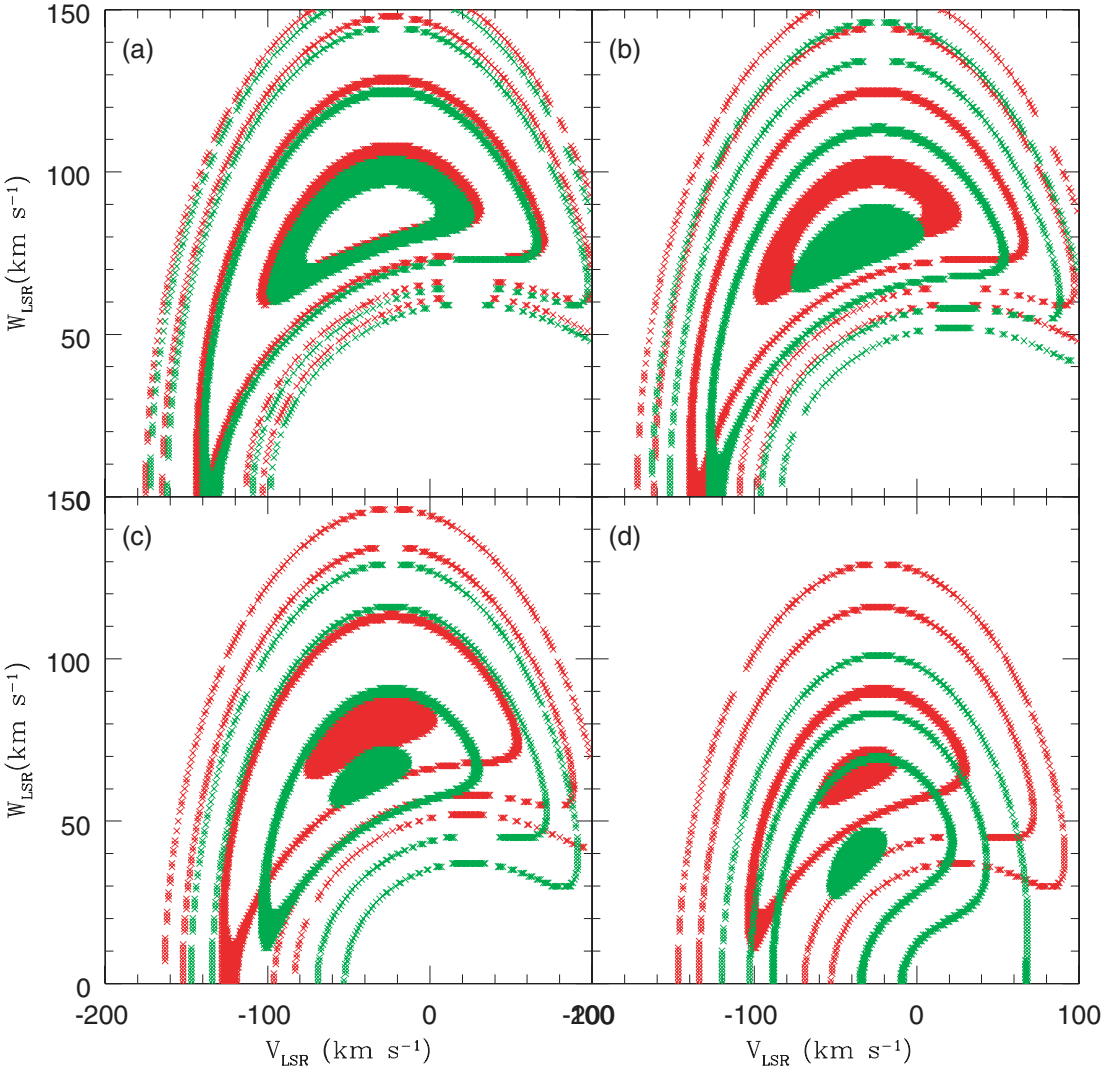

Figure 2. Probability diagram for the thick-disc component. Panels (a), (b), (c) and (d) are for the following intervals: $|U_{LSR}| = 0$–50, 50–100, 100–150 and 150–200 km s^{-1}, respectively. Contours represent equal probability P_{thick}. Probability increases from the outside to the inside contour starting at $P_{thick} = 50$ per cent and increasing to 70 per cent, 90 per cent and then $\geqslant$90 per cent. In each panel, the red contours correspond to the lower U_{LSR} and the green contours to the higher U_{LSR} for that panel.

outliers, we obtained T_{eff} spectroscopically by demanding excitation equilibrium for a set of Fe I lines.

Observed colours were not corrected for interstellar extinction for stars closer than 100 pc. For the 37 stars with distances greater than 100 pc (but less than 150 pc), a correction was estimated from Neckel, Klare & Sarcander (1980) maps. The maximum extinction is about 0.1 mag in V and, thus, 0.01 mag in K. Correction for this level of extinction, a maximum for our sample, increases the T_{eff} by about 140 K.

4.2 Metallicity, surface gravities, and microturbulence

Metallicity usually refers to the iron abundance (relative to the solar abundance) which, here, was obtained for each star from numerous well-defined Fe I lines and a few Fe II lines. Since the stellar T_{eff} except for a few exceptional cases (see above) and the surface gravity in all cases were obtained without recourse to the Fe I and Fe II lines, it is of interest to see if the Fe I and Fe II lines return the same value for the iron abundance. Non-LTE effects may affect these iron abundance estimates; overionization of neutral iron (relative to LTE) is believed to be the principal non-LTE effect so that, in an LTE analysis, the abundance from Fe I lines is less than that from Fe II lines. Fig. 7 (top panel) shows the abundance difference from Fe I and Fe II as a function of the abundance from the neutral lines. On average, the Fe I lines give a lower abundance by 0.04 ± 0.08 dex with no significant trend with [Fe/H]. (The corresponding difference for the thin-disc stars in Paper I was 0.02 ± 0.05 dex for stars with [Fe/H] from about 0.0 to -0.6.) Following Paper I, we adopt the iron abundance given by the Fe I lines because the neutral lines are many and the ionized lines few.

Photometric recipes exist for determining the metallicity, here identified with [M/H]. Here, we adopt the metallicity calibration of the Strömgren photometry provided by Hauck & Mermilliod (1997). Fig. 7 (lower panel) shows the difference between the photometric [M/H] and the spectroscopic [Fe/H] from the Fe I lines as a function of the spectroscopic [Fe/H]. The differences are generally small and the mean difference [M/H] $-$ [Fe/H] $= -0.01 \pm 0.10$. (In Paper I, the mean difference was 0.05 ± 0.09 with no detectable trend over the interval [Fe/H] from -0.2 to -0.8.) We note that discrepant iron abundances are inferred from Fe I and Fe II lines for slightly lower

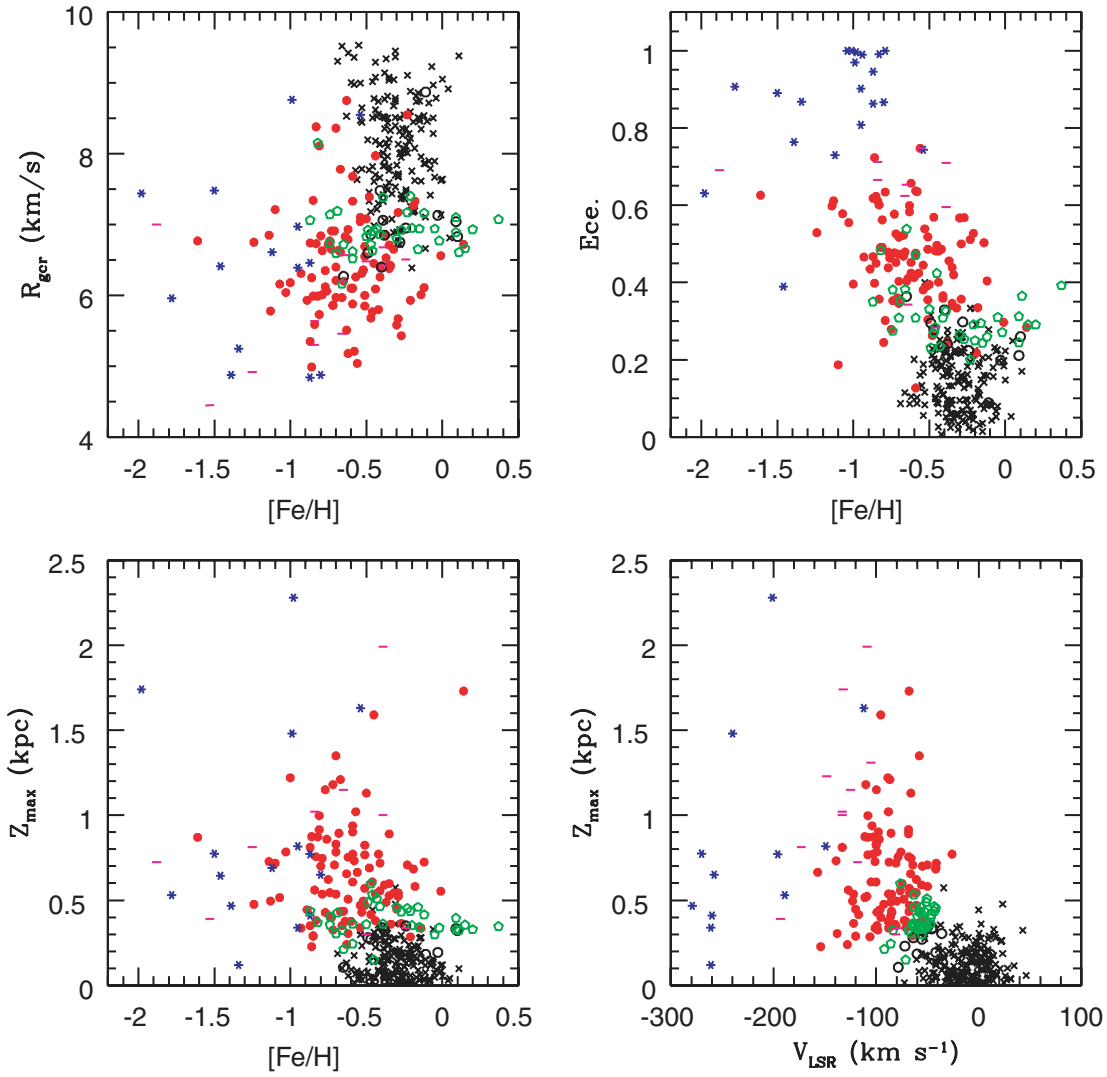

Figure 3. Plots of the orbital parameters: $R_{\rm gcr}$, eccentricity and $Z_{\rm max}$ against [Fe/H] for the current sample and that from Paper I. Also plotted is $Z_{\rm max}$ against $V_{\rm LSR}$. See the caption to Fig. 1 for the key to the symbols.

values of $T_{\rm eff}$ and, especially, more metal rich stars than in our sample (Feltzing & Gustafsson 1998; Schuler et al. 2003; Allende Prieto et al. 2004; Yong et al. 2004).

Surface gravities were obtained, as in Paper I, by a combination of stellar isochrones (Bertelli et al. 1994), $T_{\rm eff}$, [Fe/H], and the *Hipparcos* astrometry. The resulting $\log g$ values are compared for the common stars between this study and few others (see Table 3). For the microturbulent velocities ($\xi_{\rm t}$), we used the relation between $\xi_{\rm t}$, $T_{\rm eff}$ and $\log g$, derived in Paper I. The relation used from Paper I is derived using mainly thin-disc stars which cover slightly different ranges in the parameters than the thick-disc sample stars. To check the validity of the relation, we derived $\xi_{\rm t}$ values for 15 thick-disc stars using Fe I lines. The adopted values from the relation are larger by only 0.14 ± 0.17 km s^{-1} than the spectroscopically derived values. The effect of such difference on the abundances is negligible.

4.3 Model atmospheres

Stellar abundances are obtained assuming LTE line formation. Abundances are given with respect to the Sun which was analysed as described in Paper I. We used the Kurucz's (1998) LTE, plane-parallel, line-blanketed models with convective overshoot and the revised (2002) stellar abundance code MOOG (Sneden 1973). The oscillator strengths for the basic set of about 160 lines are a mixture of laboratory measured values and the astrophysically derived by inverting solar and the stellar spectra (see Paper I).

The rationale for adopting the Kurucz models with convective overshoot is described in Paper I; the thin-disc sample in Paper I is similar to the Sun for which the convective overshoot model gives a good representation. However, the current thick-disc stars are cooler, metal-poor and higher-gravity stars than the thin-disc sample; they are not close analogues of the Sun. The models with convective overshoot are not widely used in abundance analysis. For this reason, we computed the [X/Fe] of 12 representative elements, using both the models – with and without convective overshoot. 12 stars are chosen so that they cover $T_{\rm eff}$ (5000–6100 K) and [Fe/H] (0.2 to -1.6) range of the thick-disc sample. Differences (δ[X/Fe]) in [X/Fe] from the two kinds of models were δ[X/Fe] $\leqslant 0.01$ for all the elements except carbon for which 0.04 was representative. The computed abundance ratios [X/Fe] for 21 elements are given in Tables 4 and 5.

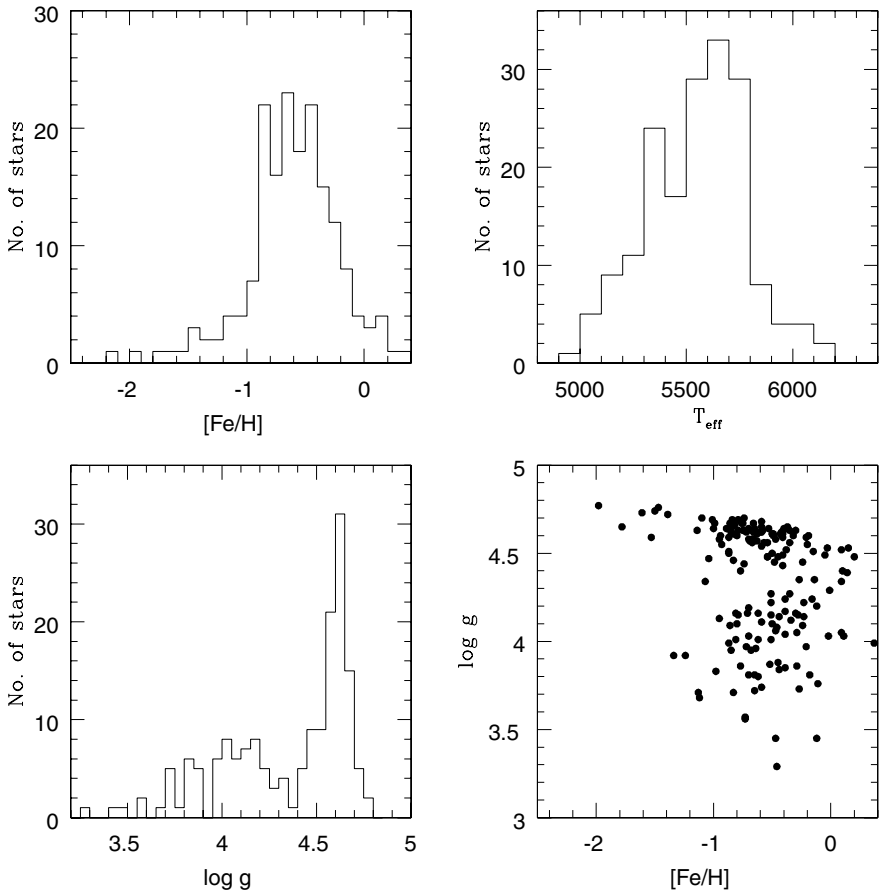

Figure 4. Distribution of the sample stars in [Fe/H], $T_{\rm eff}$ and log g. Also shown is the gravity versus metallicity.

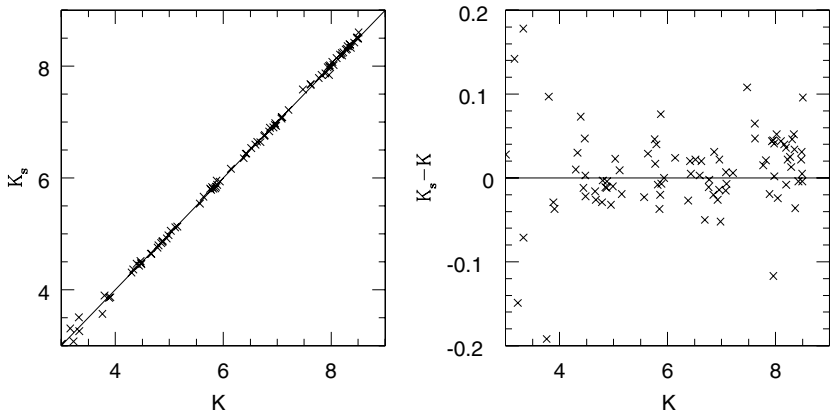

Figure 5. The broad-band K magnitudes for a sample of around 90 stars taken from Alonso et al. (1996) are compared with the $K_{\rm s}$ magnitudes taken from the 2MASS (left-hand panel) where the solid line corresponds to $K = K_{\rm s}$. The difference $K_{\rm s} - K$ against K is shown in the right-hand panel.

4.4 Abundance errors

The principal goal of this study is to define the differences in composition between thin- and thick-disc stars. It is known that the differences, even in the most striking cases, are small ($\leqslant$0.2 dex) and, therefore, attention must be paid to the errors thought to affect the abundance determinations. In addition, our sample of thick-disc stars is of a sufficient size that we may attempt to estimate the dispersion in the abundances at a given metallicity and wonder if the dispersion is due to measurement errors or may contain cosmic scatter.

The recipe used to assess the errors follows that used in Paper I. Two qualitative differences may be noted. First, the spectra for the thick-disc sample are of lower quality than those used for Paper I: signal-to-noise ratio (S/N) $\simeq$ 100–200 versus S/N $\simeq$ 200–400. Also, two spectra were generally obtained for each thin-disc star but a single one for a thick-disc star; the thick-disc stars are relatively fainter than the selected thin-disc stars. Secondly, the thick-disc stars are

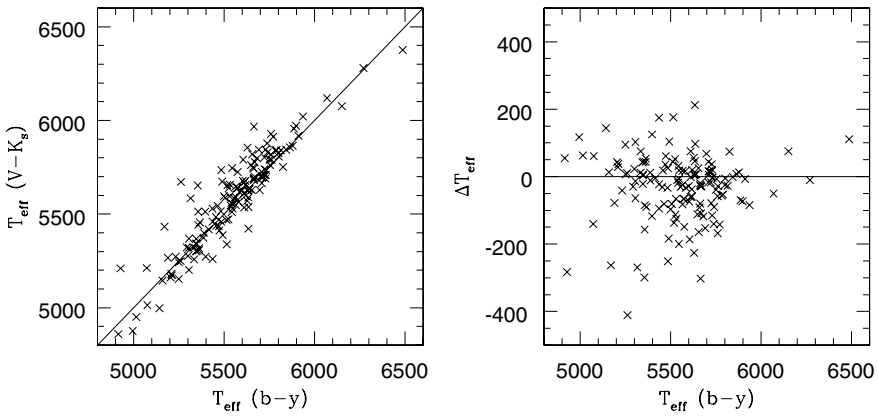

Figure 6. $T_{\rm eff}$ derived from the Strömgren colour $(b-y)$ and the broad-band colour $(V-K_{\rm s})$ (see text) in the left-hand panel where the solid line corresponds to $T_{\rm eff}(V-K_{\rm s}) = T_{\rm eff}(b-y)$. The right-hand panel shows the difference $T_{\rm eff}(b-y) - T_{\rm eff}(V-K_{\rm s})$ against $T_{\rm eff}(b-y)$.

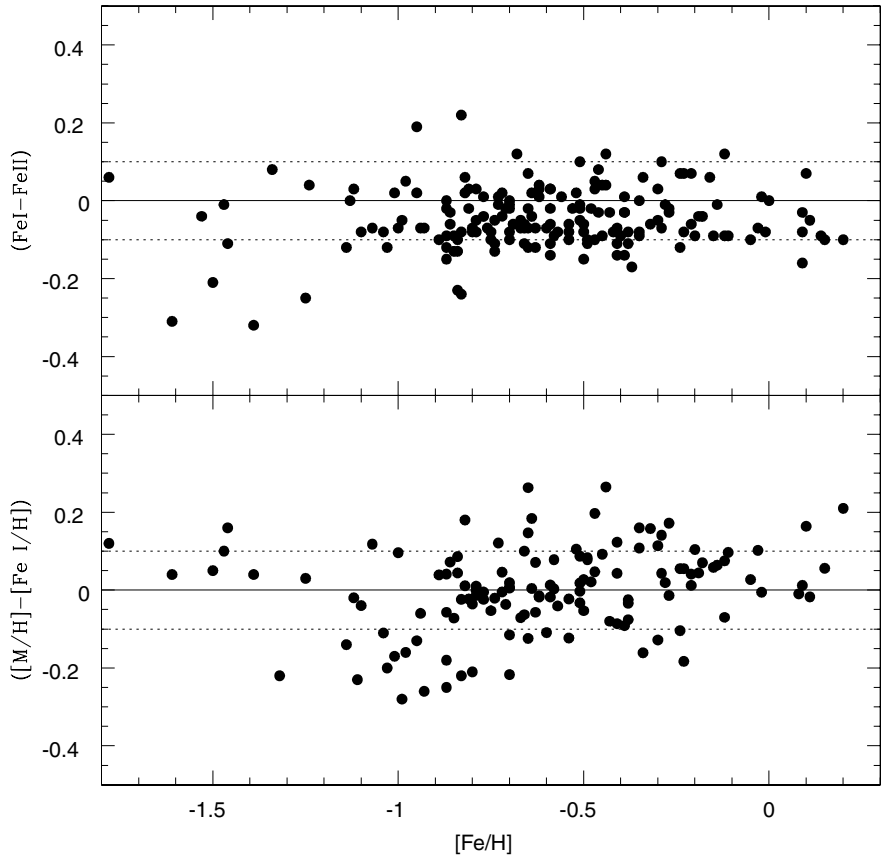

Figure 7. The difference between the spectroscopic abundances from Fe I and Fe II lines against the abundance from Fe I lines (top panel). The difference between the Strömgren photometric metallicity [M/H] and the iron abundance from the Fe I lines (bottom panel). Solid line refers to no difference in abundances. Two broken lines represent 0.1 dex above and below the solid line.

systematically cooler (and more metal poor) than the thin-disc stars; these differences lead to different sensitivities of the abundances on the atmospheric parameters.

For these reasons, we estimated the uncertainties in [X/Fe] due to the uncertainties in model parameters and measurement errors afresh for the present sample. We assumed that the errors are uncorrelated. The predicted uncertainty, $\sigma_{\rm mod}$ for a whole sample, in each abundance ratio due to the measurement errors can be written as a simple mean of the $\sigma_{\rm s}$ estimated for n representative stars:

$$\sigma_{\rm mod} = \frac{1}{n}\sum_i \sigma_i = \frac{1}{n}\sum_i \sqrt{\sum_j \left(\frac{\partial}{\partial p_j}[{\rm X/Fe}]\right)^2 (\delta p_j)^2}, \qquad (3)$$

and the parameters p_j considered here are the effective temperature, surface gravity, metallicity, microturbulence, and the equivalent width measurements. We examined five representative

Table 3. Mean differences and standard deviations of the abundance ratios [X/Fe] for stars that are common among Bensby et al. (2003, 2004) and Mishenina et al. (2004).

	Bensby–Ours		Mishenina–Ours	
Quantity	Mean difference	σ	Mean difference	σ
$T_{\rm eff}$	88	80	102	116
$\log g$	−0.05	0.08	−0.18	0.18
[Fe/H]	0.03	0.05	−0.03	0.09
[Na/Fe]	−0.02	0.05	0.03	0.08
[Mg/Fe]	0.00	0.06	0.05	0.05
[Al/Fe]	0.04	0.08	0.12	0.10
[Si/Fe]	0.00	0.06	0.16	0.09
[Ca/Fe]	0.04	0.06	0.07	0.04
[Ti/Fe]	0.08	0.04	0.10	0.08
[V/Fe]	...	...	0.05	0.09
[Cr/Fe]	0.04	0.05	0.08	0.03
[Ni/Fe]	0.01	0.04	0.05	0.02
[Zn/Fe]	0.02	0.05	...	...
[Y/Fe]	−0.08	0.04	0.01	0.05
[Ba/Fe]	0.12	0.08	0.12	0.10

thick-disc stars spanning the sample's range in $T_{\rm eff}$, [Fe/H] and $\log g$. Assuming that $\delta T_{\rm eff} = 100$ K, $\delta \log g = 0.2$, δ[M/H] = 0.2, $\delta\xi_{\rm t} = 0.25\,{\rm km\,s^{-1}}$, and $\delta W_\lambda = 2$ mÅ. The error in W_λ is estimated in the same way as in Paper I, and the resulting error in the abundance is divided by $\sqrt{N}$ where N is the number of lines used in deriving the abundance [X/H]. In Table 6, $\sigma_{\rm s}$ for each abundance ratio for five stars and the final mean value $\sigma_{\rm mod}$ and the standard deviation are given.

4.5 Ages

Stellar ages for the present sample have been computed by the method used in Paper I. Briefly, we used the stellar isochrones of Bertelli et al. (1994) and the method described in Paper I and Allende Prieto et al. (2004). The adopted isochrones do not consider compositions in which the α-elements have enhanced abundances (relative to iron). For the thin-disc stars, this is a fair approximation. However, in the present sample, there are stars belonging to the thick disc and in halo which show α/Fe ratios significantly different from zero. Neglecting the α-enhancements in the isochrones would overestimate the ages for the most-metal-poor thick-disc and halo stars by up to 2 Gyr. We thus adopted the relationship between metallicity (Z), iron abundance ([Fe/H]), and the α-enhancement proposed by Degl'Innocenti, Prada & Ricci (2005) in selecting the appropriate isochrones from the Padova grid. Reliable ages are determinable only for those stars which have evolved away from the ZAMS. Ages were estimated for 65 stars (see Table 2, column 11).

In Fig. 8, we compare our age determinations with those published in the recent survey by Nordström et al. (2004). Nordström et al. used the Padova isochrones (no α-enhancement) of Girardi et al. (2000). The 45 stars which are in common between the two surveys are overwhelmingly thin-disc stars and, therefore, in spite of the difference in the selection of the isochrones' metallicity, the two determinations agree fairly well with an average difference of 0.1 Gyr with $\sigma \approx 2$ Gyr.

5 THIN- AND THICK-DISC COMPOSITIONS

5.1 Some comparisons

Clear evidence that thick- and thin-disc stars of the same [Fe/H] showed different abundances (relative to Fe) of other elements was provided by the Furhrmann's (1998) demonstration that [Mg/Fe] was systematically greater in the thick-disc stars. Extension of this result to other elements was made by Prochaska et al. (2000), who determined the abundances of up to 20 elements in a sample of 10 stars with $V_{\rm LSR}$ from −20 to $-100\,{\rm km\,s^{-1}}$, and a $W_{\rm LSR}$ that takes a star to at least 600 pc above the Galactic plane, which virtually guarantees that the stars belong to the thick disc.

Prochaska et al.'s survey augmented by the occasional inclusion of thick-disc stars in quite extensive studies of local stars (Edvardsson et al. 1993; Chen et al. 2000; Fulbright 2000; Reddy et al. 2003) led to the finding that abundance differences between thick- and thin-disc stars appear to define two broad categories. In the first category (here, Mg-like elements) are the elements like Mg in which [X/Fe] for a thick-disc star exceeds that in a thin-disc star of the same [Fe/H]. The thick–thin difference is not the same for all elements in this category and may also be a function of [Fe/H]. The second category (here, Ni-like elements) are those elements for which [X/Fe] appears unchanged between the thin and thick disc. In reality, the thick–thin disc abundance differences may span a continuous range.

Before presenting and discussing our results in detail, we offer a few comparisons with several recent abundance analyses of thick-disc stars to highlight differences in the sizes of the samples and to examine the consistency between the different investigations with respect to the abundance ratios. The chosen analyses are those by Bensby and colleagues, Mishenina et al. (2004), and Fuhrmann (2004). For each case, we reassessed the assignments to the thick and thin discs, using our recipe for the membership probabilities.

Bensby and colleagues determined abundances for many elements in a sample of 102 F-G dwarfs of which 35 were attributed by them to the thick disc. According to our recipe, 18 of the 102 are thick-disc stars. Though the recipes for choosing thick-disc stars are basically the same, they differ in the normalization. Bensby et al. chose a relative probability ratio of thick disc and thin disc >1.0, and halo and thick-disc ratio <1.0 for a star to belong thick disc. Their criteria approximately translate into our criteria if $P_{\rm thick} >$ 50 per cent for a star to belong thick disc.

Mishenina et al. analysed 174 F-G-K dwarfs for their Mg, Si, Fe and Ni abundances. (Non-LTE effects were considered in the Mg analysis.) 30 stars were assigned to the thick disc. Adoption of our method of calculating the membership probability reduces the number of thick-disc stars to 13. The main difference between us and Mishenina et al. is in the adopted fraction for thin- and thick-disc stars. Mishenina et al. assumed 25 per cent thick-disc and 75 per cent thin-disc stars. This led to larger number of thick-disc stars in their study.

Fuhrmann (2004) following his earlier work (Fuhrmann 1998) obtained the Mg and Fe abundances for a sample of 71 nearby stars. Out of which 25 or more are deemed thick-disc stars.

In Fig. 9, we show [Mg/Fe] against [Fe/H] as provided by our sample and the three published analyses. The larger filled black symbols in the plot represent thick-disc stars based on our criteria. Stars for which the probability of thin- or thick-disc membership is below 70 per cent but greater that 50 per cent are included in the panels but with a smaller symbol. Figs 10 and 11 show the corresponding results for [Si/Fe], and [Ti/Fe], respectively. These figures show clearly the increase in the number of thick-disc stars provided by our sample. They also show broad agreement between the different studies over the behaviour of Mg-like elements with [Fe/H] in thin and thick discs: [X/Fe] of the thick disc exceeds that of the thin disc at a common [Fe/H] for [Fe/H] $\leqslant -0.3$ with an apparent merger of thin- and thick-disc behaviour for greater [Fe/H].

Table 4. Abundance ratios [X/Fe] for elements from C to V for the program stars. Note that the O abundances in column 4 are not corrected for the NLTE effect.

HIP	[Fe I/H]	C	O	Na	Mg	Al	Si	Ca	Sc	Ti	V
					Thick disc						
3086	−0.23	0.14	0.34	0.08	0.15	0.17	0.09	0.04	−0.07	0.04	0.0
3185	−0.65	0.28	0.51	0.19	0.40	0.34	0.25	0.21	0.19	0.27	0.04
3441	−0.50	0.35	0.56	0.06	0.32	0.24	0.18	0.10	0.24	0.19	0.06
4039	−1.24	....	0.71	0.22	0.30	−0.12	0.15	0.29	−0.13	0.24	...
4544	−0.87	0.26	0.49	0.09	0.39	0.24	0.21	0.11	0.12	0.22	0.24
5122	−0.62	0.44	0.56	0.11	0.26	0.30	0.20	0.12	0.11	0.18	0.12
5315	−0.47	0.37	0.51	0.20	0.46	0.32	0.23	0.27	0.22	0.29	0.17
5336	−0.86	0.49	0.72	0.13	0.24	0.30	0.28	0.22	0.18	0.26	0.15
5775	−0.59	0.48	0.79	0.17	0.32	0.26	0.28	0.22	0.29	0.23	0.25
6159	−0.67	0.42	0.59	0.10	0.33	0.23	0.18	0.12	0.17	0.20	0.13
6607	−0.41	0.26	0.48	0.08	0.18	0.19	0.19	0.09	0.22	0.18	0.03
7961	−0.64	0.44	0.68	0.16	0.35	0.35	0.26	0.22	0.08	0.24	0.04
8674	−0.60	0.56	0.58	0.06	...	0.21	0.20	0.08	0.13	0.13	0.07
9080	−0.37	0.69	0.57	−0.01	0.14	0.13	0.15	0.0	0.21	0.05	0.11
10652	−0.67	...	0.70	0.07	0.24	0.25	0.16	0.13	0.19	0.13	0.02
12579	−0.80	0.42	0.71	0.08	0.26	0.16	0.19	0.16	0.08	0.13	0.21
13366	−0.70	0.36	0.64	0.08	0.37	0.21	0.23	0.16	0.18	0.19	0.03
15126	−0.82	...	0.64	0.01	0.28	0.16	0.25	0.12	0.14	0.15	0.06
15405	−0.73	0.34	0.49	0.04	0.16	0.16	0.13	0.10	0.03	0.05	−0.01
17147	−0.87	0.32	0.72	0.10	0.44	0.22	0.24	0.21	0.16	0.21	0.19
17666	−1.03	....	0.87	0.06	0.35	0.33	0.42	0.21	0.11	0.25	0.07
22020	−0.35	0.27	0.51	0.10	0.24	0.25	0.19	0.11	0.12	0.17	0.06
22060	−0.63	0.52	0.63	0.19	0.28	0.25	0.21	0.11	0.20	0.19	−0.02
23080	−0.32	0.29	0.32	0.01	0.24	0.19	0.19	0.13	0.25	0.20	0.19
24030	−1.00	...	0.69	0.12	0.30	0.19	0.23	0.11	0.09	0.19	0.08
25860	−0.35	0.24	0.52	0.05	0.29	0.20	0.21	0.14	0.28	0.22	0.14
26452	−0.89	0.36	0.73	0.12	0.33	0.24	0.25	0.17	0.17	0.23	0.16
26828	−0.34	0.23	0.64	0.18	0.23	0.25	0.15	0.17	0.01	0.12	0.16
27128	−0.81	0.27	0.66	0.15	0.33	0.29	0.17	0.28	0.05	0.14	0.10
29269	−0.68	0.27	0.62	0.17	0.36	0.36	0.20	0.24	−0.02	0.23	0.11
31188	−0.59	0.15	0.30	−0.03	0.12	0.04	0.03	0.04	−0.01	0.05	0.01
34642	−0.44	0.18	0.44	0.04	0.10	0.21	0.11	0.04	−0.02	0.06	−0.01
35989	−0.19	0.04	0.21	−0.14	−0.03	−0.02	0.04	−0.03	0.03	0.04	0.14
36849	−0.77	0.37	0.58	0.06	0.27	0.18	0.15	0.08	0.10	0.13	0.08
37233	−0.51	0.16	0.42	0.06	0.36	0.31	0.20	0.22	0.14	0.24	0.17
38769	−0.79	0.49	0.68	0.11	0.34	0.40	0.20	0.20	0.08	0.20	0.06
39893	−0.84	0.68	0.78	0.22	0.29	0.33	0.35	0.24	0.23	0.15	0.16
40613	−0.62	0.36	0.71	0.15	0.39	0.28	0.21	0.15	0.16	0.19	0.03
43393	−0.59	...	0.57	0.07	0.20	0.26	0.25	0.11	0.14	0.25	0.19
44075	−0.86	0.39	0.64	0.09	0.27	0.24	0.19	0.17	0.12	0.15	0.03
44347	−0.85	0.44	0.68	0.08	0.43	0.25	0.30	0.25	0.22	0.26	0.11
44860	−0.51	0.36	0.58	0.17	0.37	0.32	0.24	0.19	0.11	0.24	0.08
45947	−0.46	0.35	0.57	0.11	0.25	0.32	0.24	0.22	0.15	0.33	0.19
50005	−0.53	...	0.63	0.08	0.30	0.38	0.29	0.20	0.23	0.20	0.20
50671	−0.48	0.34	0.39	0.13	0.13	0.07	0.09	0.06	0.0	−0.03	0.01
50965	−0.57	0.41	0.57	0.06	0.26	0.23	0.19	0.15	0.25	0.33	0.02
52673	−0.66	...	0.58	0.14	0.27	0.22	0.21	0.18	0.20	0.24	0.09
58843	−0.79	0.28	...	0.05	0.28	0.22	0.23	0.21	0.05	0.22	0.05
59233	−0.83	0.47	0.60	0.22	0.38	0.42	0.15	0.30	−0.17	0.22	0.28
59750	−0.74	0.28	0.74	0.15	0.32	0.25	0.25	0.17	0.08	0.17	0.02
60268	−0.72	0.39	0.65	0.08	0.28	0.29	0.21	0.19	0.17	0.21	0.09
60956	−0.58	0.47	0.56	0.07	0.22	0.23	0.21	0.15	0.19	0.22	0.2
62240	−0.83	...	0.87	0.16	0.33	0.34	0.30	0.03	0.03	0.11	0.01
64426	−0.71	0.31	0.57	0.06	0.33	0.16	0.14	0.20	0.05	0.14	−0.01
65449	−0.44	0.33	0.50	0.08	0.20	0.31	0.17	0.10	0.07	0.15	0.09
70520	−0.62	0.23	0.52	0.12	0.28	0.28	0.21	0.20	0.05	0.23	0.11
70681	−1.10	....	0.90	0.05	0.32	0.29	0.39	0.19	0.13	0.12	0.07
71819	−0.14	0.10	0.16	0.02	0.06	0.09	0.03	0.05	0.02	0.0	0.04
72407	−0.54	0.45	0.65	0.12	0.32	0.29	0.30	0.21	0.30	0.25	0.20
72803	−0.73	0.37	0.83	0.14	0.34	0.40	0.31	0.17	0.14	0.19	0.08
74033	−0.85	0.39	0.80	0.16	0.41	1.6	0.27	0.25	0.13	0.24	0.11

Table 4 – *continued*

HIP	[Fe I/H]	C	O	Na	Mg	Al	Si	Ca	Sc	Ti	V
74067	−0.75	0.42	0.63	0.05	0.31	0.27	0.20	0.13	0.19	0.15	0.05
81748	−0.01	0.14	0.23	−0.03	−0.03	0.09	0.08	−0.06	0.02	−0.08	−0.03
84781	−0.29	0.22	0.48	0.01	0.25	0.23	0.15	0.11	0.19	0.18	0.12
84803	−0.52	0.35	0.66	0.19	0.31	0.38	0.23	0.24	0.05	0.14	−0.02
84862	−0.41	0.40	0.61	0.07	0.35	0.28	0.22	0.16	0.23	0.18	0.06
85373	−0.82	...	0.42	0.01	0.18	0.26	0.34	0.05	0.30	0.15	0.19
85378	−0.51	0.27	0.57	0.12	0.34	0.35	0.21	0.23	0.12	0.23	−0.01
85757	−0.70	0.40	0.72	0.14	0.36	0.37	0.29	0.23	0.08	0.23	0.11
86013	−0.70	0.49	0.72	0.07	0.31	0.16	0.21	0.14	0.18	0.14	0.07
86830	−0.59	0.43	0.69	0.17	0.35	0.35	0.30	0.23	0.07	0.21	0.14
87089	−0.30	0.37	0.47	−0.12	...	0.06	0.14	0.10	0.16	0.26	0.24
87533	−0.21	0.12	0.22	0.08	0.15	0.16	0.04	0.08	−0.06	0.0	0.04
88039	−0.81	0.41	0.66	0.15	0.43	0.34	0.30	0.18	0.12	0.15	0.20
88166	−0.76	...	0.73	0.13	0.34	0.28	0.28	0.14	0.15	0.21	0.12
90393	−0.72	...	0.11	0.04	0.26	0.17	0.07	0.11	0.30	0.33	0.34
94129	−0.27	0.23	0.45	0.04	0.25	0.24	0.15	0.03	0.10	0.14	0.11
96185	−0.56	0.30	0.68	0.15	0.22	0.31	0.22	0.19	0.07	0.16	0.09
96902	−0.29	0.20	0.34	0.12	0.25	0.25	0.14	0.14	0.06	0.17	0.14
97846	−0.18	0.38	0.45	0.04	...	0.23	0.14	0.10	0.11	0.10	0.07
98020	−1.61	....	1.1	0.25	0.31	...	0.44	0.20	0.22	0.03	0.39
98532	−1.13	....	0.65	0.01	0.34	0.33	0.29	0.25	−0.03	0.15	0.10
99224	−0.12	0.18	0.40	0.05	0.01	0.16	0.14	0.0	0.00	−0.01	0.00
104659	−1.07	0.47	0.75	0.06	0.35	0.26	0.25	0.18	0.06	0.31	0.11
106947	−0.35	0.43	0.34	−0.01	...	0.15	0.15	0.09	0.21	0.20	0.20
107294	−1.14	....	0.73	0.23	0.25	0.26	0.25	0.22	0.09	0.27	0.24
108056	0.14	0.20	0.25	0.00	0.09	0.03	0.07	−0.08	0.08	−0.13	−0.01
109384	−0.38	0.50	0.65	0.02	0.30	0.17	0.26	0.10	0.20	0.12	0.24
110291	−0.93	0.52	0.82	0.06	0.36	0.17	0.21	0.11	0.15	0.12	0.11
111517	−0.45	0.44	0.49	0.17	0.31	0.36	0.23	0.15	0.07	0.18	0.10
112666	−0.42	0.25	0.44	0.07	...	0.21	0.21	0.13	0.14	0.10	0.17
112811	−0.70	...	0.65	0.01	0.30	0.24	0.25	0.12	0.15	0.24	0.21
113514	−0.63	0.42	0.66	0.09	0.29	0.19	0.21	0.16	0.19	0.13	0.03
116421	−0.51	0.38	0.60	0.13	0.31	0.34	0.26	0.21	0.22	0.23	0.13
117029	−0.77	0.46	0.77	0.14	0.33	0.38	0.27	0.17	0.11	0.20	0.10
					Thin Disc						
2909	−0.28	0.37	0.40	0.13	0.19	0.23	0.15	0.08	0.04	0.10	0.04
14086	−0.65	0.34	0.54	0.09	0.39	0.29	0.27	0.19	0.21	0.27	0.20
14241	−0.49	0.33	0.57	0.10	...	0.24	0.23	0.13	0.27	0.22	0.11
19696	−0.24	0.34	0.44	0.05	0.12	0.13	0.14	0.02	0.10	0.05	0.01
26437	0.10	0.02	0.07	0.00	0.07	0.06	0.01	0.00	−0.09	−0.03	−0.02
39616	−0.41	0.15	0.32	0.10	0.15	0.06	0.08	0.02	0.05	0.01	−0.04
40118	−0.47	0.41	0.54	0.08	0.21	0.22	0.21	0.10	0.23	0.15	0.08
64924	−0.03	0.18	0.07	−0.06	0.02	−0.01	0.05	−0.02	0.08	−0.06	0.00
73078	−0.11	0.30	0.47	0.04	0.15	1.3	0.18	−0.03	0.02	−0.13	−0.04
74933	−0.39	0.33	0.52	0.0	0.11	0.19	0.12	0.05	0.16	−0.02	−0.05
81681	−0.38	0.31	0.50	0.04	0.27	0.23	0.18	0.10	0.19	0.16	0.10
84506	0.09	0.50	0.43	0.14	0.04	0.24	0.20	−0.03	0.09	−0.08	−0.01
86568	−0.40	0.35	0.62	0.03	...	0.21	0.24	0.07	0.19	0.17	0.22
					Halo						
3026	−1.04	....	0.47	0.07	0.19	...	0.09	0.11	0.13	0.20	...
10449	−0.87	...	0.71	−0.04	0.26	0.18	0.24	0.18	0.19	0.12	−0.09
12294	−0.95	0.24	0.22	0.07	0.14	...	0.28	0.14	0.07	0.15	...
16072	−1.39	....	1.2	0.41	0.45	...	0.49	0.28	...	0.26	0.33
28671	−1.01	....	0.79	−0.03	0.14	...	0.17	0.16	−0.06	0.16	0.26
52771	−1.98	....	1.1	...	0.21	...	...	0.10	...	0.11	...
55592	−0.94	0.390	0.59	0.08	0.31	0.21	0.18	0.15	−0.01	0.15	0.11
57450	−1.5	....	0.99	0.18	0.36	...	0.34	0.20	0.23	0.10	0.26
58229	−0.83	...	0.67	0.06	0.18	0.13	0.10	0.07	−0.03	0.10	...
62882	−0.98	0.200	0.80	−0.02	0.26	0.12	0.27	0.19	−0.12	0.08	0.10
73385	−1.46	....	1.0	...	...	1.6	0.49	0.32	0.0	0.33	0.0
78640	−1.34	....	0.78	...	0.29	...	0.23	0.26	−0.18	0.26	0.22
80837	−0.80	0.46	0.72	0.14	0.36	0.26	0.24	0.16	0.17	0.21	0.12
86321	−0.87	0.30	0.55	0.02	0.15	0.07	0.15	0.13	0.13	0.12	0.06

Table 4 – *continued*

HIP	[Fe I/H]	C	O	Na	Mg	Al	Si	Ca	Sc	Ti	V
86431	−0.54	0.39	0.57	0.05	0.24	0.19	0.15	0.07	0.15	0.08	0.04
94449	−1.12	0.66	0.95	0.11	0.46	0.48	0.36	0.37	−0.06	0.24	0.08
100568	−0.99	...	0.68	0.01	0.20	...	0.14	0.11	0.00	0.08	0.00
109067	−0.79	0.48	0.68	0.07	0.28	0.24	0.24	0.13	0.21	0.15	0.11
111549	−0.95	...	0.40	−0.42	...	...	0.03	0.17	−0.3	0.12	0.00
115704	−1.78	....	0.67	...	...	...	...	...	...	...	...
					Thin/thick disc						
5163	−0.74	0.44	0.68	0.12	0.27	0.31	0.23	0.13	0.18	0.17	0.06
8720	−0.74	...	0.82	0.08	0.40	0.28	0.28	0.13	0.24	0.16	0.20
10711	−0.69	0.40	0.71	0.00	0.25	0.23	0.22	0.09	0.08	0.11	0.02
12381	−0.16	0.08	0.30	0.02	0.17	0.12	0.01	0.04	−0.01	−0.02	0.02
15394	−0.27	0.09	0.19	0.04	0.26	0.17	0.13	0.04	0.06	−0.02	−0.01
16738	0.37	−0.01	0.18	0.31	0.32	0.14	0.12	−0.08	−0.08	−0.17	−0.07
21227	−0.45	0.45	0.52	0.06	0.12	0.18	0.13	−0.01	0.16	0.04	−0.05
21306	−0.65	0.59	0.79	0.09	0.23	0.25	0.28	0.12	0.22	0.14	−0.02
21703	0.15	−0.01	0.17	−0.14	−0.06	−0.06	0.06	−0.14	0.08	−0.07	−0.06
21921	−0.41	0.32	0.65	0.12	0.21	0.25	0.26	0.11	0.27	0.15	0.17
24037	−0.49	0.28	0.48	0.07	...	0.19	0.19	0.08	0.15	0.17	0.11
30990	−0.87	...	0.87	0.14	0.34	0.30	0.26	0.16	0.18	0.17	−0.01
33382	−0.05	0.07	−0.01	−0.08	0.07	0.01	0.06	−0.05	0.03	−0.08	−0.04
34511	−0.15	0.19	0.17	−0.03	0.04	0.01	0.05	−0.02	0.08	−0.08	−0.04
35148	−0.30	0.22	0.36	0.02	0.17	0.12	0.06	0.0	0.00	−0.05	−0.03
40023	−0.12	0.01	0.08	0.03	0.03	0.13	0.04	0.05	−0.12	0.08	0.07
42734	−0.70	0.42	0.68	0.19	0.31	0.32	0.24	0.21	0.08	0.22	0.26
47588	−0.47	0.34	0.53	0.23	0.28	0.29	0.20	0.10	0.22	0.16	0.23
52015	−0.02	0.13	0.26	0.09	0.05	0.16	0.11	−0.01	0.02	−0.05	−0.01
53535	0.11	0.25	0.35	0.11	−0.06	0.15	0.17	−0.03	0.04	−0.11	−0.05
54196	−0.39	0.11	0.24	0.01	0.16	0.06	0.04	0.04	−0.05	0.02	0.03
62077	−0.59	0.53	0.76	0.13	0.31	0.27	0.23	0.11	0.25	0.21	0.10
62507	−0.24	0.16	0.27	0.06	0.15	0.14	0.09	0.03	−0.12	−0.03	0.01
64103	−0.21	0.16	0.19	−0.09	0.13	0.04	0.04	−0.03	0.02	−0.02	0.02
74442	−0.23	0.52	0.41	−0.01	0.16	0.10	0.09	0.04	0.03	−0.08	−0.09
74443	−0.59	0.62	0.63	0.13	0.12	0.26	0.25	0.14	0.21	0.26	0.25
80162	−0.66	0.75	0.73	0.10	0.06	0.34	0.31	0.11	0.26	0.25	0.22
82265	0.09	0.05	0.08	−0.06	0.17	0.06	0.05	−0.02	0.11	0.02	0.03
85653	−0.43	0.35	0.45	0.06	...	0.23	0.19	0.13	0.11	0.21	0.19
89583	−0.20	0.05	0.22	0.0	0.27	0.16	0.13	0.04	0.26	0.11	0.06
90745	−0.50	0.42	0.64	0.12	0.36	0.25	0.20	0.10	0.07	0.09	0.04
94615	0.20	−0.01	−0.06	−0.16	−0.01	−0.05	−0.02	−0.06	0.11	−0.02	0.06
99938	−0.54	0.36	0.72	0.05	0.30	0.15	0.16	0.09	0.34	0.17	0.06
102081	0.09	0.12	0.20	−0.04	0.20	0.05	0.05	−0.03	0.00	−0.11	−0.09
107236	−0.50	0.43	0.60	0.10	0.29	0.21	0.22	0.06	0.19	0.09	0.05
115721	−0.46	0.45	0.53	0.11	0.26	0.19	0.16	0.12	0.16	0.08	0.07
					Thick disc/halo						
7452	−1.53	....	0.78	...	0.18	0.65	0.77	0.20	0.24	0.28	...
14594	−1.88	....	0.58	...	...	...	0.64	0.28	...	0.50	...
20298	−0.84	0.67	0.93	0.08	0.42	0.41	0.38	0.28	0.20	0.23	0.00
23922	−0.66	...	0.63	0.05	0.29	0.12	0.18	0.13	0.19	0.18	0.08
26617	−0.75	0.50	0.83	0.04	0.23	0.25	0.25	0.19	0.13	0.13	0.08
42864	−1.47	....	0.95	...	0.40	...	0.55	0.20	...	0.22	0.34
43595	−0.84	0.52	0.71	0.05	0.29	0.32	0.17	0.13	0.12	0.24	0.06
48209	−0.65	0.39	0.66	0.10	0.21	0.24	0.22	0.11	0.22	0.18	0.08
51477	−1.25	....	1.4	0.14	0.44	0.42	0.53	0.26	0.08	0.11	−0.02
60331	−0.64	...	0.82	0.07	0.22	0.35	0.27	0.05	0.27	0.14	0.10
71019	−0.39	0.41	0.66	0.04	0.23	0.33	0.23	0.12	0.20	0.13	0.07
85650	−0.39	0.34	0.60	0.13	0.25	0.35	0.25	0.17	0.16	0.17	0.11

Inspection of Figs 9–11 shows that a majority of stars from Bensby et al.'s sample which we put in the thin–thick group with [Fe/H] $\leqslant -0.3$ are thick-disc stars as judged by Mg, Si and Ti abundances. Mishenina et al.'s results give marginal support to the difference in [Mg/Fe] and [Si/Fe] between thin and thick discs.

A comparison of abundances for stars in common shows that the different studies are consistent. We have 10 stars (no distinction is made according to thin or thick disc) in common with the Bensby and colleagues' total sample of 102 stars. We have five stars in common with Mishenina et al. (2004). Mean difference and standard deviations for the samples of common stars are summarized in Table 3

Table 5. Abundance ratios [X/Fe] for elements from V to Eu for the program stars.

HIP	[Fe/H]	Cr	Mn	Co	Ni	Cu	Zn	Y	Ba	Ce	Nd	Eu
						Thick disc						
3086	−0.23	−0.04	−0.18	0.02	−0.03	−0.06	0.14	−0.16	−0.15	0.04	0.14	0.23
3185	−0.65	0.08	−0.19	0.12	0.04	−0.09	0.14	0.04	−0.06	0.12	0.34	0.60
3441	−0.50	−0.03	−0.32	0.08	0.05	−0.08	0.23	0.04	−0.09	0.18	0.26	0.42
4039	−1.20	0.07	−0.51	0.28	−0.08	−0.48	0.08	0.05	0.30	...	...	0.88
4544	−0.87	−0.09	−0.40	0.13	0.0	−0.05	0.08	−0.02	−0.14	...	0.58	0.53
5122	−0.62	0.00	−0.22	0.11	0.05	0.11	0.09	−0.03	−0.16	−0.02	0.20	0.40
5315	−0.47	0.00	−0.18	0.12	0.03	0.14	0.23	0.07	−0.20	0.08	0.19	0.43
5336	−0.86	0.00	−0.23	0.18	0.12	0.02	0.16	−0.02	−0.23	0.05	0.14	0.34
5775	−0.58	0.06	−0.16	0.12	0.04	0.00	0.21	0.22	0.08	0.07	...	0.43
6159	−0.67	−0.04	−0.26	0.06	0.04	0.03	0.08	−0.01	−0.14	0.22	0.25	0.46
6607	−0.41	−0.01	−0.15	0.14	0.04	0.02	0.01	0.06	−0.08	0.21	0.36	0.41
7961	−0.64	−0.01	−0.28	0.07	0.02	−0.2	0.1	−0.03	−0.20	−0.04	0.07	0.28
8674	−0.60	−0.03	−0.24	0.08	−0.01	0.01	0.26	0.69	0.57	0.64	0.89	0.45
9080	−0.37	−0.05	−0.04	0.10	0.11	0.03	0.02	−0.28	−0.11	0.21	0.27	0.19
10652	−0.67	−0.01	−0.33	0.06	0.02	−0.02	0.10	−0.07	−0.09	−0.07	...	0.39
12579	−0.80	−0.08	−0.42	0.17	−0.05	−0.09	0.11	0.05	−0.04	−0.05	0.20	0.37
13366	−0.70	−0.06	−0.30	0.06	−0.01	−0.05	0.14	−0.07	−0.15	−0.10	0.18	0.29
15126	−0.82	−0.04	−0.40	0.11	−0.03	−0.14	0.13	−0.05	−0.07	...	...	0.49
15405	−0.73	−0.05	−0.30	0.07	−0.03	0.04	0.11	−0.13	−0.12	0.16	0.08	0.24
17147	−0.87	−0.03	−0.39	0.11	−0.02	−0.08	0.15	0.22	0.00	0.13	0.25	0.42
17666	−1.0	−0.03	−0.29	0.22	−0.01	−0.13	0.21	0.31	0.11	0.25	0.43	0.57
22020	−0.35	−0.03	−0.23	0.09	−0.01	0.04	0.11	−0.13	−0.06	0.02	...	0.21
22060	−0.63	−0.07	−0.28	0.02	0.00	0.00	0.14	0.10	−0.05	0.23	−0.02	0.47
23080	−0.32	−0.03	−0.13	0.15	0.04	0.09	0.11	0.08	−0.06	0.24	0.16	0.40
24030	−1.0	−0.05	−0.53	0.02	0.04	−0.33	0.13	0.21	0.02	...	...	...
25860	−0.35	0.01	−0.20	0.16	0.04	0.10	0.17	0.07	−0.08	0.26	0.22	0.35
26452	−0.89	−0.03	−0.38	0.2	−0.01	−0.08	0.13	0.09	−0.20	...	0.24	0.41
26828	−0.34	−0.07	−0.28	0.05	−0.04	−0.10	0.02	−0.13	−0.12	...	...	0.13
27128	−0.81	−0.14	−0.39	0.16	−0.02	−0.09	0.11	−0.02	−0.12	−0.01	...	0.40
29269	−0.68	0.00	−0.28	0.05	0.01	−0.03	0.17	−0.14	−0.10	−0.08	0.07	0.29
31188	−0.59	−0.12	−0.15	0.03	−0.06	−0.07	−0.02	−0.06	−0.07	−0.01	0.04	0.17
34642	−0.44	−0.04	−0.27	0.02	−0.02	−0.10	−0.04	−0.16	0.00	−0.23	0.08	0.15
35989	−0.19	−0.04	−0.11	−0.02	−0.03	−0.25	−0.02	−0.33	−0.21	0.18	0.01	0.13
36849	−0.77	−0.14	−0.40	0.02	−0.04	−0.10	0.10	−0.10	−0.12	0.02	...	0.39
37233	−0.51	0.00	−0.27	0.10	0.02	−0.04	−0.03	−0.11	−0.12	−0.12	0.04	0.36
38769	−0.79	−0.06	−0.54	0.02	0.01	0.0	0.17	−0.05	−0.12	0.00	...	0.26
39893	−0.84	−0.02	−0.25	0.16	0.02	−0.05	0.19	−0.16	−0.14	0.18	0.31	0.53
40613	−0.62	−0.03	−0.31	0.09	−0.04	−0.04	0.10	−0.05	−0.19	−0.15	0.07	0.24
43393	−0.59	−0.01	−0.28	0.09	0.02	0.02	0.10	−0.10	−0.22	−0.02	0.15	0.33
44075	−0.86	−0.07	−0.35	0.11	−0.06	−0.12	0.10	0.09	−0.06	0.12	0.14	0.35
44347	−0.85	−0.08	−0.43	0.21	0.05	−0.13	0.19	0.13	0.10	0.13	0.35	0.52
44860	−0.51	0.00	−0.20	0.14	0.05	0.09	0.17	0.09	−0.10	0.08	0.08	0.39
45947	−0.46	0.04	−0.21	0.06	0.03	0.22	0.13	0.06	−0.11	−0.04	0.13	0.57
50005	−0.53	0.02	−0.22	0.23	0.03	0.14	0.05	0.09	−0.19	...	...	0.42
50671	−0.48	−0.02	−0.13	−0.02	0.02	0.05	0.09	−0.05	0.03	−0.01	0.02	0.17
50965	−0.57	−0.04	−0.22	0.13	0.02	0.00	0.10	0.03	−0.07	0.02	...	0.34
52673	−0.66	0.02	−0.20	0.11	0.04	0.02	0.23	0.15	−0.01	0.03	0.19	0.40
58843	−0.79	0.00	−0.33	0.13	0.03	−0.03	0.09	0.18	0.00	0.08	0.09	0.44
59233	−0.83	0.07	−0.08	0.06	−0.01	0.02	0.17	−0.40	−0.25	−0.08	0.05	0.12
59750	−0.74	−0.09	−0.35	0.09	0.02	−0.08	0.12	0.07	−0.14	...	...	0.32
60268	−0.72	0.02	−0.26	0.10	0.05	0.08	0.17	0.00	−0.14	0.07	0.17	0.41
60956	−0.58	−0.02	−0.18	0.08	0.05	0.04	0.15	0.06	−0.10	0.22	0.29	0.44
62240	−0.83	0.03	−0.32	0.19	0.07	−0.11	0.04	0.04	−0.28	0.21	0.22	0.57
64426	−0.71	−0.09	−0.36	0.09	−0.04	−0.08	0.04	−0.07	−0.21	0.09	0.21	0.21
65449	−0.44	0.03	−0.22	0.04	−0.01	0.09	0.04	−0.16	−0.14	−0.27	0.00	0.29
70520	−0.62	0.00	−0.25	0.12	0.01	−0.02	0.09	−0.06	−0.22	0.11	0.07	0.28
70681	−1.1	−0.06	−0.47	0.07	−0.01	−0.33	0.08	0.29	0.10	...	0.34	0.53
71819	−0.14	−0.01	−0.07	0.02	0.0	0.01	0.02	−0.02	−0.06	0.03	0.16	0.03
72407	−0.54	0.05	−0.20	0.14	0.10	0.08	0.17	0.13	−0.13	0.09	0.29	0.56
72803	−0.73	−0.05	−0.26	0.11	0.09	0.01	0.09	−0.01	−0.28	0.07	0.19	0.42
74033	−0.85	0.00	−0.35	0.20	0.03	−0.09	0.18	0.17	−0.11	0.02	0.19	0.34

Table 5 – *continued*

HIP	[Fe/H]	Cr	Mn	Co	Ni	Cu	Zn	Y	Ba	Ce	Nd	Eu
74067	−0.75	−0.06	−0.32	0.01	0.01	−0.07	0.14	0.09	−0.10	0.14	0.21	0.48
81748	−0.01	−0.01	−0.09	−0.03	−0.03	−0.01	−0.08	−0.04	−0.19	0.16	0.10	0.04
84781	−0.29	0.00	−0.23	0.09	0.03	0.13	0.14	0.10	−0.01	0.22	0.18	0.45
84803	−0.52	0.02	−0.19	0.11	0.05	0.04	0.03	−0.08	−0.32	0.09	0.14	0.25
84862	−0.41	−0.03	−0.24	0.12	0.04	0.02	0.26	0.10	−0.12	0.06	0.32	0.45
85373	−0.82	0.04	−0.30	0.23	0.08	−0.2	0.10	0.05	−0.31	...	0.63	0.71
85378	−0.51	−0.04	−0.24	0.09	0.04	−0.02	0.09	−0.01	−0.15	0.08	0.22	0.36
85757	−0.70	−0.03	−0.29	0.10	0.03	−0.02	0.10	0.03	−0.17	−0.10	0.14	0.09
86013	−0.70	−0.11	−0.32	0.08	−0.03	−0.13	0.11	0.02	−0.13	−0.02	0.30	0.35
86830	−0.59	0.01	−0.22	0.14	0.05	0.00	0.04	−0.09	−0.27	−0.07	0.10	0.25
87089	−0.30	−0.03	−0.05	0.12	0.06	0.06	0.04	0.05	−0.10	0.32	0.28	0.46
87533	−0.21	−0.01	−0.12	−0.04	−0.02	−0.04	−0.01	−0.13	−0.14	−0.08	−0.06	−0.06
88039	−0.81	−0.09	−0.35	0.07	0.04	−0.07	0.22	0.01	−0.14	0.04	0.09	0.26
88166	−0.76	−0.01	−0.27	0.11	0.03	−0.05	0.14	0.09	−0.21	0.26	0.17	0.52
90393	−0.72	0.05	−0.15	0.14	0.05	−0.06	0.04	0.09	−0.24	0.23	0.61	...
94129	−0.27	−0.01	−0.17	0.10	0.01	0.03	0.13	0.00	0.06	−0.04	0.08	0.30
96185	−0.56	−0.09	−0.32	0.10	0.0	−0.03	0.04	0.01	−0.34	−0.06	0.17	0.20
96902	−0.29	−0.02	−0.17	0.09	0.03	0.09	0.08	−0.15	−0.22	−0.06	−0.02	0.14
97846	−0.18	0.01	0.02	0.08	0.04	0.08	0.19	−0.08	−0.02	0.03	0.19	0.12
98020	−1.6	−0.16	−0.48	0.16	0.00	−0.66	0.56	−0.01	−0.04	0.65	0.57	...
98532	−1.13	−0.03	−0.44	0.03	0.00	−0.40	0.07	0.20	0.04	0.05	0.23	0.31
99224	−0.12	−0.04	−0.16	0.02	−0.02	0.05	0.07	−0.04	−0.12	0.00	0.14	0.08
104659	−0.95	−0.19	−0.56	−0.06	−0.05	−0.23	0.11	−0.12	−0.18	...	...	0.27
106947	−0.39	−0.02	−0.05	0.12	0.05	0.11	0.13	0.0	0.05	0.28	0.24	0.47
107294	−1.14	−0.03	−0.28	0.25	0.11	−0.50	0.04	0.22	0.11	...	...	...
108056	0.14	−0.06	−0.14	−0.03	−0.01	0.04	0.04	0.06	0.15	−0.05	...	−0.12
109384	−0.38	−0.04	−0.06	0.16	0.04	0.04	0.19	0.13	−0.2	0.29	0.17	0.34
110291	−0.93	−0.12	−0.41	0.04	−0.04	−0.21	0.09	0.03	−0.03	...	0.03	0.40
111517	−0.49	0.06	−0.13	0.18	0.09	0.16	0.16	−0.08	−0.22	−0.11	−0.02	0.36
112666	−0.42	−0.03	−0.14	0.09	−0.01	0.01	0.07	−0.09	−0.13	0.27	0.16	0.43
112811	−0.63	−0.10	−0.37	0.07	−0.02	−0.11	0.00	0.07	−0.19	−0.10	−0.05	0.28
113514	−0.64	−0.05	−0.24	0.04	0.0	0.08	0.16	0.08	−0.03	0.07	0.35	0.43
116421	−0.50	−0.01	−0.24	0.12	0.03	0.0	0.07	0.03	−0.13	0.0	0.19	0.23
117029	−0.76	−0.02	−0.31	0.13	0.04	−0.03	0.11	−0.04	−0.27	0.05	0.18	0.25
						Thin disc						
2909	−0.28	−0.01	−0.15	0.08	0.03	0.04	−0.01	−0.08	−0.12	0.02	0.12	0.16
14086	−0.65	0.01	−0.23	0.14	0.05	0.07	0.06	0.09	−0.18	0.06	0.28	0.39
14241	−0.49	−0.01	−0.19	0.15	0.04	0.15	0.16	0.16	−0.06	0.13	0.22	0.48
19696	−0.24	−0.01	−0.14	0.06	0.00	0.10	0.19	0.08	0.02	0.07	0.20	0.25
26437	0.10	0.00	−0.05	−0.04	0.00	−0.02	−0.11	−0.05	−0.13	−0.16	0.02	−0.08
39616	−0.41	−0.05	−0.15	−0.02	−0.04	−0.06	0.06	0.05	0.12	0.21	0.27	0.12
40118	−0.47	−0.05	−0.19	0.10	0.01	0.10	0.16	0.00	−0.06	0.17	0.32	0.38
64924	−0.03	−0.03	−0.06	0.01	−0.05	0.00	0.07	−0.08	0.03	0.17	0.26	0.15
73078	−0.11	−0.04	−0.07	0.04	0.05	0.02	0.02	−0.09	−0.41	0.13	0.18	−0.10
74933	−0.39	−0.08	−0.20	−0.02	−0.04	−0.03	0.09	0.02	0.05	0.04	0.16	0.24
81681	−0.38	−0.05	−0.22	0.09	0.04	0.10	0.12	0.05	−0.15	0.10	0.35	0.30
84506	0.09	0.02	−0.07	0.08	0.06	0.15	0.05	0.01	−0.08	0.03	0.00	−0.11
86568	−0.40	−0.05	−0.16	0.17	0.04	0.04	0.13	−0.07	−0.07	0.20	0.18	0.49
						Halo						
3026	−1.0	−0.21	−0.52	0.31	−0.01	...	0.03	0.06	0.09	...	...	...
10449	−0.87	−0.01	−0.41	0.13	−0.06	−0.20	0.14	0.07	−0.01	0.29	...	0.49
12294	−0.95	0.09	−0.35	...	0.04	−0.37	...	0.01	−0.12	...	0.80	...
16072	−1.39	−0.02	−0.28	...	−0.01	−0.32	0.33	0.36	0.14	...	...	...
28671	−1.01	0.02	−0.48	0.01	−0.03	−0.42	0.15	0.10	−0.15	...	...	0.42
52771	−2.0	...	−0.47	0.78	−0.06	...	0.17	...	−0.27	...	...	...
55592	−0.94	−0.11	−0.42	−0.02	−0.05	−0.34	0.17	0.09	0.13	0.12	...	0.40
57450	−1.50	−0.09	−0.40	...	−0.11	−0.36	0.08	−0.04	−0.05	...	...	...
58229	−0.83	−0.35	−0.40	0.26	−0.05	−0.44	0.02	0.03	−0.13	...	...	...
62882	−0.98	−0.07	−0.61	−0.15	−0.08	−0.55	0.12	0.08	−0.06	0.07	0.10	0.12
73385	−1.46	0.18	−0.39	...	0.07	−0.46	0.20	0.20	0.07	0.27	...	0.31
78640	−1.34	...	−0.34	0.41	−0.03	...	−0.07	−0.07	−0.28	...	0.14	0.06
80837	−0.80	0.05	−0.27	0.22	0.04	0.01	0.15	0.06	−0.13	−0.05	0.14	0.29
86321	−0.87	−0.07	−0.34	0.20	−0.04	−0.43	0.08	0.07	0.03	...	...	0.36

Table 5 – *continued*

HIP	[Fe/H]	Cr	Mn	Co	Ni	Cu	Zn	Y	Ba	Ce	Nd	Eu
86431	−0.54	−0.08	−0.23	0.05	−0.05	−0.03	0.07	0.00	−0.07	0.03	0.33	0.30
94449	−1.12	−0.08	−0.36	0.14	−0.01	−0.40	0.03	−0.12	−0.27	0.11	...	0.10
100568	−0.99	−0.06	−0.51	−0.07	−0.12	−0.45	−0.06	−0.17	−0.23	0.11	0.14	0.41
109067	−0.73	−0.16	−0.40	0.06	−0.05	−0.22	0.1	0.13	−0.10	0.04	0.01	...
111549	−0.95	−0.04	−0.34	−0.06	−0.07	−0.40	−0.03	−0.29	−0.24	...	−0.01	0.27
115704	−1.78	...	...	...	...	...	...	...	...	...	...	...
						Thin/thick disc						
5163	−0.74	0.00	−0.25	0.10	0.06	0.07	0.06	0.03	−0.09	0.25	...	0.38
8720	−0.74	−0.03	−0.19	0.25	0.07	−0.01	0.13	0.02	−0.20	0.17	0.15	0.45
10711	−0.69	−0.11	−0.42	0.11	−0.06	−0.13	0.11	0.02	−0.13	0.13	...	0.27
12381	−0.16	−0.06	−0.25	0.0	−0.09	−0.01	−0.07	0.12	−0.02	−0.27	...	0.14
15394	−0.27	0.00	−0.09	0.02	0.01	−0.02	0.12	−0.08	−0.15	0.02	0.09	0.09
16738	0.37	−0.01	0.01	0.03	0.06	0.22	0.18	−0.08	0.12	...	...	...
21227	−0.45	−0.12	−0.26	0.0	−0.02	−0.04	0.03	0.02	−0.08	0.08	0.49	0.37
21306	−0.67	−0.05	−0.33	0.08	0.02	−0.05	0.17	0.07	−0.10	0.24	0.24	0.29
21703	0.15	−0.08	−0.09	−0.01	0.01	−0.01	−0.01	0.13	−0.04	0.14	0.15	0.14
21921	−0.41	−0.01	−0.20	0.12	0.03	0.02	0.11	0.06	−0.13	0.12	0.39	0.47
24037	−0.49	−0.01	−0.19	0.13	0.04	0.15	0.14	0.05	−0.07	0.06	0.33	0.38
30990	−0.87	−0.07	−0.48	0.14	−0.01	−0.15	0.12	−0.10	−0.21	0.04	...	0.29
33382	−0.05	−0.05	−0.12	−0.01	−0.03	0.01	−0.08	−0.04	−0.04	0.04	0.13	0.08
34511	−0.15	−0.03	−0.09	−0.06	−0.05	−0.01	−0.03	0.11	0.11	0.09	0.25	0.11
35148	−0.30	−0.06	−0.17	−0.04	−0.07	−0.06	−0.07	−0.16	−0.15	−0.12	0.05	0.08
40023	−0.12	0.04	−0.04	0.02	−0.03	0.08	−0.10	−0.18	−0.04	−0.07	−0.01	−0.05
42734	−0.70	0.05	−0.23	0.12	0.01	0.01	0.11	−0.14	−0.13	−0.01	0.02	0.34
47588	−0.47	−0.03	−0.22	0.19	0.02	0.08	0.10	−0.05	−0.19	−0.20	0.07	0.26
52015	−0.02	0.00	−0.04	0.04	−0.01	0.05	0.02	−0.08	−0.10	−0.02	0.06	−0.03
53535	0.11	0.00	−0.08	0.07	0.01	0.10	0.02	−0.13	−0.11	−0.06	0.20	−0.16
54196	−0.39	−0.04	−0.21	0.04	−0.04	0.00	0.03	−0.10	−0.14	−0.13	−0.03	0.17
62077	−0.59	−0.02	−0.22	0.17	0.02	0.10	0.09	−0.03	0.01	0.05	...	0.36
64103	−0.21	−0.06	−0.13	−0.06	−0.05	−0.03	0.01	−0.05	−0.02	0.11	0.14	0.17
74442	−0.23	−0.06	−0.13	−0.05	−0.02	−0.02	0.05	−0.02	−0.14	0.08	0.0	0.07
74443	−0.59	0.01	−0.08	0.20	0.06	0.00	0.13	−0.06	−0.22	−0.03	0.07	0.44
80162	−0.66	−0.02	−0.17	0.12	0.08	0.05	0.16	−0.01	−0.20	0.15	0.15	0.41
82265	0.09	−0.03	−0.04	0.04	0.01	0.04	−0.03	0.01	−0.04	0.14	0.14	0.22
85653	−0.43	0.00	−0.22	0.13	0.05	0.11	0.12	0.37	0.17	0.10	0.39	0.41
89583	−0.20	−0.05	−0.15	0.10	0.03	0.11	0.03	0.03	−0.04	0.06	0.19	0.40
90745	−0.50	−0.01	−0.20	0.06	0.02	0.04	0.06	−0.02	−0.11	−0.04	0.07	0.22
94615	0.20	0.01	−0.07	1.3	−0.02	0.06	−0.02	0.07	0.12	0.23	0.19	0.06
99938	−0.54	−0.10	−0.26	0.03	0.0	−0.03	0.06	0.02	−0.08	0.05	0.21	0.37
102081	0.09	−0.06	−0.09	0.0	−0.03	−0.03	0.04	0.04	−0.02	0.00	−0.04	−0.01
115721	−0.46	−0.01	−0.29	0.04	−0.01	0.11	0.17	−0.02	−0.02	0.07	0.05	0.30
						Thick disc/halo						
7452	−1.53	0.38	...	...	...	...	0.02	0.23	−0.01	0.12	...	...
14594	−1.88	...	...	0.91	0.44	...	0.33	...	−0.16	1.0e+03	1.0e+03	1.0e+03
20298	−0.84	−0.04	−0.43	0.07	−0.07	0.05	0.20	0.34	−0.02	0.16	0.28	0.29
23922	−0.66	−0.08	−0.31	0.07	−0.02	−0.04	0.17	0.09	−0.11	−0.09	0.11	0.35
26617	−0.75	−0.05	−0.30	0.18	0.0	−0.21	0.09	0.12	−0.06	0.21	0.25	0.39
42864	−1.47	−0.17	−0.58	...	0.24	−0.16	0.39	...	0.04	1.0e+03	1.0e+03	1.0e+03
43595	−0.84	−0.04	−0.29	0.14	−0.01	−0.03	0.20	0.07	−0.11	0.26	0.23	0.36
48209	−0.65	−0.01	−0.18	0.09	0.06	0.06	0.12	0.04	−0.09	0.09	0.10	0.35
51477	−1.2	0.00	−0.47	0.15	0.01	−0.24	0.22	0.26	0.02	0.11	0.25	0.29
60331	−0.64	0.21	−0.35	0.17	−0.06	...	0.28	−0.05	−0.25	−0.08	...	0.58
62507	−0.24	−0.04	−0.13	0.01	−0.03	−0.04	0.12	−0.16	−0.17	−0.20	0.07	−0.05
71019	−0.39	0.00	−0.27	0.07	0.03	0.04	0.15	−0.15	−0.10	0.02	0.09	0.21
85650	−0.39	0.01	−0.18	0.12	0.0	0.00	0.19	−0.08	−0.14	0.23	0.24	...
107236	−0.50	−0.04	−0.18	0.17	0.07	0.05	0.10	0.07	−0.15	0.11	0.15	0.42

for the atmospheric parameters, the Fe abundance, and the [X/Fe] values. We have six stars in common with Fuhrmann (2004). The mean difference between him and us, for [Fe/H] is 0.0 ± 0.05 and [Mg/Fe] is 0.03 ± 0.12. The Fuhrmann's $T_{\rm eff}$ and log g values are systematically hotter by 125 ± 23 K and lower by 0.19 ± 0.06 dex, respectively. Brewer & Carney (2006) analysed 23 G dwarfs of which four were analysed by us. Their and our adopted atmospheric parameters and derived abundances are in excellent agreement, for example, differences in $T_{\rm eff}$, log g, and [Fe/H] run from −43 to + 14 K, −0.2 to 0.0 cgs units, and −0.08 to +0.06 dex, respectively.

Table 6. Abundance uncertainties due to estimated uncertainties in atmospheric parameters for five representative stars. The values of σ are the quadratic sum of the variations in the abundance ratios, [X/Fe], due to the uncertainties in model parameters. The column $\sigma_{\rm mod}$ is the mean of the values of σ and the quoted error 's.d.' is the standard deviation per measurement.

	HIP 17666	HIP 15405	HIP 5122	HIP 3086	HIP 16738	
$T_{\rm eff}$	5000 K	5107 K	5204 K	5697 K	6000 K	
[Fe/H]	−1.03	−0.73	−0.55	−0.23	+0.36	
	σ_1	σ_2	σ_3	σ_4	σ_5	$\sigma_{\rm mod} \pm$ s.d.
[Fe/H]	0.07	0.09	0.09	0.08	0.09	0.08 ± 0.01
[C/Fe]	0.07	0.21	0.10	0.16	0.16	0.14 ± 0.06
[O/Fe]	0.21	0.21	0.20	...	0.15	0.19 ± 0.03
[Na/Fe]	0.06	0.05	0.04	0.03	0.04	0.05 ± 0.02
[Mg/Fe]	0.05	0.05	0.04	0.04	0.06	0.05 ± 0.01
[Al/Fe]	0.04	0.05	0.05	0.05	0.05	0.05 ± 0.01
[Si/Fe]	0.09	0.10	0.08	0.03	0.06	0.07 ± 0.03
[S/Fe]	0.07	0.18	0.17	0.12	0.13	0.13 ± 0.04
[Ca/Fe]	0.07	0.04	0.03	0.02	0.01	0.03 ± 0.03
[Sc/Fe]	0.10	0.13	0.11	0.09	0.13	0.11 ± 0.02
[Ti/Fe]	0.09	0.07	0.06	0.04	0.04	0.06 ± 0.02
[V/Fe]	0.10	0.07	0.05	0.03	0.02	0.06 ± 0.03
[Cr/Fe]	0.05	0.03	0.03	0.02	0.02	0.03 ± 0.01
[Mn/Fe]	0.05	0.08	0.07	0.05	0.04	0.06 ± 0.02
[Co/Fe]	0.02	0.03	0.03	0.03	0.02	0.03 ± 0.01
[Ni/Fe]	0.05	0.04	0.03	0.03	0.04	0.04 ± 0.01
[Cu/Fe]	0.05	0.03	0.04	0.05	0.03	0.04 ± 0.01
[Zn/Fe]	0.09	0.11	0.11	0.07	0.10	0.10 ± 0.02
[Y/Fe]	0.09	0.12	0.13	0.12	0.07	0.11 ± 0.03
[Ba/Fe]	0.11	0.11	0.13	0.13	0.13	0.12 ± 0.01
[Ce/Fe]	0.10	0.11	0.12	0.11	...	0.11 ± 0.01
[Nd/Fe]	0.08	0.11	0.13	0.12	...	0.11 ± 0.02
[Eu/Fe]	0.12	...	0.14	0.13	...	0.13 ± 0.01

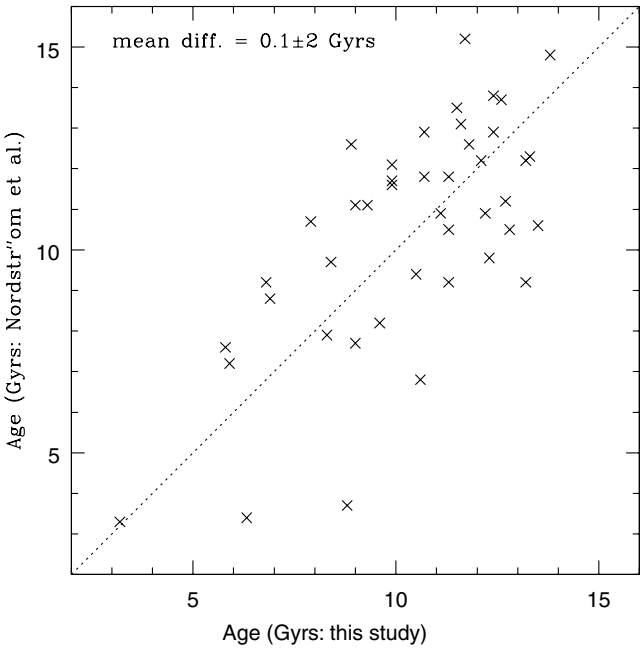

Figure 8. Stellar ages from this study against the ages from Nordström et al. (2004). The dotted line corresponds to equal ages from the two sources.

An analogous and equally satisfactory comparison was made in Paper I for thin-disc stars and the large surveys by Edvardsson et al. (1993), Chen et al. (2000), and Fulbright (2000). These analyses of stars in common with our studies suggest that results from different studies could be combined to enlarge the sample size for thick- and thin-disc stars.

5.2 Thin and thin–thick disc stars

Our discussion of the thick-disc composition is based on the 95 thick stars chosen by the requirement that $P_{\rm thick} > 70$ per cent. Here, we consider the 13 stars assigned to the thin disc and the 34 stars in the thin–thick disc category. Fig. 12 shows in separate panels the run of [α/Fe] ratio versus [Fe/H] for thick, thin–thick, and thin-disc stars from our present sample with the thin-disc stars from Paper I shown in each panel. The ratio [α/Fe] is defined as simple mean of the four ratios [Mg/Fe], [Si/Fe], [Ca/Fe] and [Ti/Fe]. Clearly, the samples of thick–thin and thin-disc stars both contain thick stars, as judged by [α/Fe]. This mixing and contamination must in part result from the fact that the assignment to the thin or the thick disc is based on a probability. Given that Fig. 12 (and other figures) convey the impression that thin- and thick-disc abundance relations are distinct, the collection of thick-disc stars might be augmented by stars from the thin–thick disc category, and even the thin-disc category. We do not act on the second suggestion, but reconsideration of the procedure for categorizing disc stars would be a useful exercise.

5.3 Our halo stars

The probability criteria yielded 20 halo stars. Most of them, as expected, have very negative $V_{\rm LSR} \leqslant -180\,{\rm km\,s^{-1}}$ and orbits of extreme eccentricity (0.7 to 1.0). A few stars are on retrograde orbits,

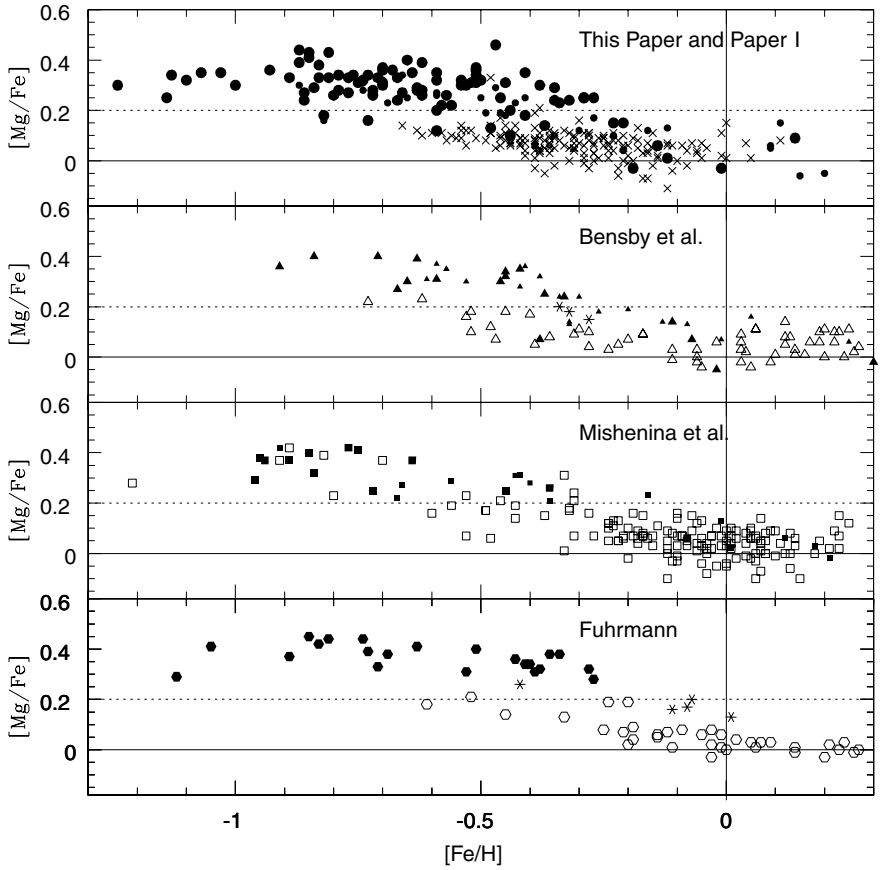

Figure 9. Abundance ratios [Mg/Fe] against [Fe/H] for four samples are shown. In all the panels, the filled symbols denote the thick-disc stars and the open symbols denote the thin-disc stars as classified by the respective studies. Large filled symbols in all the panels represent stars that have probability $P_{\rm thick} \geqslant 70$ per cent as followed by the criteria employed in this study. The smaller filled symbols represent stars whose probability $P_{\rm thick} < 70$ but >50 per cent according to our criteria. Solid lines represent solar ratios of [X/Fe] and [Fe/H] = 0, and the broken line indicates ratio [X/Fe] = +0.2.

that is, $V_{\rm LSR} < -220\,{\rm km\,s^{-1}}$. The halo stars in the sample span the [Fe/H] range −0.6 to −2.0.

Mg-like elements show overabundances similar to thick-disc stars and may show a mild trend of [X/Fe] with [Fe/H]. At overlapping metallicities, the [α/Fe] of the halo stars are in agreement with the thick-disc ratios. Ni-like elements for the halo stars track the Fe similar to thin- and thick-disc stars. The scatter in [X/Fe] ratios for both the Mg- and Ni-like elements for the halo stars appears similar to that for the thick-disc stars.

The [α/Fe] ratio, for the halo stars in our sample is about 0.25 dex, in agreement with our thick-disc stars. This value is in good agreement with the [α/Fe] results for halo stars from Gratton et al. (2003) in the same [Fe/H] range. Their results also do not show a trend of [α/Fe] with [Fe/H].

5.4 The Mg-like elements

One subset of the Mg-like elements are the so-called α-elements: C, O, Mg, Si, Ca and Ti. Our results for these elements are shown in Figs 13 and 14. Other Mg-like elements are Al, Sc, V, Co, and possibly Zn (Fig. 15).

The trend of [X/Fe] against [Fe/H] for Mg-like elements in the thick disc may be characterized by a shallow slope for [Fe/H] $\leqslant$ −0.3 and from the trend for thin-disc stars. For each Mg-like element, we compute the slope ($B_{\rm thick}$) from a linear regression fit to the [X/Fe] from [Fe/H] = −0.3 to −1.0. The offset between the thick and thin trends is obtained by calculating the mean value ($M_{\rm thick}$ or $M_{\rm thin}$) in the bin of [Fe/H] from −0.45 to −0.55. Quantities $B_{\rm thin}$, $B_{\rm thick}$, $M_{\rm thin}$ and $M_{\rm thick}$ are given in Table 7, together with the thick–thin disc offset Δ[X/Fe] = $M_{\rm thick} - M_{\rm thin}$. The behaviour of the Mg-like elements for [Fe/H] > −0.3 is discussed below. Below we make few remarks on individual elements.

Carbon. We obtained abundances for stars with [Fe/H] $\geqslant -1.2$; the chosen C I lines are too weak to measure in more-metal-poor stars. Abundance ratios [C/Fe] for the thick-disc sample stars below [Fe/H] < −0.4 as shown in Fig. 13 are on average larger than the thin-disc stars of the same [Fe/H]. Although the scatter is quite large, carbon is seen to behave like Mg and other α-elements. Similar behaviour of [C/Fe] with [Fe/H] is seen by Shi, Zhao & Chen (2002) for nearby F, G and K dwarfs. They also noted that the non-LTE corrections are negligibly small. Our thin-disc [C/Fe] (Paper I), also from the C I lines, are in agreement with the results obtained from [C I] line at 8727 Å by Gustafsson et al. (1999) and Allende Prieto et al. (2004), for samples dominated by thin-disc stars. Contrary to the above studies, the recent study by Bensby et al. (2005) based on the [C I] line at 8727 Å for a small sample of both thick- and thin-disc stars shows almost a flat trend of [C/Fe] below [Fe/H] $\approx$ −0.2.

Oxygen. The permitted O I lines at 7771 Å are used to get O abundances for all stars. These lines are known to be subject to non-LTE effects. We apply the empirical calibration to correct for these effects that was developed in Paper I, using abundances from the

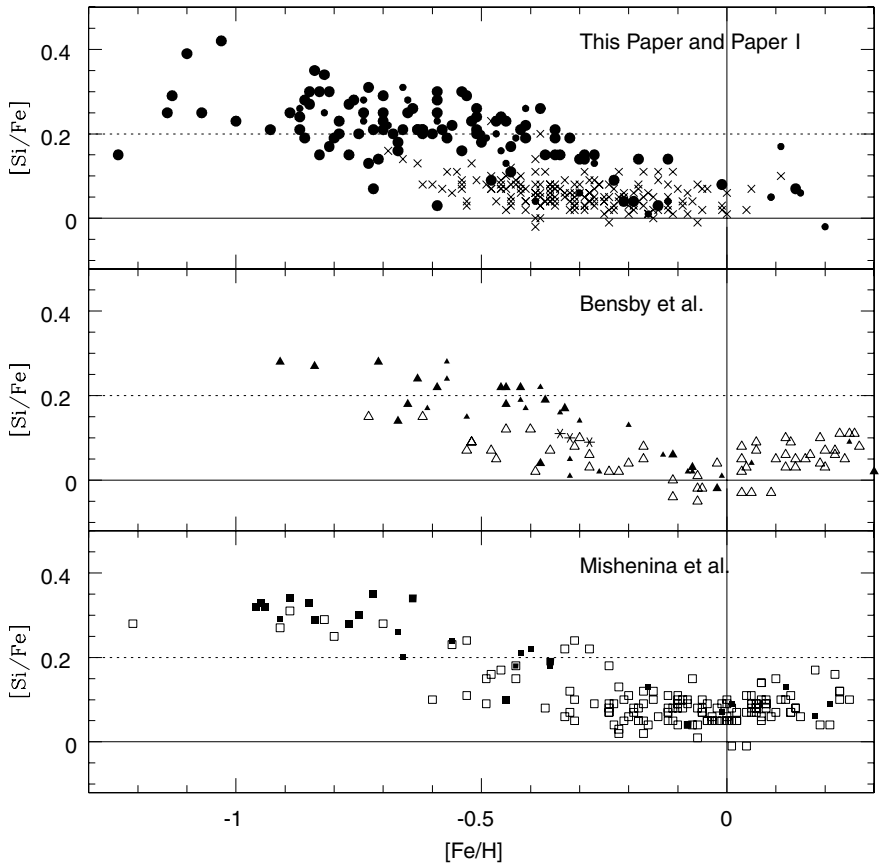

Figure 10. Same as previous figure but for the [Si/Fe] ratio.

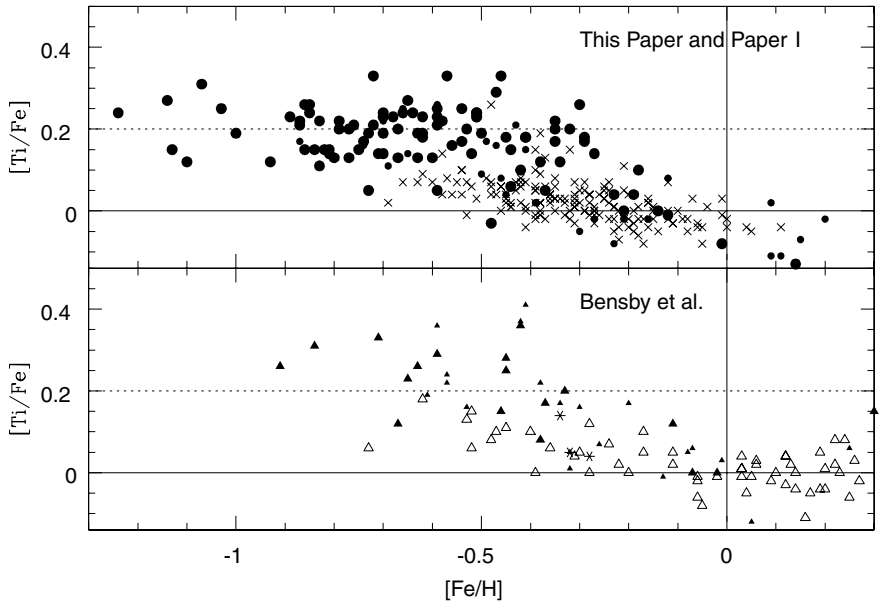

Figure 11. Same as previous figure but for the [Ti/Fe] ratio.

[O I] and O I lines for the same stars. The resulting [O/Fe] ratios are shown against [Fe/H], which shows oxygen to behave as an Mg-like element (Fig. 13). Full non-LTE corrected O abundances will be discussed in a separate publication (see Ramírez, Allende Prieto & Lambert, private communication).

The α-elements: Mg, Si, Ca and Ti. The runs of abundance ratios [X/Fe] against [Fe/H] are shown in Fig. 14. For [Fe/H] < -0.3, [X/Fe] for the thick-disc stars are distinctly larger than for the thin-disc stars. In the [Fe/H] range -0.3 to -0.6 where thin- and thick-disc stars are well represented, there is a clear separation between

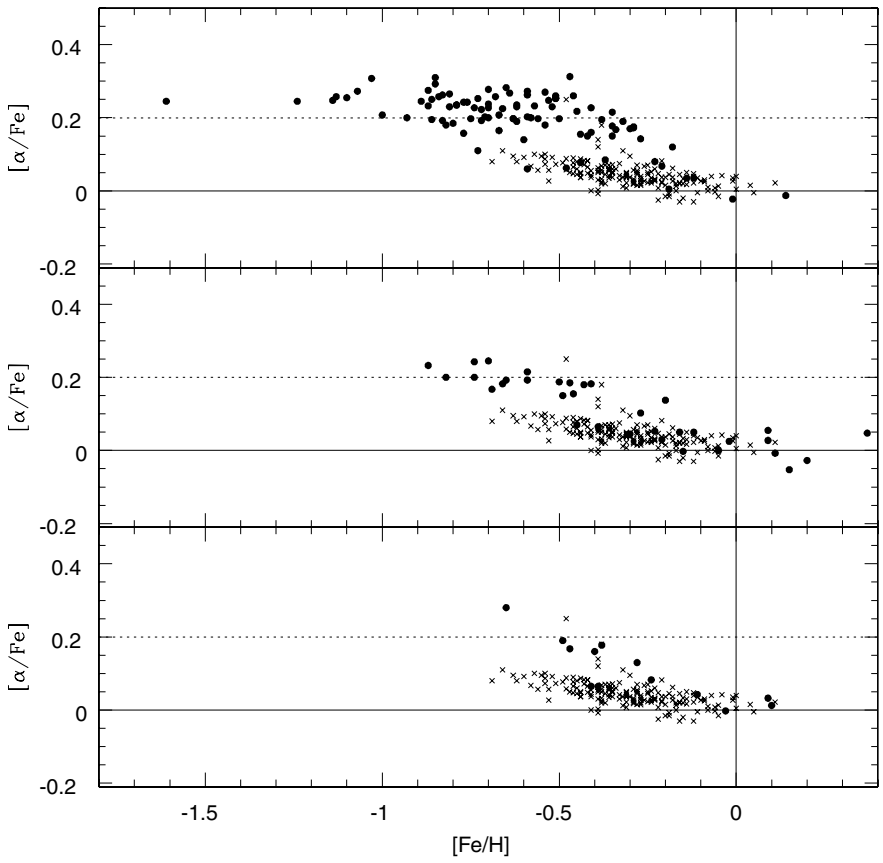

Figure 12. Run of [α/Fe] with [Fe/H] for thick ($P_{\rm thick} \geqslant 70$ per cent: top panel), thick/thin (50 per cent $< P_{\rm thick} < 70$ per cent: middle panel), and thin ($P_{\rm thin} \geqslant 70$ per cent: bottom panel) for the present sample. Also shown are thin-disc stars from Paper I (crosses).

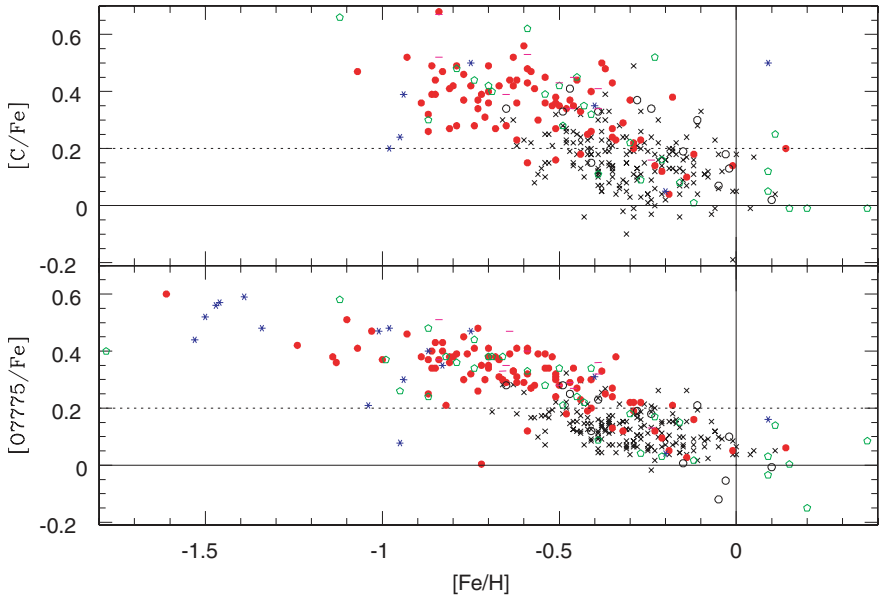

Figure 13. Abundance ratio [X/Fe] of C and O against [Fe/H] for the present sample (circles) and the thin-disc sample (crosses) from Paper I. Present disc sample is divided according to probability of belonging to the thick disc (filled red circles), the thin disc (open red circles), the halo (blue circles), and the stars which might belong to either the thin or the thick disc (green pentagons), and stars which might belong to either the halo and the thick disc (magenta dashes).

[α/Fe] of Mg, Si, Ti, and probably also Ca for thin- and thick-disc stars. For metal-rich stars of [Fe/H] $\geqslant -0.3$, the thin- and thick-disc stars show similar abundances. We comment below (see Section 6) on the possibility that there is a smooth transition for [X/Fe] from a positive displacement above its thin-disc value for [Fe/H] < -0.3 to the thin-disc value for [Fe/H] > 0.0. The thick-disc [X/Fe] ratios smoothly merge with the halo ratios in the overlapping metallicity range.

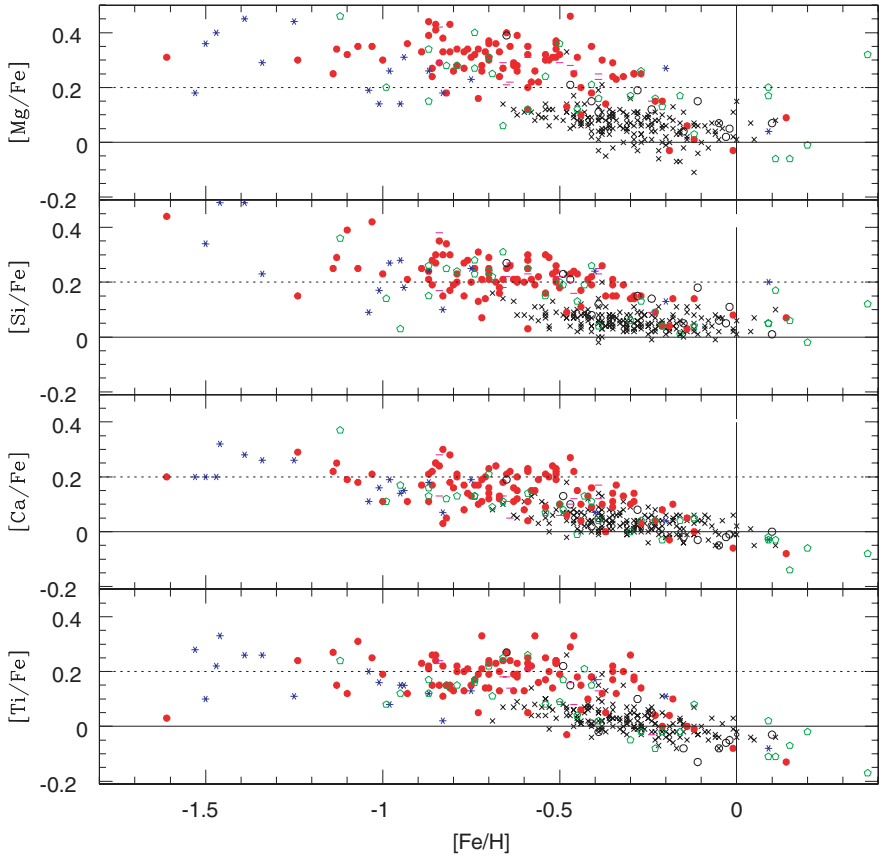

Figure 14. Abundance ratio [X/Fe] for the Mg-like elements Mg, Si, Ca and Ti against [Fe/H] for the present sample (circles) and the thin-disc sample (crosses) from Paper I. Key for the symbols is same as is earlier figures.

Our results for the α-elements in the thick disc agree very well with Prochaska et al.'s (2000) results for their sample of 10 stars with [Fe/H] between -0.5 and -1.2. Our results also agree with the results from Fuhrmann (1998, 2004) for Mg, and Bensby et al. (2005) for Mg, Si, Ca and Ti (see Figs 9–11).

Aluminium. An odd-Z element Al might have been expected to behave like Na, another odd-Z light element. This expectation is not met (Fig. 15); Al is Mg-like and Na is Ni-like. Our results below solar metallicity agree with those by Prochaska et al. (2000) and Bensby et al. (2005). Above [Fe/H] = 0.0, Bensby et al., also Chen et al. (2000), showed [Al/Fe] increasing with increasing [Fe/H]. Our samples contain too few metal-rich stars to detect this interesting trend. Below the metal-poor end of our sample, [Al/Fe] ratios for halo stars are seen to be sharply decreasing with decreasing [Fe/H] (e.g. Spite & Spite 1980; Gehren et al. 2004).

Scandium. The ratio [Sc/Fe] with [Fe/H] shows an interesting trend. Above [Fe/H] = -0.3, [Sc/Fe] ratios are similar for thin- and thick-disc stars. Below [Fe/H] = -0.3, [Sc/Fe] appears constant with an excess – albeit slight – above thin-disc values, a characteristic of an Mg-like element. A keen eye may suggest that [Sc/Fe] slowly increases and then decreases at around [Fe/H] ≈ -0.5 and returns to the solar ratio.

A similar trend of increasing [Sc/Fe] with [Fe/H] and then decreasing was seen for disc F- and G- dwarfs (Nissen et al. 2000; Prochaska & McWilliam 2000). For their thick-disc stars with [Fe/H] range of -0.4 to -1.2, Prochaska et al.'s results agree with our larger data set in magnitude and trend.

Vanadium. Below [Fe/H] = -0.3, [V/Fe] of thick-disc stars is slightly larger than for thin-disc stars. In the [Fe/H] range -0.3 to -1.6, [V/Fe] is almost flat with [Fe/H]. Our thick-disc results are consistent with those from Prochaska et al. (2000).

Peterson (1981) derived [V/Fe] ratios for 22 moderately metal-poor ([Fe/H] = -0.5 to -1.5) F-G-K dwarfs. Her results showed a clear and approximately uniform enhancement of [V/Fe] relative to solar except for two stars at the low [Fe/H] limit of the sample. A quick look at the kinematics of her sample showed many of them to have $V_{\rm LSR} \leqslant -40\,{\rm km\,s^{-1}}$, indicating membership of the thick disc or the halo.

Cobalt. Fig. 15 shows that cobalt is an Mg-like element. For thick-disc stars, [Co/Fe] is almost flat with [Fe/H], in good agreement with the results obtained by Prochaska et al. (2000). For thin-disc stars, a weak trend of decreasing [Co/Fe] with increasing [Fe/H] is apparent in the range $-0.5 <$ [Fe/H] < 0.0. This is consistent with the results of Allende Prieto et al. (2004) for that interval (with the exception of a small-scale offset).

Zinc. Zinc appears to be indistinguishable between the thin-disc and thick-disc stars in the common metallicity range. We note, however, that for thin-disc stars, there is evidence for a mild trend of increasing [Zn/Fe] with decreasing [Fe/H], as previously reported by Nissen et al. (2004), Allende Prieto et al. (2004) and Bensby et al. (2005). The latter two studies also reported an increase of the Zn/Fe ratios at [Fe/H] > 0.

5.5 The Ni-like elements

The Ni-like elements include Na, Mn, Cr, Ni and Cu. Prochaska et al. were the first to show that these elements (relative to Fe) behaved similarly in thick- and thin-disc stars. Bensby et al. (2005)

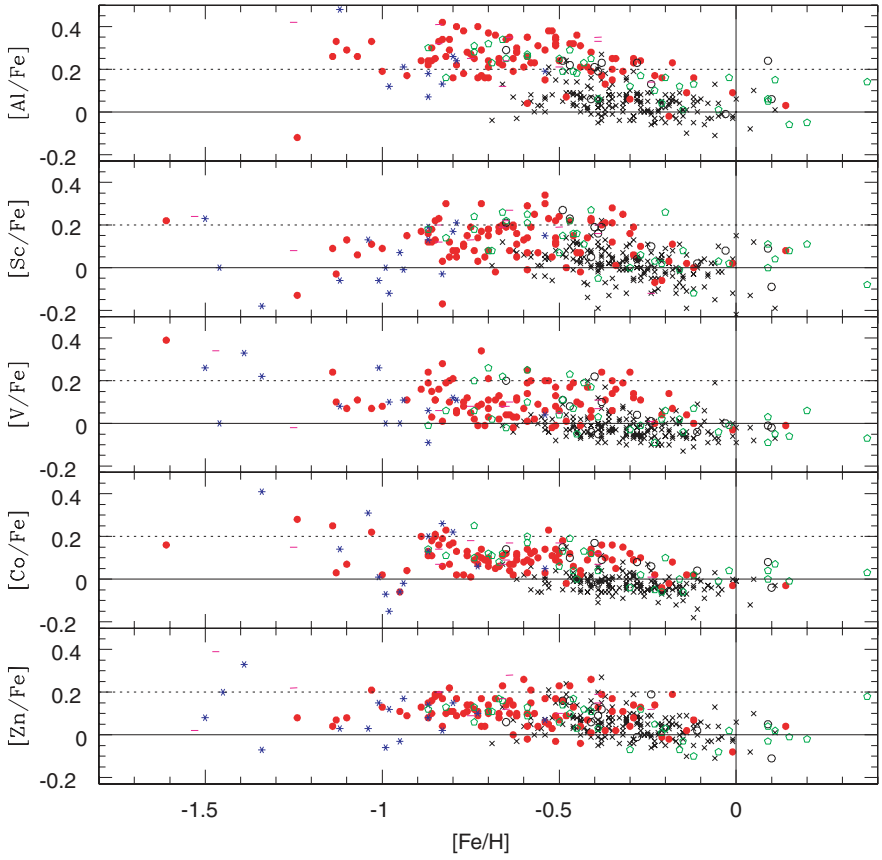

Figure 15. Abundance ratio [X/Fe] for the Mg-like elements Al, Sc, V, Co and Zn against [Fe/H] for the present sample (circles) and the thin-disc sample (crosses) from Paper I. Key for the symbols is same as in Fig. 13.

Table 7. Mean [X/Fe] values (M) in the bin of [Fe/H] -0.45 to -0.55 and the the coefficients (B) of the slope of the linear regression fit to the runs of [X/Fe] versus [Fe/H] in the metallicity range -0.3 to -1.0 for the thin- and thick-disc stars. The value Δ[X/Fe] in column 6 is the difference between $M_{\rm thick}$ and $M_{\rm thin}$.

[X/Fe]	$M_{\rm thin}$	$B_{\rm thin}$	$M_{\rm thick}$	$B_{\rm thick}$	Δ[X/Fe]
[C/Fe]	0.22 ± 0.08	-0.23 ± 0.04	0.35 ± 0.08	-0.23 ± 0.06	0.13
[O/Fe]	0.24 ± 0.07	-0.19 ± 0.03	0.36 ± 0.19	-0.25 ± 0.05	0.12
[Na/Fe]	0.09 ± 0.04	-0.15 ± 0.03	0.12 ± 0.05	-0.06 ± 0.04	0.03
[Mg/Fe]	0.11 ± 0.06	-0.15 ± 0.03	0.32 ± 0.06	-0.10 ± 0.03	0.21
[Al/Fe]	0.12 ± 0.06	-0.11 ± 0.03	0.30 ± 0.09	-0.01 ± 0.06	0.18
[Si/Fe]	0.08 ± 0.05	-0.09 ± 0.02	0.22 ± 0.06	-0.11 ± 0.03	0.14
[Ca/Fe]	0.06 ± 0.04	-0.13 ± 0.02	0.18 ± 0.06	-0.12 ± 0.02	0.12
[Sc/Fe]	0.05 ± 0.05	-0.17 ± 0.04	0.17 ± 0.10	$+0.14 \pm 0.05$	0.12
[Ti/Fe]	0.06 ± 0.05	-0.18 ± 0.02	0.21 ± 0.09	-0.03 ± 0.03	0.15
[V/Fe]	-0.01 ± 0.04	-0.10 ± 0.03	0.10 ± 0.08	$+0.02 \pm 0.04$	0.11
[Cr/Fe]	-0.02 ± 0.02	$+0.03 \pm 0.01$	0.00 ± 0.04	$+0.04 \pm 0.03$	0.02
[Mn/Fe]	-0.18 ± 0.05	$+0.16 \pm 0.02$	-0.22 ± 0.05	$+0.38 \pm 0.04$	-0.04
[Co/Fe]	0.00 ± 0.05	-0.10 ± 0.02	0.11 ± 0.06	-0.03 ± 0.03	0.11
[Ni/Fe]	0.00 ± 0.02	-0.00 ± 0.01	0.04 ± 0.03	-0.03 ± 0.04	0.04
[Cu/Fe]	-0.01 ± 0.04	-0.05 ± 0.04	0.06 ± 0.09	$+0.48 \pm 0.06$	0.07
[Zn/Fe]	0.09 ± 0.07	-0.14 ± 0.07	0.12 ± 0.07	-0.11 ± 0.08	0.03
[Y/Fe]	-0.03 ± 0.1	0.16 ± 0.04	0.01 ± 0.08	-0.10 ± 0.06	-0.04
[Ba/Fe]	-0.04 ± 0.11	$+0.09 \pm 0.06$	-0.19 ± 0.08	-0.10 ± 0.07	-0.10
[Ce/Fe]	-0.01 ± 0.10	$+0.00 \pm 0.05$	0.03 ± 0.09	$+0.00 \pm 0.06$	0.04
[Nd/Fe]	0.04 ± 0.18	-0.03 ± 0.06	0.15 ± 0.10	-0.04 ± 0.04	0.11
[Eu/Fe]	0.15 ± 0.06	-0.26 ± 0.03	0.38 ± 0.11	-0.20 ± 0.09	0.23

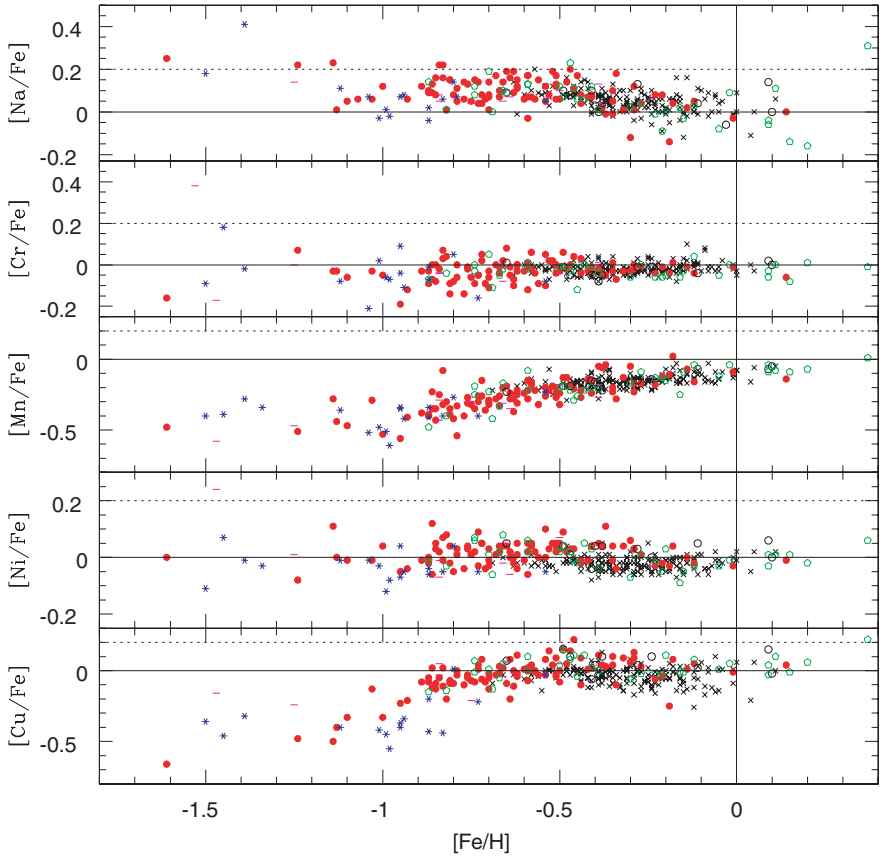

Figure 16. Abundance ratio [X/Fe] for the Ni-like elements Na, Mn, Cr, Ni and Cu against [Fe/H] for the present sample (circles) and the thin-disc sample (crosses) from Paper I. Key for the symbols is same as in earlier figures.

confirmed the Ni-like behaviour of Na, Cr and Ni, but did not consider either Mn or Cu in their analyses. Our results for the quintet are shown in Fig. 16. Of special interest, perhaps, is the example of Mn where [Mn/Fe] is a quite steeply increasing function of Fe, yet thin- and thick-disc stars form a single relation. The contrast between the odd–even Na (Ni-like) and Al (Mg-like) is also interesting.

Sodium. This odd-Z and proton-capture element seems to be a difficult one for which to obtain consistent values. We suspect departures from LTE are behind these difficulties. There are several studies but no two are in very good agreement. For example, Chen et al.'s (2000) study of disc F- and G- dwarfs showed a flat trend of [Na/Fe] with [Fe/H] without Na enhancement. Edvardsson et al.'s (1993) results suggested that [Na/Fe] increases with [Fe/H] for stars of [Fe/H] > 0.0, and an apparent slow rise in [Na/Fe] with decreasing [Fe/H] for stars with [Fe/H] < 0.0. Prochaska et al. (2000) found an enhancement of Na for 10 thick-disc stars without any trend with [Fe/H].

The results from our study are based on the two Na I lines: 6154 and 6160 Å. Results indicate no visible (Fig. 16) demarcation between the thin- and thick-disc samples. Examination of the plot indicates a possible slow increase of [Na/Fe] with decreasing [Fe/H], reaching a maximum value of [Na/Fe] ≈ 0.15 at [Fe/H] ≈ -0.6. From the maximum, [Na/Fe] may fall with decreasing [Fe/H]. Recent analysis of disc dwarfs by Shi, Gehren & Zhao (2004) using the same lines as we did but with NLTE treament suggests a similar trend of [Na/Fe] in [Fe/H] range 0.0 to -1.0. For metal-rich stars, they confirm Edvardsson et al.'s (1993) results.

Chromium and Nickel. Chromium shows [X/Fe] $\simeq 0.02 \pm 0.04$ between thick- and thin-disc stars. Chromium tracks Fe well up to around [Fe/H] $\simeq -0.6$, but [Cr/Fe] is negative for lower [Fe/H]. Nickel tracks Fe throughout the [Fe/H] range. Possibly, [Ni/Fe] is larger for thick-disc stars compared to thin disc but the mean difference is just 0.04 ± 0.03. A small overabundance of Ni for the thick-disc stars is suggested by the equivalent figures given by Prochaska et al. (2000) and Bensby et al. (2005).

Manganese. As shown in Fig. 16, [Mn/Fe] is a function of [Fe/H]. [Mn/Fe] ratios at a given [Fe/H] for thin, thick, and halo stars are the same. Below [Fe/H] $= -1.0$, [Mn/Fe] shows a flat trend with [Fe/H]. Above [Fe/H] $= -1.0$, Mn steadily increases with increasing [Fe/H]. Our results are in agreement with Mn results for disc and halo stars (Nissen et al. 2000), and the 10 thick-disc stars analysed by Prochaska et al. (2000).

Copper. Copper is a Ni-like element in the [Fe/H] interval populated by both thin- and thick-disc stars; there is a hint that [Cu/Fe] is slightly greater for the thick-disc stars: Δ[Cu/Fe] $= +0.07$ (Table 7). This result was shown by Prochaska et al. (2000). At [Fe/H] < -0.8, [Cu/Fe] falls below the solar value, possibly in a precipitous way. Our results generally confirm earlier results for disc and halo stars (Sneden, Gratton & Crocker 1991; Mishenina et al. 2002; Bihain et al. 2004; Simmerer et al. 2004).

5.6 The *s*- and *r*-process elements

Synthesis of elements beyond the iron group occurs by two neutron-capture processes: the *s*-process occurring in asymptotic giant

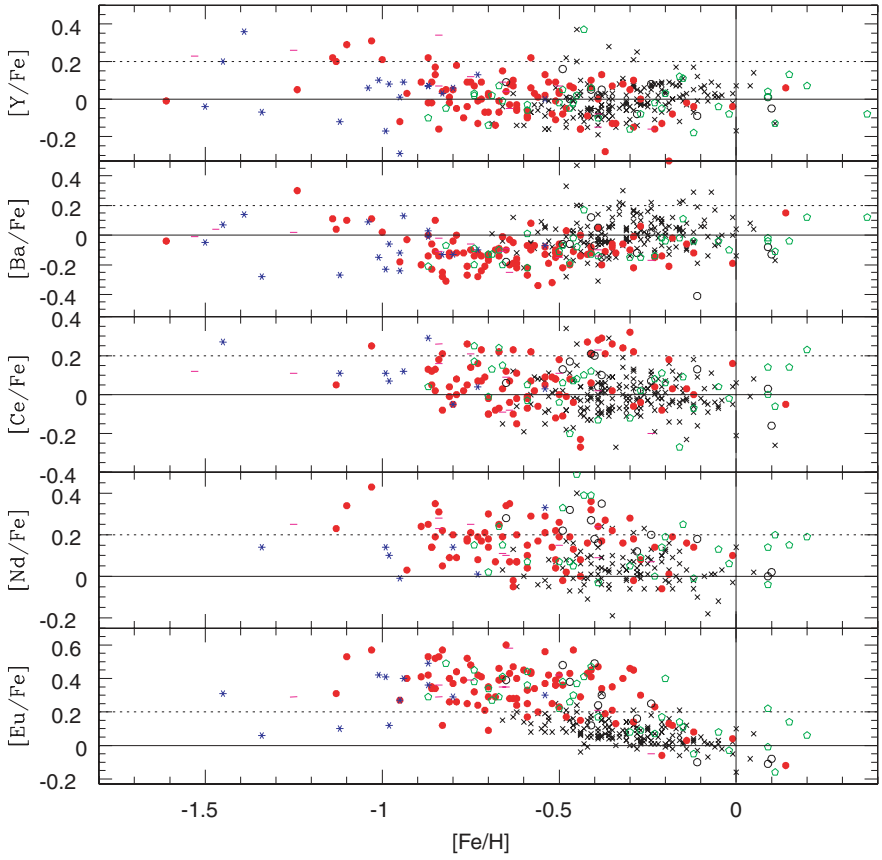

Figure 17. Abundance ratio [X/Fe] for Y, Ba, Ce, Nd, and Eu against [Fe/H] for the thick-disc stars(circles) and the thin-disc stars (crosses) from Paper I. Key for the symbols is same as in earlier figures.

branch (AGB) stars, and the *r*-process occurring (probably) in Type II supernovae (SN II). In the solar system mix of elements, barium is predominantly an *s*-process product and europium an *r*-process product. Our suite of neutron-capture elements includes not only Ba and Eu, but also Y, Ce and Nd. According to Burris et al.'s (2000) resolution of the solar elemental abundances, the contributions from the *s*-process are 72 per cent for Y, 85 per cent for Ba, 81 per cent for Ce, 47 per cent for Nd, and merely 3 per cent for Eu. Bensby et al. (2005) determined abundances for Y, Ba and Eu showing differences in the behaviour of the *s*- and *r*-process contributions between the thin and thick discs.

Our abundances for Y, Ba, Ce, Nd and Eu are based with one exception on the lines used in Paper I. The exception concerns Eu for which we use the resonance line at 4129 Å, but in Paper I we used the subordinate line at 6645 Å. The atomic data for the 4129-Å line are taken from Kurucz (1998), and the isotopic abundance ratio was set at the solar value: $^{151}\mathrm{Eu}/^{153}\mathrm{Eu} = 53/47$. The 4129-Å line was analysed in all stars of the present sample and also those in Paper I. The Eu abundances from the 4129- and 6645-Å lines are in good agreement for the Paper I's stars.

The trends of the abundances of Y, Ba, Ce, Nd and Eu with [Fe/H] (Fig. 17) show a difference between the contributions of the *s*-process and *r*-process to the thin and thick discs, as found by Bensby et al. The elements – Y, Ba and Ce – expected to have a dominant *s*-process contribution are Ni-like elements. Our results for Y agree with thick-disc results from Prochaska et al. (2000). However, Bensby et al. (2005) found [Y/Fe] ratios showing a slow decreasing trend with decreasing [Fe/H], but the [Y/Fe] ratios at given [Fe/H] are almost same for both thin- and thick-disc stars, similar to our present results. In the case of Ba, our [Ba/Fe] ratios for thick-disc stars are on average smaller by 0.1 dex than for thin-disc stars. There also may be small trend of decreasing [Ba/Fe] with decreasing [Fe/H]. Again our and Prochaska et al.'s results for Ba agree, both in trend and magnitude. Both Bensby et al. (2005) and Allende Prieto et al. (2004) found thin-disc stars to show a possible maximum of [Ba/Fe] at [Fe/H] ~ -0.2, but such feature is not present in our data.

Europium is an Mg-like element. The scatter in [Eu/Fe] at a given [Fe/H] is attributable to the measurement errors. The large scatter in Eu results for the thick compared to the thin disc may be attributed to large number of cooler stars in thick-disc sample. Continuum placement at 4129 Å is more difficult for the cooler stars, and also sensitivity to the model parameters is different. Eu results agree quite well with the Eu results from Prochaska et al. (2000) and Bensby et al. (2005).

Neodymium which is provided about equally by the *s*- and *r*-process in the solar mix of abundances can be imagined from Fig. 17 to be a mix of an Mg-like and an Ni-like element. We do not confirm the trend of increasing [Nd/Fe] with decreasing [Fe/H] reported by Allende Prieto et al. (2004) for thin-disc stars.

5.7 Cosmic scatter

In Paper I, we showed that the scatter of the [X/Fe] values about the mean trend was entirely dominated by the measurement errors, that is, there was no hint of a cosmic scatter in the values found for

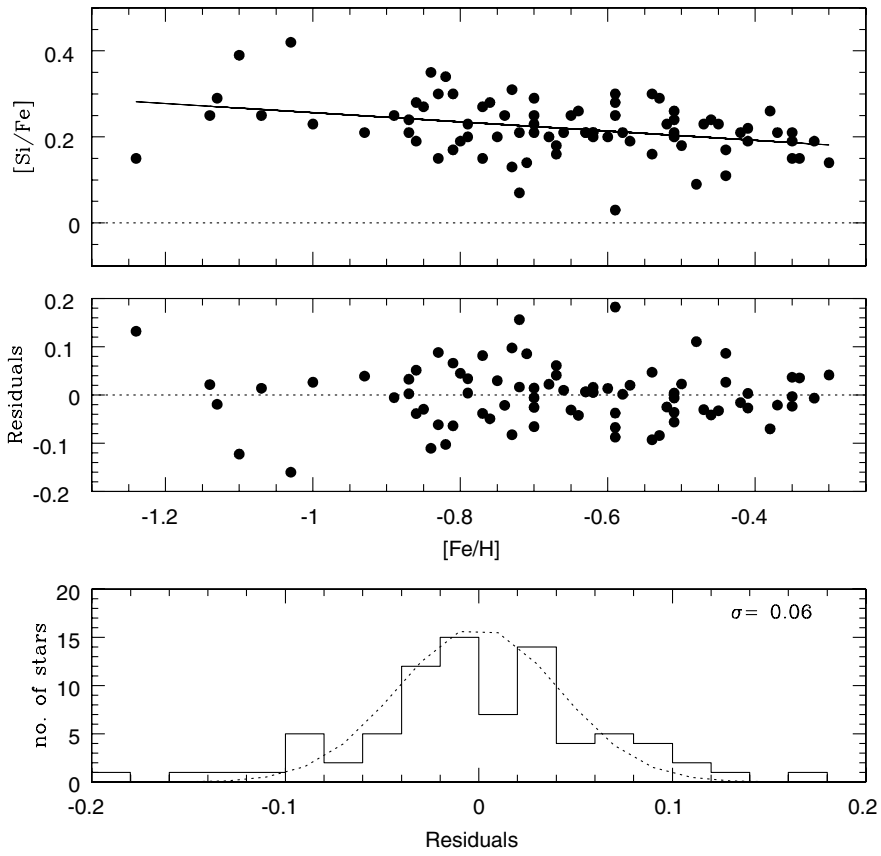

Figure 18. Top panel: [Si/Fe] against [Fe/H]. The solid line is the linear regression fit to the data. Middle panel: the residuals around the mean fit. Bottom panel: histogram and the Gaussian fit to the residuals.

the thin-disc stars. It is of value to determine if the thick-disc stars betray cosmic scatter in their [X/Fe] values.

We estimate the scatter in [X/Fe] for the thick disc by removing the linear fit made to the data points for [Fe/H] < -0.3 and fitting a Gaussian to the residuals – see Fig. 18 for [Si/Fe]. In Table 8, we list the Gaussian $\sigma_{\rm Gau}$ and the expected $\sigma_{\rm mod}$ from the congeries of measurement errors. The same quantities from Paper I are also tabulated. The comparison of $\sigma_{\rm Gau}$ with $\sigma_{\rm mod}$ (Fig. 19) shows that they are very similar, that is, there is no detectable cosmic scatter for the sampled elements for thick-disc stars with [Fe/H] < -0.3. Oxygen's $\sigma_{\rm mod}$ determined from the [O/Fe] obtained from the O abundances based on the O I 7772 Å line, after introducing an empirical correction for departures from LTE, greatly exceeds the measured scatter ($\sigma_{\rm Gau}$) which is apparently overestimated for these high-excitation lines.

6 CHEMICAL EVOLUTION OF THE THICK DISC

By chemical evolution is meant the run of [X/Fe] versus [Fe/H] for a suite of elements X sampling the major sites and processes of stellar nucleosynthesis. Here, the Mg-like elements separate the thick- from thin-disc stars, and it is their evolution that we address first. To reduce the observational uncertainties as much as possible, we use the composite index [α/Fe] from the average of the four indices [X/Fe] for X = Mg, Si, Ca and Ti. The individual indices are given equal weight. The index [α/Fe] versus [Fe/H] is shown in Fig. 20. Two representations of the thick-disc chemical evolution are suggested by the inspection of Fig. 20.

Table 8. The predicted uncertainty, $\sigma_{\rm mod}$ and the $\sigma_{\rm Gau}$ resulting from a Gaussian fit to the residuals for the thin- and thick-disc stars are given.

[X/Fe]	Thin disc		Thick disc	
	$\sigma_{\rm mod}$	$\sigma_{\rm Gau}$	$\sigma_{\rm mod}$	$\sigma_{\rm Gau}$
[Fe/H]	0.07	...	0.08	...
[C/Fe]	0.14	0.07	0.14	0.09
[O/Fe]	0.16	0.07	0.19	0.07
[Na/Fe]	0.03	0.04	0.05	0.07
[Mg/Fe]	0.04	0.04	0.05	0.07
[Al/Fe]	0.04	0.05	0.05	0.08
[Si/Fe]	0.05	0.04	0.07	0.06
[Ca/Fe]	0.03	0.04	0.03	0.06
[Sc/Fe]	0.11	0.05	0.11	0.09
[Ti/Fe]	0.03	0.04	0.06	0.06
[V/Fe]	0.04	0.04	0.06	0.10
[Cr/Fe]	0.02	0.03	0.03	0.04
[Mn/Fe]	0.04	0.04	0.03	0.04
[Co/Fe]	0.02	0.04	0.03	0.06
[Ni/Fe]	0.02	0.03	0.04	0.04
[Cu/Fe]	0.02	0.06	0.04	0.08
[Zn/Fe]	0.05	0.06	0.10	0.06
[Y/Fe]	0.09	0.07	0.11	0.12
[Zr/Fe[	0.10	0.07	0.11	0.12
[Ba/Fe]	0.12	0.08	0.12	0.11
[Ce/Fe]	0.11	0.08	0.11	0.10
[Nd/Fe]	0.10	0.07	0.11	0.09
[Eu/Fe]	0.11	0.08	0.13	0.08

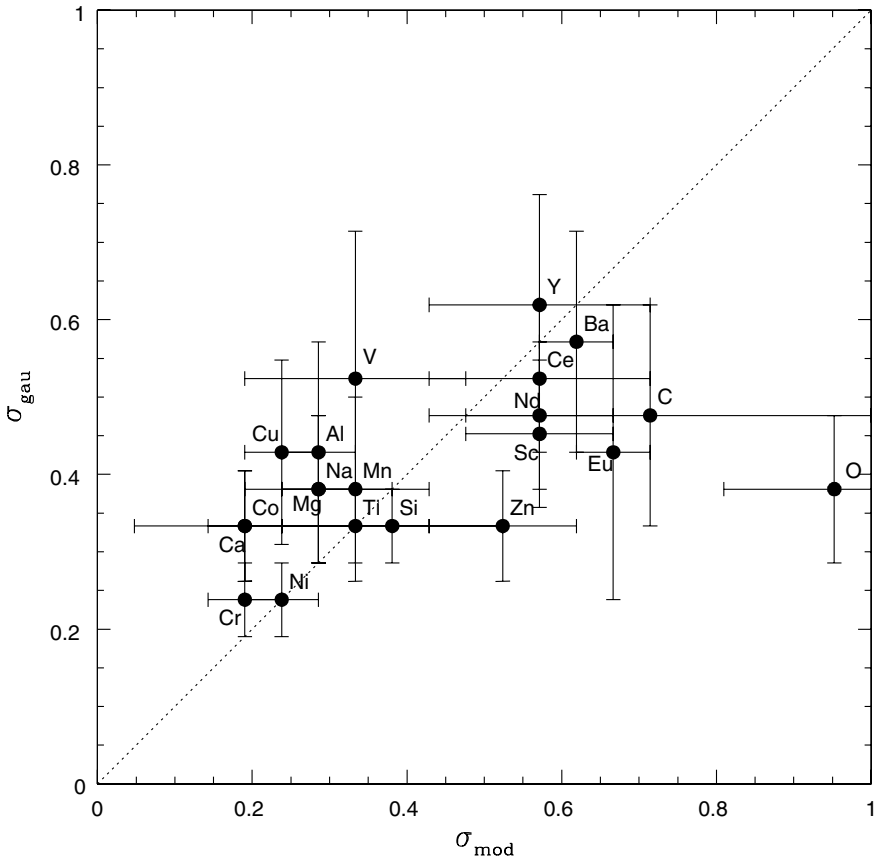

Figure 19. The errors in the abundance ratios [X/Fe] as represented by σ_{mod} are compared with σ_{Gau}, the dispersion of the Gaussian distribution of the [X/Fe] residuals.

First, as proposed by Bensby et al. (2003), [α/Fe] of the thick disc is greater than for the thin disc for [Fe/H] < -0.3, but at about an [Fe/H] of -0.3, the [α/Fe] appears to tend towards thin-disc values and for [Fe/H] > -0.2, thick- and thin-disc stars are chemically identical to within the measurement errors. Bensby et al. spoke of a 'knee' linking the thick-disc stars of [Fe/H] < -0.3 with those of [Fe/H] > -0.2. This puts all but a few of our thick-disc stars into a single relation. The exceptions are the five stars in Fig. 20 with [Fe/H] < -0.3 with thick-disc kinematics but a thin-disc [α/Fe].

In an alternative representation proposed here, the thick disc is restricted to [Fe/H] less than about -0.3, and the above five exceptions with thin-disc compositions but thick-disc kinematics are considered to form a single relation with the thick-disc stars of [Fe/H] > -0.3. Thirteen of our thick-disc stars from across the [Fe/H] spanned by the thin disc form this latter relation which is

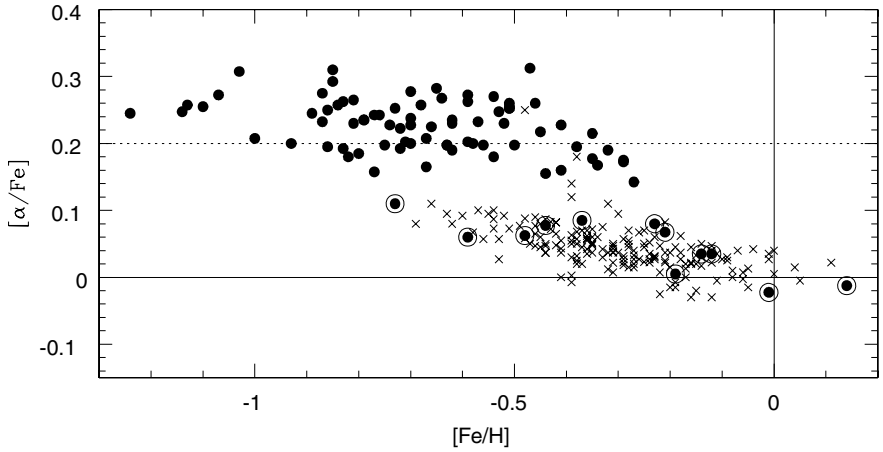

Figure 20. Abundance ratios [α/Fe] versus [Fe/H] for the thick- and thin-disc stars. Solid lines represent solar ratios of [α/Fe] and [Fe/H] = 0, and the broken line indicate a value of [α/Fe] = +0.2.

considered distinct from the more populated thick-disc relation between [α/Fe] and [Fe/H] < -0.3. In this representation, there is no knee connecting thick- and thin-disc stars.

Before commenting further on the two representations, we remark upon the stars – five in one and 13 in the other representation – with the kinematics of the thick disc but abundances of the thin disc: here, we refer to these as the TKTA stars.

6.1 The TKTA stars

The TKTA stars have *contaminated* some previous studies. For example, the eight thick-disc stars in Mishenina et al.'s (2004) sample with [Fe/H] > -0.3 had the abundance pattern of the thin disc. Application of our membership criteria reduces the octet to a single thick-disc star. Although all eight have a negative $V_{\rm LSR}$ (-40 to $-100\,{\rm km\,s^{-1}}$) outside the normal range for thin-disc stars, they with a single exception have a low $W_{\rm LSR}$ and so remain close to the Galactic plane, a fact noted by Mishenina et al. The exception at [Fe/H] of $+0.12$ is a TKTA star by our definition.

Bensby et al. (2003, 2005) were the first to suggest that thin- and thick-disc abundance patterns converged for [Fe/H] > -0.2. According to our criteria, 17 of their stars belong to the thick disc. One of the 17 is a TKTA star with [Fe/H] $= -0.37$. Other potential TKTA stars are at metallicities for which thin and thick disc have the same abundance pattern.

In our larger sample, we have five TKTA stars at a low [Fe/H] such that their abundances clearly separate them from the majority of the thick-disc stars. It is unlikely that the five are mistakenly identified as the TKTA stars through a conspiracy of errors. The individual [X/Fe] contributing to the [α/Fe] each mark them out as having thin-disc abundances. One of the five (HIP 50671) was earlier analysed by Edvardsson et al. (1993) who obtained a similar [Fe/H] (-0.42 versus our -0.48) and [α/Fe] (0.05 versus our 0.06). Another (HIP 31188) was treated by Fuhrmann (1998) whose [Fe/H] was -0.81 versus our -0.59 and [Mg/Fe] was $+0.22$ versus our $+0.12$. If placed in Fig. 9, the star would fall on an extension of the Fuhrmann's thin-disc abundances and below his thick-disc abundance of [Mg/Fe] of 0.4 for his [Fe/H]. It should be considered a possible TKTA star when judged solely by Fuhrmann et al.'s abundances. A fresh study of HIP 31188 may be desirable but we note that our Si, Ca, and Ti abundances support our low value of [Mg/Fe].

The set of 13 TKTA stars with the additional examples from Mishenina et al. and Bensby and colleagues run in [Fe/H] over the entire metallicity spread of the thin disc. The close correspondence between the compositions of the TKTA stars and thin disc suggest that there is a close relation between the two groups. Heating of the thin disc is a well-known phenomenon: the dispersion of the components ($U_{\rm LSR}$, $V_{\rm LSR}$, $W_{\rm LSR}$) increases with age. Nordström et al. (2004) provided a recent determination of the dispersion–age relations. Perhaps, the TKTA stars are thin-disc stars which have been heated to resemble the genuine thick-disc stars. The old ages of the TKTA stars favour above average heating and, perhaps, owing to the stochastic nature of the heating processes, the TKTA stars were subjected to much greater than normal heating. Low-mass analogues of the runaway B stars are a possibility. Against the association of the TKTA stars with the thin disc is the fact that on average the TKTA stars appear to be systematically a couple of Gyr older than the oldest thin-disc stars (Fig. 24 below).

The TKTA stars appear to be confined to certain parts of the ($U_{\rm LSR}$, $V_{\rm LSR}$, $W_{\rm LSR}$) space. Fig. 21 using [α/Fe] to distinguish thick- from thin-disc stars shows that the TKTA stars tag on to the low-$V_{\rm LSR}$ tail of the thin-disc stars. The TKTA stars favour positive $U_{\rm LSR}$ over negative values but are distributed in $W_{\rm LSR}$ in a similar way to thick-disc stars. A wider exploration of ($U_{\rm LSR}$, $V_{\rm LSR}$, $W_{\rm LSR}$) space may reveal some clumping of TKTA stars, an indication of a moving group.

6.2 The knee

In the representation in which TKTA stars are given an identity apart from the thick-disc stars (i.e. thin-disc stars with special kinematics), thick-disc stars are restricted to [Fe/H] less than about < -0.3 or -0.2. The alternative representation proposed by Bensby et al. (2003) introduces a knee in the thick-disc [X/Fe] versus [Fe/H] for an Mg-like element such that the near-constant [X/Fe] for [Fe/H] < -0.3 merges smoothly with the lower [X/Fe] values of thin- and thick-disc results for [Fe/H] > -0.1 or so. (The TKTA stars with [Fe/H] < -0.3 still require a special interpretation in this scenario.) Interpretations of the chemical evolution of the thick disc differ for these different representations.

The leading suggestion of a 'knee' was made by Bensby and colleagues. Comparison with our results is made by combining the index [α/Fe] from the abundances obtained by Bensby and colleagues with our probability criteria for stellar populations. Fig. 22 shows the result where thick-disc stars by our criteria are shown by the larger filled triangles and thin-disc stars by small open triangles. Small filled triangles represent stars with a probability of 50 to 70 per cent of belonging to the thick disc (these were assigned to the thick disc by Bensby et al.). Compare this figure with Fig. 20. Although a knee could be drawn in Fig. 22, our representation of a thick disc terminating at about [Fe/H] of -0.3 and a separate thin-disc relation with superposed TKTA stars would appear to be as satisfactory a fit. Fig. 22 shows one TKTA star (HIP 3704) with [Fe/H] < -0.3 but three with [Fe/H] > -0.1. The thick-disc relation may show a slight drop in [α/Fe] near [Fe/H] $= -0.3$.

Bensby et al. would likely contend that the principal evidence for the knee lies in their results for oxygen (Bensby et al. 2004, 2005) which show a near-linear and continuous relation for [O/Fe] versus [Fe/H] in thick-disc stars with no hint of a discontinuity at [Fe/H] ~ -0.3. Existence of the knee would appear to depend, however, on the [O/Fe] values for just two to four stars in the interval [Fe/H] of about -0.3 to 0.0. The oxygen abundances derived from the [O I] 6300 Å line (corrected for a blending Ni I line) provide the clearest evidence for the continuous relation. Abundances from the O I 7772 Å triplet do not offer decisive evidence in favour of a continuous relation for the thick-disc stars. Ramírez et al. (private communication), who performed a non-LTE analysis of the O I 7772 Å triplet for a large sample of thick-disc stars (our present sample plus about an additional 20 stars) suggest that the thick-disc [O/Fe] versus [Fe/H] relation shows no clear signs of a knee.

Marsakov & Borkova (2005) attempted to separate chemical evolution for thick and thin discs by discussing [Mg/Fe] indices compiled from the published values collated by Borkova & Marsakov (2005) who attempted to place the collated results for [Fe/H] and [Mg/Fe] from about 80 publications on common scales. Velocity components (U, V, W) are also provided. Thick-disc stars are separated from thin-disc stars by criteria that give results similar to ours. Marsakov & Borkova concluded that [Mg/Fe] for the thick disc starts to decline steeply from [Mg/Fe] $\simeq +0.4$ at [Fe/H] $\simeq -0.5$ to [Mg/Fe] $\simeq +0.1$ at [Fe/H] $= -0.3$ with a subsequent less-steep decline. This interpretation is based on the abundances for 133 thick-disc stars.

The separation in [Mg/Fe] at [Fe/H] $\simeq -0.3$ between thick- and thin-disc stars is not large (say, 0.2 dex) and, therefore, close

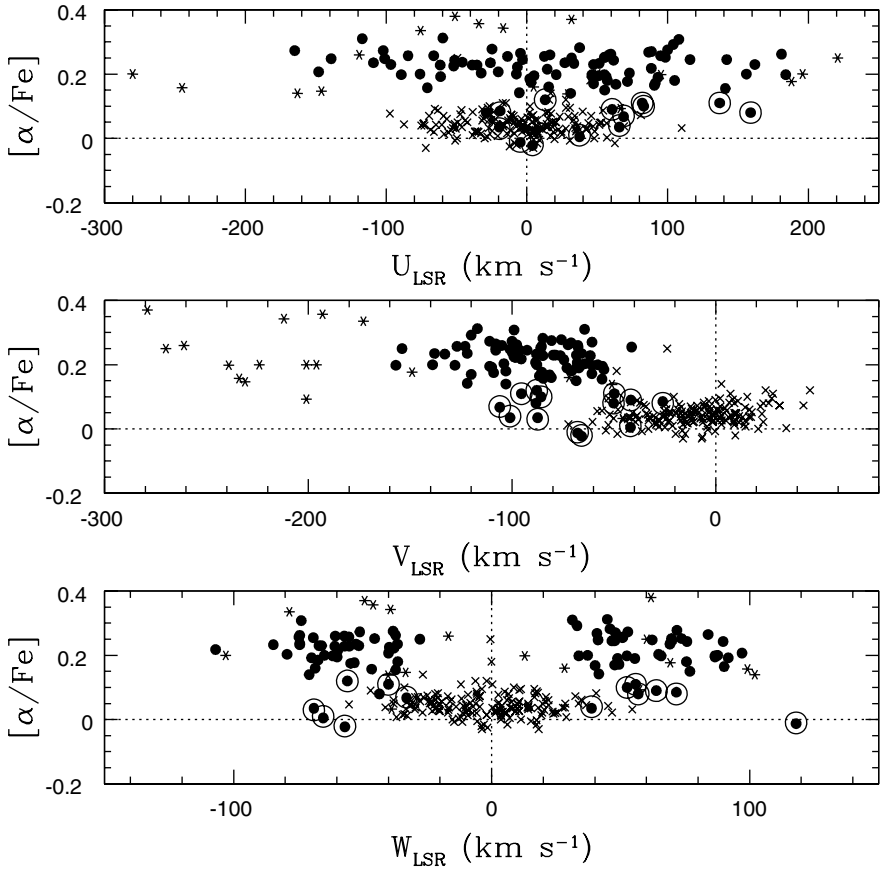

Figure 21. Ratio [α/Fe] verus $U_{\rm LSR}$, $V_{\rm LSR}$ and $W_{\rm LSR}$ for thick-disc (filled circles), thin-disc (crosses), halo (star symbols), and the TKTA stars (embedded filled circles).

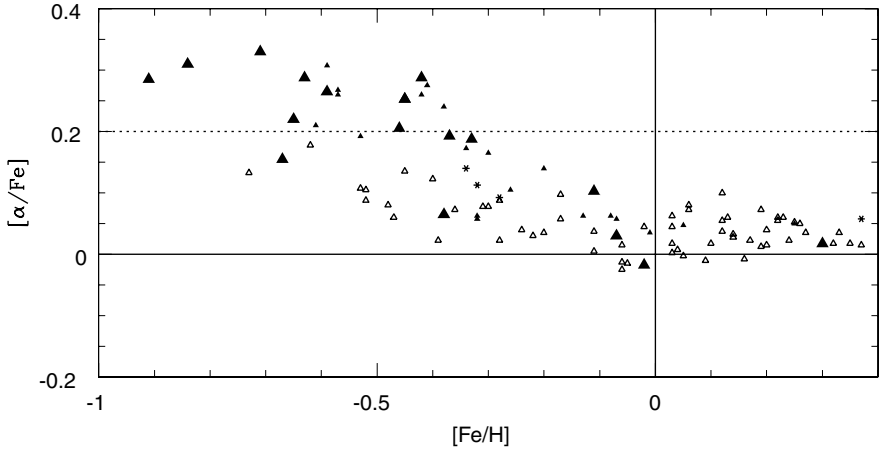

Figure 22. [α/Fe] index versus [Fe/H] for thick-disc (filled triangles), thin-disc (open triangles), and transition objects (star symbols) from Bensby and colleagues is shown. Large filled triangles represent thick-disc stars according to our criteria.

attention must be paid in combining measurements from different authors to relative precision and to normalization to common abundance scales for Mg and Fe. If selection of thick-disc stars is restricted to those stars with [Mg/Fe] from two or more sources, the evidence for the knee is greatly weakened (see Marsakov & Borkova's fig. 2b) for lack of thick-disc stars with [Fe/H] > -0.3 (three only). Only when stars with a single measurement of [Mg/Fe] are included is the thick disc quite well represented across the full [Fe/H] range (their fig. 2c), but the clean separation between thin- and thick-disc stars clearly obtained by Bensby et al. and by us is not found. This lack of a separation must cast doubt on the conclusions drawn by Marsakov & Borkova.

On applying our criteria to the space velocities given in the Borkova & Marsakov's (2005) catalogue and adopting their recommended [Mg/Fe], we obtain the results shown in Fig. 23 for stars with [Fe/H > -2.0. The top panel shows results for thick-disc stars alone; the majority of these 84 stars are drawn from the studies we have commented upon. This panel provides no support for a knee.

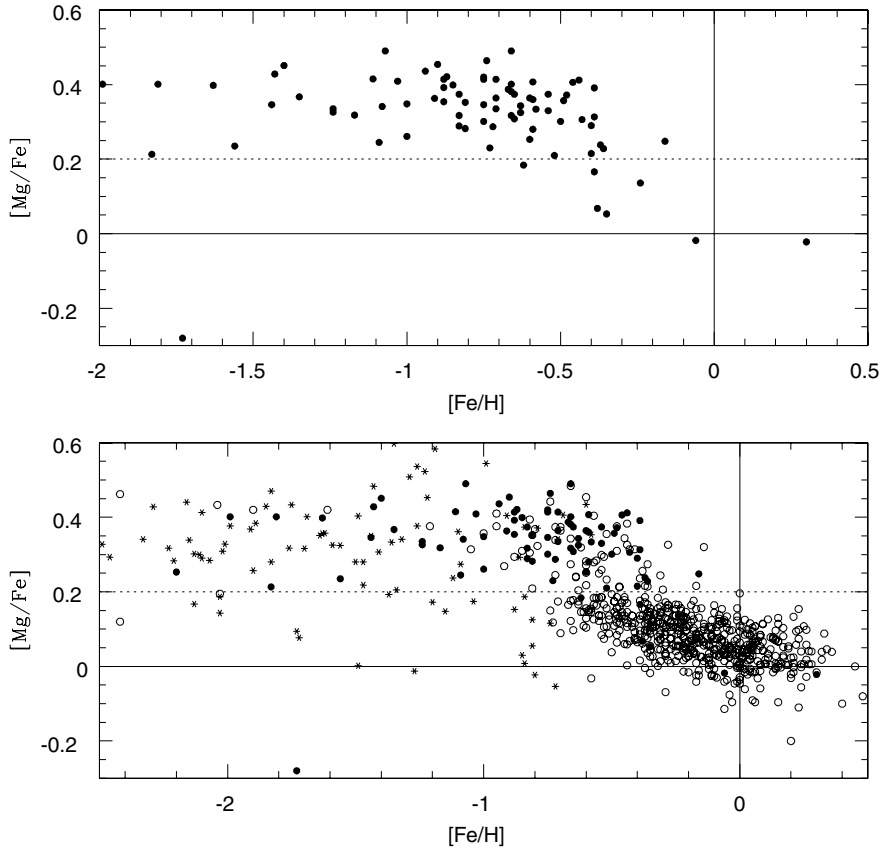

Figure 23. The catalogue (Borkova & Marsakov 2005) of published values of [Fe/H] and [Mg/Fe], and kinematics are subjected to our criteria for separating stars into thin-disc (open circles), thick-disc (filled circles), and halo components (star symbols). In the top panel, only stars with $P_{\rm thick} \geqslant 70$ (thick-disc stars) are shown. In the bottom panel, all the stars belonging to three components are shown.

The lower panel includes the thin and halo stars drawn again using our criteria from the catalogue. There is a large number of stars classified as belonging to the thin disc with an [Mg/Fe] of the thick disc.

Very recently, Brewer & Carney (2006) offered evidence in favour of a knee. Their sample of 23 G dwarfs contained, by their method of assigning population membership (see Venn et al. 2004), nine thin-disc and 14 thick-disc stars. The method overlooks the fact the three categories of membership (halo, thin and thick disc) are not represented equally in the solar neighbourhood (thin-disc stars dominate the stellar population). On applying the method in Section 3.2 in which the membership fractions are considered, we find that 18 of the 23 stars are thin-disc stars, the other five fall in our thin/thick-disc group with a maximum probability of belonging to the thick disc of under 50 per cent, and not a single star would be assigned the thick-disc status by us. None the less, consistent with our results in Fig. 12, the Brewer & Carney's precise abundances delineate the thin- and thick-disc trends of [α/Fe] with [Fe/H]. There may be evidence from stars with [Fe/H] ~ -0.2 and higher of a knee, but this comes from stars we would classify as belonging to the thin disc.

6.3 Stellar ages

Interpretations of the chemical evolution of the thick disc, as represented by a plot of [X/Fe] versus [Fe/H], should take account of the ages of thick- and thin-disc stars. There is a consensus that the mean age of the thick disc is about 5 Gyr greater than that of the thin disc when isochrone ages are estimated for stars in the solar neighbourhood. Evidence, described as tentative, also exists that thick-disc stars describe an age–metallicity relation (Bensby et al. 2004, 2005). Here, the age–metallicity relation and some connections between the ages and other properties are presented for our sample of thick-disc stars.

Determination of stellar ages was discussed in Section 4.5. Ages were obtained for 43 of the 95 thick-disc stars. Fig. 24 shows [Fe/H] versus age for these stars together with the ages for 150 thin-disc stars from Paper I. This figure gives an impression of a continuous age–metallicity relation. For the thin-disc stars, this is a false impression because Paper I did not fairly represent stars with [Fe/H] > -0.2 for which the age spread is very similar to that of the thin-disc stars with [Fe/H] < -0.2. The thick-disc stars were not knowingly selected by [Fe/H] but by kinematic criteria. There is an age–metallicity relation for the thick disc: metallicity increases to about [Fe/H] ~ -0.3 in 5 Gyr from -1.5. This result is consistent with previous studies. The maximum ages given the measurement errors are consistent with the *Wilkinson Microwave Anisotropy Probe* (*WMAP*) age of just under 14 Gyr. Thus, as emphasized recently by Schuster et al. (2006) from ages of halo stars, star formation began within 1 Gyr of the big bang.

Those stars with well-determined ages may be used to examine the velocity–age relations. Nordström et al. (2004, their fig. 30) showed the growth of $U_{\rm LSR}$, $V_{\rm LSR}$ and $W_{\rm LSR}$ with age for their sample, which is dominated by thin-disc stars. This figure serves to indicate the outer boundaries for the growth in these velocity components arising from dynamical heating of thin-disc stars. (We

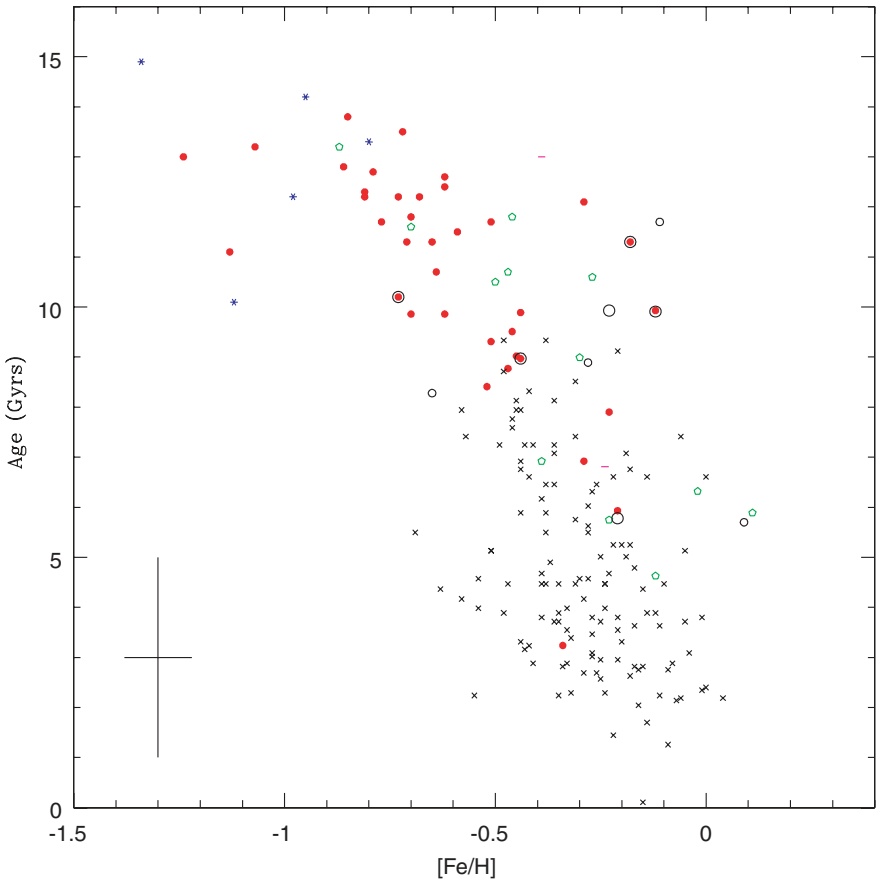

Figure 24. Age versus [Fe/H] for the thick-disc sample of 68 stars with accurate age determinations. Also shown are the 151 thin-disc stars from Reddy et al. (2003). Symbols and the colours represent the stars same as in earlier plots. Typical error bars in [Fe/H] and Age are shown.

showed earlier that our ages were in fair agreement with those of Nordström et al.'s.) In Fig. 25, we show these boundaries in the three panels showing velocity versus age. Stars of Paper I fall in the main between the broken lines. In Nordström et al.'s fig. 30, the area between the broken lines is filled with stars to about ages of 15 Gyr, but note that their ages systematically differ from ours for the most-metal-poor stars (see Section 4.5).

Our thick-disc stars are, as expected, displaced outside the area between the broken lines in the $V_{\rm LSR}$ versus age plot. In $W_{\rm LSR}$ versus age, the thick-disc stars fall along the broken lines, and in $U_{\rm LSR}$ versus age the thick-disc stars fall within and outside the area between the broken lines.

7 MERGERS AND ABUNDANCES

Today, the origin of the thick disc is believed to lie in the formation of the early Galaxy through mergers of smaller (proto-) galaxies in the context of a Lambda cold dark matter (ΛCDM) universe. Simulations of galaxy construction by mergers are regularly reported in the literature. Reviews are written to correlate observational and theoretical evidence on the thick disc not only of the Galaxy, but also of (edge-on) spiral galaxies. Here, we restrict remarks largely to interpretations of the abundance differences between thick and thin disc and the similarities between the thick disc and the halo. The reader is referred to comprehensive reviews for a more detailed discussion of observations and theory – see, for example, Majewski (1993) and Freeman & Bland-Hawthorn (2002). Our discussion is obviously influenced by the recent commentaries by Dalcanton, Seth & Yoachim (2006) and Wyse & Gilmore (2005).

Recent detections of the accretion of dwarf galaxies show that merger is a continuing way of life for the Galaxy (e.g. Ibata et al. 1997; Yanny et al. 2003). Theoretical ideas about mergers in the usual ΛCDM universe predict that the rate of mergers was much higher in the past with a marked decline in the rate at (say) a redshift $z \sim 1$ or about 8 Gyr ago. Coupling of the history of mergers with the formation of thick-disc stars explains why the Galactic thick-disc stars are old. One additional condition is required: the system of thick-disc stars must be created free of gas in order that star formation is cut off and young thick-disc stars are not formed. Thin-disc stars form from gas – likely, a mixture of pre-merger gas of the Galaxy and infall of gas following the mergers.

A defining characteristic of the thick disc is the large vertical scaleheight, that is the high vertical velocity dispersion (σ_W). Dalcanton et al. (2006) noted that there are three ways in which a high σ_W may be achieved through merging: (A) heating of a thin disc in a merger (which may or may not lead to the disruption of the thin disc); (B) direct accretion of stars from satellite galaxies; and (C) star formation in merging gas-rich systems. There is the real possibility that the three ways each contributed to the formation of our thick (and thin) disc.

7.1 Scenario A

The Galaxy develops a thin disc with the ongoing star formation. Merger with one or more satellite galaxies occurs. Thin-disc stars

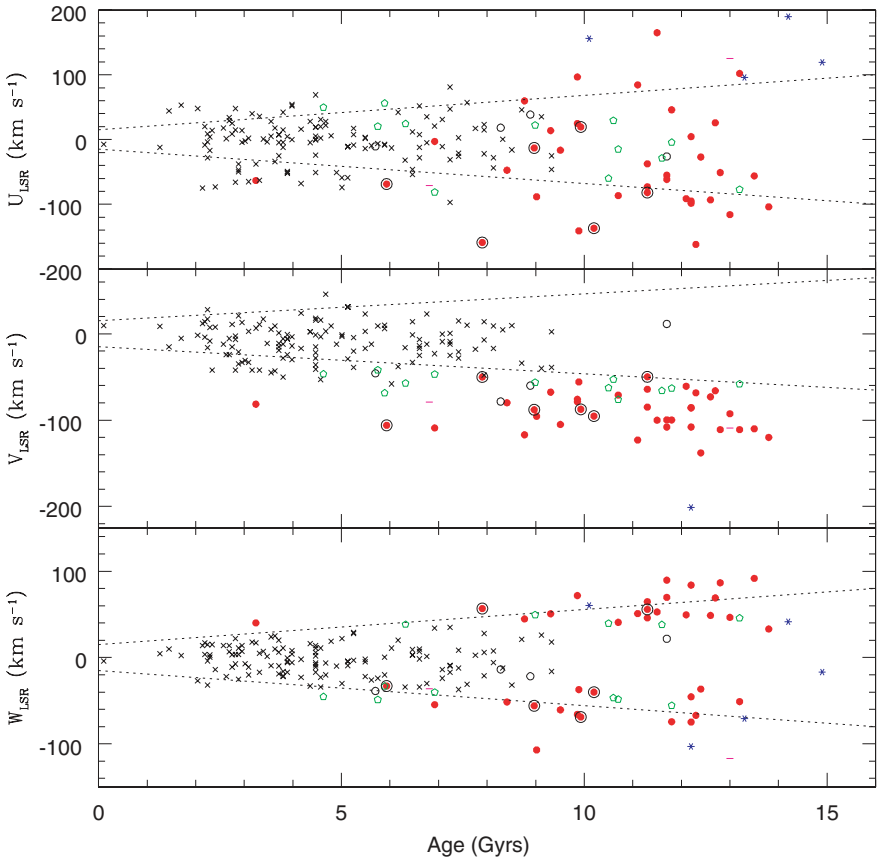

Figure 25. Space velocities as a function of age for thin- and thick-disc stars. Cones (dashed lines) in the $U_{\rm LSR}$, $V_{\rm LSR}$ and $W_{\rm LSR}$ and age plots represent the solar neighbourhood disc stars from Nordström et al. (2004). Note the increasing thickness of the disc as it ages. For more details see the text.

are heated in the merger to create a thick disc of stars but not gas. Thick-disc stars are fossils from the early years of the thin disc. This thin disc of gas is largely destroyed but reforms following the mergers by accreting gas from the original thin disc, the satellites, and, perhaps, the proverbial infall of (primordial?) gas. After a hiatus, star formation resumes in the thin disc from gas having an initial abundance set by the compositions of the contributors of gas and may be also by the Type Ia supernovae (SN Ia) from the generations of thick-disc stars. Quinn, Hernquist & Fullagar (1993) is commonly cited as providing a description of thick-disc formation through a merger.

As pointed out by Dalcanton et al. (2006), vertical heating does not change angular momentum significantly. For example, Quinn et al. (1993) showed only a mild reduction of about 10 km s^{-1} in the rotational velocities of the stars after disc heating by a satellite merger. Thus, in this scenario, it may be difficult to explain the larger differences observed between the asymmetric drifts of the thin and thick discs.

7.2 Scenario B

An alternative consequence of galaxy growth through mergers is that the thick disc is composed of stars accreted from satellite galaxies. Abadi et al. (2003a,b) described results from a single simulation of galaxy formation in a ΛCDM universe. Many structural and dynamical properties of the Galaxy are satisfactorily reproduced including a disc with well-defined thin- and thick-disc components. The majority (about 60 per cent) of the thick-disc stars are stars captured from satellite galaxies. This percentage increases with age; 90 per cent of thick-disc stars older than about 10 Gyr were provided by satellite galaxies. In addition, about 15 per cent of the oldest thin-disc stars are from the satellites.

One of the most interesting predictions of the Abadi et al. scenario is that the thick-disc stars acquired from any given satellite do not end up at all galactocentric distances, but they rather form a ring-like structure. Thus, different satellites may dominate the thick-disc population at different radii. However, the peak of the metallicity distribution of thick-disc stars appears to be fairly uniform between 4 and 14 kpc from the Galactic Centre (Allende Prieto et al. 2006).

The demonstrated uniformity of composition among thick-disc stars in the solar neighbourhood (see Section 5.7), and the lack of cosmic scatter, would suggest that these stars may not have come from a variety of satellites, each with a different, if similar, chemical history. It may be noted too that abundance analyses of stars in dwarf spheroidal galaxies and the Magellanic Clouds (Shetrone et al. 2003; Hill 2004) show a variety of [X/Fe] versus [Fe/H] relations, each unlike those of the thick disc. However, the satellites that merged long ago may have had abundance patterns distinct from those of the surviving dwarf spheroidal and irregular galaxies. Abadi et al. stressed that they have only a single simulation and, perhaps, other simulations will provide a Galaxy with a thick disc free of a significant population of accreted stars. (Abadi et al. predicted that one in two stars in the halo is from a satellite galaxy. Star-to-star scatter in [X/Fe] including [α/Fe] may exist among halo stars.)

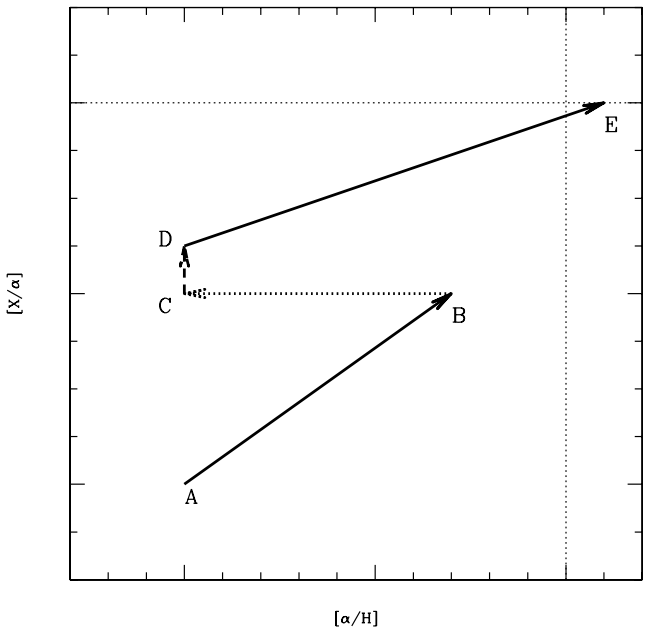

Figure 26. Schematic diagram for the Galactic disc evolution from thick-disc (A–B) and the thin-disc evolution (D–E). The points B and C may refer to merger event and the birth of the thin disc, respectively.

The mergers disrupt the gas of the early thin disc. Just prior to its disruption, a part of the thin disc had attained [Fe/H] $\simeq -0.3$, the maximum metallicity of the thick disc. After the merger, the thin disc is reconstituted from the gas of the former thin disc and the metal-poor (presumably) gas of the satellite galaxies. One supposes that the present thin disc began life with [Fe/H] ~ -0.7, the low metallicity bound to the present thin-disc stars. In the hiatus before the reconstitution of the thin disc, the gas is contaminated by the ejecta from SNe Ia, as in scenario (C) – see, our discussion of Figs 26 and 27 which is also pertinent to this scenario.

7.3 Scenario C

The thick disc is formed during an early period of multiple mergers involving gas-rich systems. A high star formation rate is associated with this period. Interactions between the merging systems and the nascent galaxy lead to a relatively hot system of stars supported by rotation – that is, a thick disc. Subsequent to this early period, the thin disc is formed from infalling gas.

This scenario is developed by Brook et al. (2004, 2005, 2006). Their 2005 paper presented abundance predictions, specifically [α/Fe] versus [Fe/H], for several simulated galaxies provided from an N-body smoothed particle hydrodynamics (SPH) code. These predictions (figs 12–15 from Brook et al. 2005) bear a remarkable resemblance to the observed abundance patterns of the halo, thick and thin discs.

For example, the predicted metal content of thick-disc stars is approximately uniform, across different Galactocentric distances and with the height from the Galactic plane, in agreement with the recent SDSS observations (Allende Prieto et al. 2006). Of particular note is the clear separation in the [α/Fe] versus [Fe/H] relations of the thick and thin disc with each trend showing a weak [Fe/H] dependence. In the reported simulations, the thick disc extends in [Fe/H] variously from about -1.5 to an upper limit in the range -0.1 to -0.5. The thick-disc [α/Fe] at the upper limit in two of the four reported simulations remained separated from the thin disc's [α/Fe] and in the other two approached but did not merge with the [α/Fe] of the thin disc (i.e. the simulations do not predict a knee). The lower [α/Fe] of the thin disc results from the contamination of the thin disc by the ejecta from SNe Ia from thick-disc binaries. The thin disc has a metallicity spread of -0.5 to $+0.4$ in three of the four simulations and -0.9 to -0.1 in the fourth. Halo stars extend to [Fe/H] of about -0.9 to -0.6 with a [α/Fe] very similar to that of the thick disc in three simulations and about 0.2 dex larger in the fourth simulation.

7.4 An observer's scenario

Our data on thick- and thin-disc abundances may be used to characterize the pollution of the gas by SN Ia ejecta (and AGB stars). Ages of thin- and thick-disc stars show (Fig. 24) that several Gyr elapsed between the formation of the first thick- and the first thin-disc stars and, thus, time aplenty for SNe Ia (and AGB stars) to cause pollution. Compositions of thick-disc stars up to the most metal rich (in our interpretation) at [Fe/H] $= -0.3$ are dominated by contributions from SN II. Addition of SN Ia ejecta to gas, as recognized in a classic paper by Tinsley (1979), increases the abundance ratio of the iron-group elements to α-elements.

This episode in the chemical evolution of the Galactic disc is represented schematically by Fig. 26 in which we plot [X/α] versus [α/H]. The α abundances are dominated by SN II products but not without an SN Ia contribution, especially for the heavier α-elements. Oxygen would probably provide a cleaner measure of SN II products, albeit with a bias to the SN II from the most massive stars but, at present, we do not have non-LTE corrected O abundances for all of our stars. Evolution of the thick disc is represented by the track A to B; pristine gas is contaminated by SN II ejecta raising [α/H] and, in this example, also raising [X/α]; X is here an element whose yield from SN II is metallicity-dependent. For elements whose yield from SN II is independent of metallicity, the track A to B will be parallel to the x-axis. Stars formed as the gas composition evolves from A to B become today's thick-disc stars.

Star formation ceases as a thin disc forms from the gas of the satellites that gave the thick-disc stars and infalling more-metal-poor gas. On the assumption that the thick-disc gas of the composition corresponding to point B is diluted with very metal-poor gas, the thin disc will initially have the composition corresponding to point C. Following the period of active merger, there will be a hiatus before star formation in the thin disc resumes. In and following the interval of very low star formation, SNe Ia pollute the gas. Pollution prior to the resumption of star formation is represented by the track C to D; in this example, the products of SNe Ia include notable amounts of X but not of the α-elements. (If α-elements are produced, the track C to D is slanted.) Finally, the composition of the gas (and stars) of the new thin disc evolves along the track D to E in response to the contributions by the SN II arising from massive stars formed in the new thin disc, SN Ia in the thick disc and later of the thin disc, and AGB stars of the thick and thin discs.

Evolution from A to E will depend on the element X, as we illustrate in Fig. 27, where derived abundances for four representative elements – Mn, Fe, Ni and Eu – are shown with a track A to E superimposed with point B placed at [[α/H] $= -0.1$, and C placed, somewhat arbitrarily, at [α/H] $= -0.6$. The increase in [Mn/α] along A to B is attributed to a metallicity-dependent Mn yield from SN II (McWilliam et al. 2003). This is supported by the observation that the track C to D for Mn is short. Iron offers a contrasting track: along the thick-disc segment, A to B, [Fe/α] is essentially constant indicating that the relative yields of Fe and α-elements

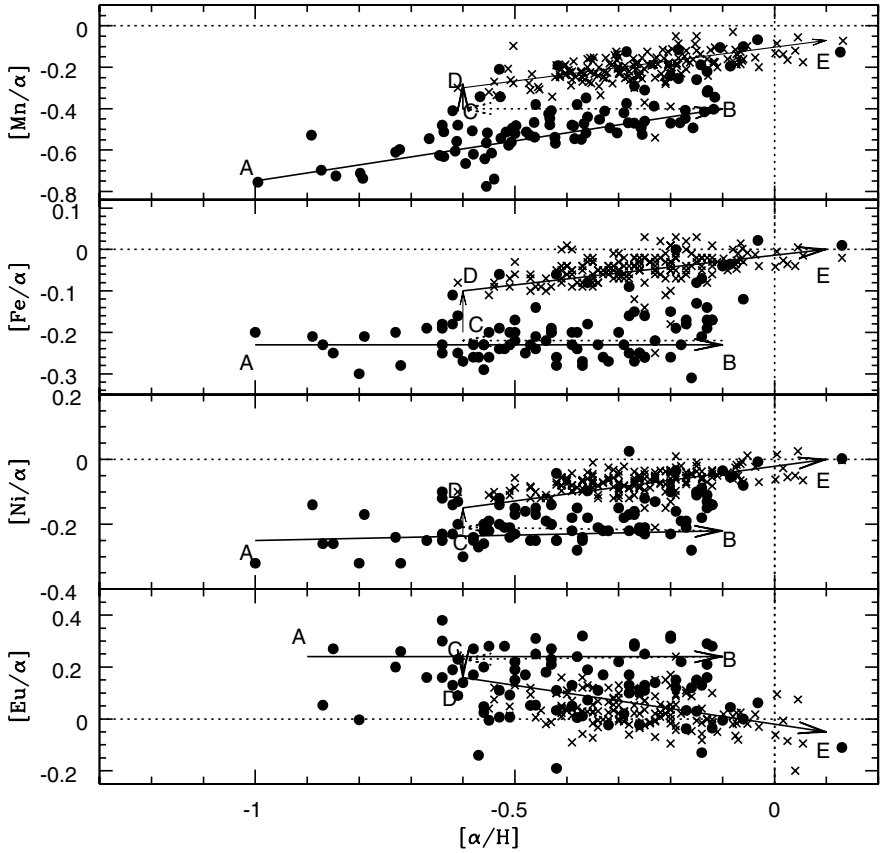

Figure 27. Plots for abudance ratios [X/α] against [α/H] for Mn, Fe, Ni and Eu for thin-disc (crosses) and the thick-disc stars (filled circles). See the text for the details.

are metallicity-independent; the large jump from C to D shows, as anticipated, that Fe is a principal product of SNe Ia; and the slope to the track D to E reflects the combined contributions of SN II and SN Ia to the continuing evolution of the thin disc. Behaviour of Ni is similar to that of Fe but the increment in [X/α] from C to D is less for Ni than for Fe. For Eu, [Eu/α] is approximately constant along the track A to B, indicating a lack of a metallicity dependence of the Eu to α-element yields from SN II. The track C to D shows a decrease in [Eu/α] resulting from α-element production by SN Ia with the absence of Eu production. The track D to E is controlled by the yields from SN II and SN Ia. In summary, chemical evolution of the disc as depicted by Fig. 26 offers a qualitative account of the compiled data on the abundances of thin- and thick-disc stars.

This scenario for the formation of the thick disc offers a fine account of the observed abundance pattern of the Galaxy's halo, thick and thin discs. Brook et al. described how their simulations fit other observed characteristics of the Galaxy and external disc galaxies. They also remarked that the accretion of stars from satellites, after the formation of the thin disc, may contribute to the population of the thick disc and halo, that is, the first scenario (above) may have a role to play.

A potential problem with this scenario, pointed out by Dalcanton et al. (2006), is that it will be the same gas from the merging blocks which will give birth to the thick-disc stars first and to the thin-disc population later. This situation could make it difficult to have quite different scalelengths for the two discs. However, as we discussed above, in order to match the observed abundances of thin- and thick-disc stars, a significant contribution of metal-poor gas must be made available before star formation begins in the thin disc. Only in this way, the last stars formed in the thick disc can have higher metal abundances than thin-disc stars formed at a later time. In the models reported by Brook et al., the scalelength of the thin disc, we note, is significantly different from that of the thick disc (a ratio of 1.6), but with the thick disc being more compact than the thin disc, which is opposite to the behaviour observed in most galaxies, including the Milky Way.

8 CONCLUDING REMARKS

On the basis of the available abundance data on the thin and thick discs and of the published simulations of disc formation through mergers in a ΛCDM universe, scenario (C) appears to be a plausible leading explanation for the origin of the thick and thin discs. In terms of a continued exploration of the observational frontiers, there is, for example, a need for (i) a detailed abundance analysis of stars apparently attributable to an extension of the thick disc to metallicities below [Fe/H] of -1, that is, the so-called metal-weak thick disc, which comprises only 1 per cent of the thick disc (Martin & Morrison 1998); (ii) a more complete investigation of the four-dimensional space (U, V, W, [Fe/H]), for example, the pursuit of stars at low $W_{\rm LSR}$ with [Fe/H] less than about -0.7, stars, which, if present, would be assigned to the thin disc; (iii) an analysis of a larger sample of stars with [Fe/H] greater than about -0.3 and well-determined kinematics is needed to confirm or deny the presence of the knee in the thick-disc Mg-like abundances connecting to the thin-disc abundances for the most-metal-rich stars; (iv) a larger sample of thick-disc stars is needed to determine the radial and vertical gradients in the compositions of the thick-disc stars. The vertical

gradient, if any, appears to be very shallow (e.g. Allende Prieto et al. 2006; Bensby et al. 2005).

The realization that thick- and thin-disc stars of the same [Fe/H] differ in composition and the strong suggestion that thick- and thin-disc stars span overlapping but distinctly different ranges in [Fe/H] (see, e.g. Schuster et al. 2006) has consequences for the cottage industry providing models of chemical evolution of the Galactic disc, especially for models of the solar neighbourhood. The industry standard supposes that the chemical evolution as represented by a plot of [X/Y] versus [Y/H], where Y is traditionally taken to be Fe or sometimes O, is a continuous process from the halo to the disc, that is, initially, metal-free gas experiences star formation leading to the halo stars, collapse of gas to a disc with enrichment from stellar nucleosynthesis and possibly continuing infall of gas leads to a steady continuous chemical evolution. No account is taken of the fact that the disc has the two components – thin and thick – from different origins and, most probably, covering different metallicity ranges. The time has come to change the industry standard.

ACKNOWLEDGMENTS

We thank Jocelyn Tomkin, Kameswara Rao and Gajendra Pandey for many spirited and useful discussions. This research has been supported in part by the Robert A. Welch Foundation of Houston, Texas. This research has made use of the SIMBAD data base, operated at CDS, Strasbourg, France, and the NASA ADS, USA.

REFERENCES

Abadi M. G., Navarro J. F., Steinmetz M., Eke V. R., 2003a, ApJ, 591, 499
Abadi M. G., Navarro J. F., Steinmetz M., Eke V. R., 2003b, ApJ, 597, 21
Adelman-McCarthy et al., 2006, ApJS, 162, 38
Allende Prieto C., Barklem P. S., Lambert D. L., Cunha K., 2004, A&A, 420, 183
Allende Prieto C., Beers T. C., Wilhelm R., Newberg H. J., Rockosi C. M., Yanny B., Lee Y. S., 2006, ApJ, 636, 804
Alonso A., Arribas S., Martinez-Roger C., 1996, A&A, 313, 873
Andersson H., Edvardsson B., 1994, A&A, 290, 590
Barbier-Brossat M., Figon P., 2000, A&AS, 142, 217
Bensby T., Feltzing S., Lundström I., 2003, A&A, 410, 527
Bensby T., Feltzing S., Lundström I., 2004, A&A, 415, 155
Bensby T., Feltzing S., Lundström I., Ilyin I., 2005, A&A, 433, 185
Bertelli G., Bressan A., Chiosi C., Fagotto F., Nasi E., 1994, A&AS, 106, 275
Bihain G., Israelian G., Rebolo R., Bonifacio P., Molaro P., 2004, A&A, 423, 777
Borkova T. V., Marsakov V. A., 2005, ARep, 49, 405
Brewer M-M., Carney B. W., 2006, AJ, 131, 431
Brook C. B., Kawata D., Gibson B. K., Freeman K. C., 2004, ApJ, 612, 894
Brook C. B., Gibson B. K., Martel H., Kawata D., 2005, ApJ, 630, 298
Brook C. B., Veilleux V., Kawata D., Martel H., Gibson B. K. 2006, in de Jong R. S., ed., Island Universes, Structure and Evolution of Disc Galaxies. Springer, Dordrecht, in press (astro-ph/0511002)
Buser R., Rong J., Karaali S., 1999, A&A, 348, 98
Burris D. L., Pilachowski C. A., Armandroff T. E., Sneden C., Cowan J. J., Roe H., 2000, ApJ, 544, 302
Cabrera-Lavers A., Garzón F., Hammersley P. L., 2005, A&A, 433, 173
Carney B. W., Latham D. W., Laird J. B., Aguilar L. A., 1994, AJ, 107, 2240
Chen Y. Q., Nissen P. E., Zhao G., Zhang H. W., Benoni T., 2000, A&AS, 141, 491
Cutri R. M. et al., 2003, VizieR Online Data Catalog, 2246. Originally published in: Univ. of Massachusetts and Infrared Processing and Analysis Centre, IPAC/California Institute of Technology
Dalcanton J. J., Seth A. C., Yoachim P., 2006, in de Jong R. S., ed., Island Universes, Structure and Evolution of Disc Galaxies. Springer, Dordrecht, in press (astro-ph/0509700)
Degl'Innocenti S., Prada Moroni P. G., Ricci B., 2005, preprint (astro-ph/0504611)
Dehnen W., Binney J. J., 1998, MNRAS, 298, 387
Edvardsson B., Andersen J., Gustafsson B., Lambert D. L., Nissen P. E., Tomkin J., 1993, A&A, 275, 101
Famaey B., Jorissen A., Luri X., Mayor M., Udry S., Dejonghe H., Turon C., 2005, A&A, 430
Feltzing S., Gustafsson B., 1998, A&AS, 129, 237
Feltzing S., Bensby T., Lundström I., 2003, A&AL, 397, 1
Freeman K., Bland-Hawthorn J., 2002, ARA&A, 40, 487
Fulbright J. P., 2000, AJ, 120, 1841
Fuhrmann K., 1998, A&A, 338, 161
Fuhrmann K., 2004, AN, 325, 3
Gehren T., Liang Y. C., Shi J. R., Zhang H. W., Zhao G., 2004, A&A, 413, 1045
Gilmore G., Reid N., 1983, MNRAS, 202, 1025
Girardi L., Bressan A., Bertelli G., Chiosi C., 2000, A&AS, 141, 371
Gratton R. G., Carretta E., Matteucii F., Sneden C., 1996, in Morrison H., Sarajedini A., eds, ASP Conf. Ser. Vol. 92, Formation of the Galactic Halo . . . inside and out. Astron. Soc. Pac., San Francisco, p. 307
Gratton R. G., Carretta E., Desidera S., Lucatello S., Mazzei P., Barbieri M., 2003, A&A, 406, 131
Gustafsson B., Karlsson T., Olsson E., Edvardsson B., Ryde N., 1999, A&A, 342, 426
Hauck B., Mermilliod M., 1997, yCat, 2215, 0
Hill V., 2004, in McWilliam A., Rauch M., eds, Origin and Evolution of the Elements. Carnegie Observatories, Pasadena, p. 205
Ibata R. A., Wyse R. F. G., Gilmore G., Irwin M. J., Suntzeff N. B., 1997, AJ, 113, 634
Juric M. et al., 2005, preprint (astro-ph/0510520)
Kurucz R. L., 1998, http://kurucz.harvard.edu (online reference only)
Latham D. W., Stefanik R. P., Torres G., Davis R. J., Mazeh T., Carney B. W., Laird J. B., Morse J. A., 2002, AJ, 124, 1144
McWilliam A., Rich R. M., Smecker-Hane T. A., 2003, ApJ, 592, L21
Majewski S. R., 1993, ARA&A, 31, 575
Malaroda S., Levato H., Galliani S., 2001, Complejo Astronomico El Leoncito (CASLEO). San Juan, Argentina
Marsakov V. A., Borkova T. V., 2005, Astron. Lett., 31, 515
Martin J. C., Morrison H. L., 1998, AJ, 116, 172
Mishenina T. V., Kovtyukh V. V., Soubiran C., Travaglio C., Busso M., 2002, A&A, 396, 189
Mishenina T. V., Soubiran C., Kovtyukh V. V., Korotin S. A., 2004, A&A, 418, 551
Neckel Th., Klare G., Sarcander M., 1980, A&AS, 42, 252
Nidever D. L., Marcy G. W., Butler R. P., Fischer D. A., Vogt S. S., 2002, ApJS, 141, 503
Nissen P. E., Chen Y. Q., Schuster W. J., Zhao G., 2000, A&A, 353, 722
Nissen P. E., Chen Y. Q., Asplund M., Pettini M., 2004, A&A, 415, 993
Nordström B. et al., 2004, A&A, 418, 989
Ojha D. K., 2001, MNRAS, 322, 426
Ojha D. K., Bienayme O., Robin A. C., Creze M., Mohan V., 1996, A&A, 311, 456
Ojha D. K., Bienaymé O., Mohan V., Robin A. C., 1999, A&A, 351, 945
Peterson R. C., 1981, ApJ, 244, 989
Prochaska J. X., McWilliam A., 2000, ApJ, 537, L57
Prochaska J. X., Naumov S. O., Carney B. W., McWilliam A., Wolfe A. M., 2000, AJ, 120, 2513
Quinn P. J., Hernquist L., Fullagar D. P., 1993, ApJ, 403, 74
Reddy B. E., Tomkin J., Lambert D. L., Allende Prieto C., 2003, MNRAS, 340, 304 (Paper I)
Robin A. C., Reylé C., Derrière S., Picaud S., 2003, A&A, 409, 523
Schuler S. C., King J. R., Fisher D. A., Soderblom D. R., Jones B. F., 2003, AJ, 125, 2085
Schuster W. J., Moitinho A., Marquez A., Parrao L., Covarrubias E., 2006, A&A, 445, 939

Shetrone M., Venn K. A., Tolstoy E., Primas F., Hill V., Kaufer A., 2003, AJ, 125, 684
Shi J. R., Zhao G., Chen Y. Q., 2002, A&A, 381, 982
Shi J. R., Gehren T., Zhao G., 2004, A&A, 423, 683
Simmerer J., Sneden C., Cowan J. J., Collier J., Woolf V. M., Lawler J. E., 2004, ApJ, 617, 1091
Sneden C., 1973, PhD thesis, Univ. of Texas, Austin
Sneden C., Gratton R. G., Crocker D. A., 1991, A&A, 246, 354
Soubiran C., Bienaymé O., Siebert A., 2003, A&A, 398, 141
Spite M., Spite F., 1980, A&A, 89, 118
Takada-Hidai M., Saito Yu-Ji., Takeda Y., Honda S., Sadakane K., Masuda S., Izumiura H., 2005, PASJ, 57, 347
Tinsley B. M., 1979, ApJ, 229, 1046
Tull R. G., MacQueen P. J., Sneden C., Lambert D. L., 1995, PASP, 107, 251
Venn K. A., Irwin M., Shetrone M. D., Tout C. A., Hill V., Tolstoy E., 2004, AJ, 128, 1177
Yong D., Lambert D. L., Allende Prieto C., Paulson D. B., 2004, ApJ, 603, 697
Yanny B. et al., 2003, ApJ, 588, 824
York D. G. et al., 2000, AJ, 120, 1579
Wyse R. F. G., Gilmore G., 2005, in Valls-Gabaud D., Chavez M., eds, ASP Conf. Ser., Resolved Stellar Populations. Astron. Soc. Pac., San Francisco, in press (astro-ph/0510025)

This paper has been typeset from a TEX/LATEX file prepared by the author.